POLITECNICO DI MILANO

Chemistry, Materials and Chemical Engineering Department

"Giulio Natta"

This Thesis is submitted for the degree of Master of Science in

Materials Engineering

TERNARY BLENDS FOR ORGANIC PHOTOVOLTAICS

By

Alberto Scaccabarozzi

755762

Supervised by Dr Natalie Stingelin

Prof Chiara Bertarelli

A.A. 2011/2012

Ai miei genitori, per avermi insegnato a guardare lontano.

I Abstract

Organic photovoltaics (OPV) have attracted increasing interest over the last decade resulting in their efficiencies to have risen to over 10 %. This development is driving organic photovoltaic technologies towards commercialization. To full exploit their touted potential, however, other prerequisites need to be fulfilled: for example, beside a sufficient device performance, OPVs ideally should also feature a good mechanical stability. In addition, they should be amenable to straight-forward processing routes. So far it has, however been challenging to introduce such features. One reason for this is the small thickness of the OPV active layers (generally < 100 nm) that is required for optimal performance of the solar cells, limiting both, mechanical robustness and ease of processing of such structures.

In this thesis, a range of optoelectronic and structural properties of ternary blends for photovoltaic applications, previously shown to display favourable rheological and mechanical properties compared to the common donor:acceptor binaries, are explored to address this issue. To this end, we selected the electrically insulating high-density polyethylene (HDPE) as a third component of systems comprising the donor:acceptor combination of poly(3-hexylthiophene) and phenyl-C_{61}-butyric acid methyl ester (PCBM).

Binary systems were first studied in order to explore the influence of HDPE on the properties of the neat P3HT and PCBM. Thereby, P3HT:HDPE and PCBM:HDPE binary blends were first analysed. In a second set of experiments, we then focused on ternary blends comprising P3HT, PCBM and HDPE.

The weight ratio between the active components was for this purpose kept to 1:1, while the HDPE content was varied. We find that various electronic and morphological properties strongly depend on the active layers' thickness and provide evidence that films comprising the ternary blend display sufficiently high photovoltaic properties at larger thicknesses compared to the common donor:acceptor binaries. These observations are supported by a study using other OPV blends. We concentrate here on those comprising a diketopyrrolopyrrole (DPPTTT) derivative as donor polymer.

II Estratto

Negli ultimi anni i semiconduttori organici, polimeri e small molecules, hanno attirato un interesse sempre maggiore della comunità scientifica per l'ottimale combinazione di alcune loro caratteristiche, quali ad esempio: buone proprietà optoelettroniche, leggerezza, flessibilità e facilità di deposizione.

Uno degli ambiti d'applicazione di tali materiali è il fotovoltaico, dove i materiali organici si propongono come alternativa al silicio. Nonostante le celle fotovoltaiche al silicio siano caratterizzate ancora da maggiore efficienza, sono anche contraddistinte da un elevato costo ed elevato impatto ambientale del processo di produzione.

Al fine di migliorare l'efficienza delle celle fotovoltaiche organiche è necessario utilizzare un blend di due diversi materiali, un donatore ed un accettore. In tal senso il sistema ampiamente più studiato è la miscela binaria tra poli(3-esiltiofene) (P3HT) ed estere metilico dell'acido [6,6]-fenil C_{61}-butirrico (PCBM).

Il lavoro di tesi in oggetto si propone di studiare un sistema ternario con l'aggiunta di polietilene ad alta densità (HDPE) al blend binario. La miscela è dunque del tipo P3HT:PCBM:HDPE. L'idea è quella di aggiungere un ulteriore polimero, inattivo dal punto di vista elettronico, con il quale è però possibile migliorare le proprietà reologiche e meccaniche del film, facilitando così la scalabilità industriale.

Studi preliminari hanno dimostrato che il blend con HDPE non peggiora la mobilità delle cariche, ma in alcuni casi ha effetti migliorativi, anche per elevate percentuali di polietilene. [1] Altri studi dimostrano inoltre come tali miscele possano essere utilizzate in applicazioni fotovoltaiche senza peggiorare necessariamente i rendimenti. [2]

Tuttavia l'effetto dell'utilizzo del HDPE su alcune proprietà dei film non è ancora stato oggetto di studi approfonditi. Tali proprietà comprendono: aggregazione delle macromolecole di P3HT, formazione di aggregati di PCBM, quenching dell'eccitone e generazione di cariche libere. In questa tesi ci si propone dunque di studiare tali proprietà al variare della quantità di polietilene aggiunto e dei parametri di processo.

Inizialmente sono stati studiati dei blend binari tra HDPE ed i materiali attivi, di conseguenza sono state analizzate miscele P3HT:HDPE e PCBM:HDPE. Successivamente l'attenzione è stata rivolta sullo studio di miscele ternarie. Il rapporto in peso tra P3HT e PCBM è stato mantenuto costante (1:1), mentre il contenuto del

HDPE è stato variato sistematicamente. La caratterizzazione dei film è stata eseguita utilizzando principalmente le seguenti tecniche: spettroscopia UV-vis, spettroscopia di fluorescenza (PL), transient absorption spectroscopy (TAS), microscopio ottico, calorimetria differenziale a scansione (DSC).

Nella tesi vengono proposti tra gli altri i risultati sperimentali in cui si mette in luce una forte dipendenza tra alcune proprietà optoelettroniche con lo spessore dei film. Nel caso di miscele binarie P3HT:PCBM, sono necessari film molto fini (< 100 nm) per ottimizzare i rendimenti delle celle. Film ternari prodotti con questi spessori forniscono proprietà insoddisfacenti; se però gli spessori vengono aumentati (~500 nm), le proprietà migliorano e tornano ad essere compatibili con i requisiti necessari per applicazioni fotovoltaiche. Questo risultato è confortante in quanto l'obiettivo iniziale era quello di migliorare le prestazioni meccaniche del film, dunque l'interesse era proprio quello di produrre film più spessi.

In questa tesi è anche proposto lo studio di un altro polimero semiconduttore, utilizzandolo al posto del P3HT. Il polimero utilizzato è un derivato del dichetopirrolpirrolo, DPPTTT. Vengono presentati inizialmente i risultati concernenti il blend binario DPPTTT:PCBM e successivamente quelli relativi altre miscele binarie e ternarie con il HDPE, descrivendone le caratteristiche e i possibili vantaggi.

III Acknowledgements

I would like to thank my supervisor at Imperial College, Dr Natalie Stingelin, for giving me the opportunity of working in her group. I appreciated her effort and enthusiasm in guiding me through this experience. I would also like to thank all of the staff and students working in the group: Dr Ester Buchaca Domingo, Dr Christoph Hellmann, Dr Manuela Russo, George Richardson, Paul Westacott, Liyang Yu.

I also want to acknowledge my supervisor at Politecnico di Milano, Prof.ssa Chiara Bertarelli for bringing me closer to these topics and for her helpfulness during these months of work.

Last but not least, I would like to thank my parents for their support throughout the years of my studies, especially for the period I spent in London to work on this thesis.

IV Scope and survey of the thesis

This thesis intends to investigate the influences of high-density polyethylene (HDPE) on the electronic properties of a common binary system used for organic photovoltaics, poly(3-hexylthiophene):phenyl-C_{61}-butyric acid methyl ester (P3HT:PCBM). Previous studies highlight how such a ternary blends enables intriguing perspectives both for Organic Field Effect Transistor (OFET) and Organic Photovoltaics (OPV) applications.
Mechanical properties are strongly upgraded thanks to the use of polyethylene leading to an easier processability and better applicability of these films with practical uses of solar cells, with a similar role that has got the compounding for polymer industry.
The idea of this blend is thus in agreement with a possible industrial production and commercialization of solar cells, consequently a fundamental requirement is to use a scalable deposition technique, like wire-bar coating.
In order to study the properties of the ternary blends different techniques has been employed: UV-vis spectroscopy, Photoluminescence Spectroscopy (PL), Transient Absorption Spectroscopy (TAS), Optical Microscopy (OM), Differential Scanning Calorimetry (DSC).
In the last part of my work I used another donor polymer, a diketopyrrolopyrrole derivative, called DPPTTT, instead of P3HT. A preliminary study of a binary blend with PCBM was investigated, as well as an examination of the applicability of a ternary blend with HDPE.

Table of Contents

1. Introduction

1.1 Organic electronics

Organic electronics is a subject attracting progressively more attention in the last years. Since 1950s when the first organic semiconductors were reported [3] and especially after 1977 when Shirakawa, MacDiarmid and Heeger managed to obtain high conductive polyacetylene, this new field of research flourished. [4]

After this discovery many research groups have been working on this issue, developing new materials and devices that enable organic electronics to be present nowadays not only in academia, but also in the industry. Organic electronics can be divided in three fields: Organic Light Emitting Diodes (OLED), that have already reached a good level of industrialization, Organic Field Effect Transistors (OFET) and Organic Photovoltaics (OPV). See Figure 1.1 for some example of current commercial applications.

Figure 1.1: Example of commercial applications of OLED (on the left) and solar cells (on the right)

The reason of the strong interest on this topic is explained by the promise for low-cost, flexibility, lightness, production simplification that organic compounds offer compared to inorganic materials. Another important advantage lies in the possibility of changing easily the properties of organic materials by modifying the synthetic pathways and processing. This is impossible for silicon based materials.

1.2 Organic semiconductors

Polymers are an extraordinary versatile class of materials, not only because there are many different types of them, but also because processing can radically modify the properties. For example, polyethylene is one of the most common polymers, it is used in different applications and it is normally considered a mechanically weak material. However if anisotropy is given to the material through use of suitable processing conditions, fibres can be obtained of mechanical properties that exceed those of steel.

In the same way, polymers are normally considered non-conductive materials and they are usually employed in electronics as insulators. However the development of organic semiconductors is changing completely this perception.

The inspiration for the development of organic semiconductors resulted from the work of Shirakawa, MacDiarmid and Heeger who discovered how doping polyacetylene with chlorine, bromine or iodine vapour, increases the conductivity of this polymer by 10^9 times. With their work they pointed out the importance of doping and innustrated why neat polyacetylene, although having conductive appearance, was not conductive.

Organic semiconducting materials are normally classified in two categories: polymers and small molecules. This classification is not particularly accurate from a pure materials science point of view; indeed many organic semiconductors considered polymers have relatively short chains, with hundreds of repeat units, compared to conventional polymers, in which a typical number of repeat units is 20000.

1.2.1 Conductivity in materials

Conductivity is defined as the ability of the material to conduct an electrical current, it is expressed as σ and is measured in Siemens per meter (Sm^{-1}); the reciprocal of conductivity is the resistivity ρ, measured in Ohm·meter (Ωm).

Materials can be divided in insulators, semiconductors and conductors, depending on their conductivity, see Figure 1.2.

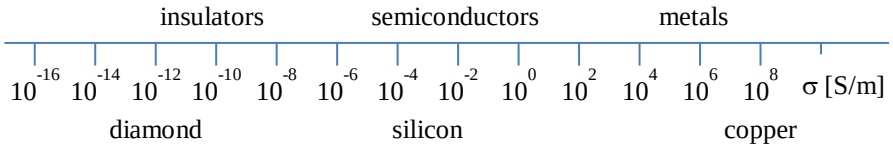

Figure 1.2: Conductivity of materials

Conductivity is directly proportional to the number of free charges (n) and to their mobility (μ), i.e. the ability of charges to move in a medium. In metals the conductivity is the consequence of the complete delocalization of atomic orbitals and it is related to the solid-state structure. If N atoms interact, N molecular orbitals are formed, each one with an energy higher than the previous one. Thus if N is really high (for metals $N=10^{22}$ for a $1cm^3$ metal piece) a continuous band forms and only the lowest half N orbitals are occupied, in this situation once an electron is injected, it's free to jump to a highest level.

When non-metallic bonds are present, i.e. covalent bonds, and provided the atoms are equal or their electronegativity is similar, two different bands are formed, separated one from the other by a certain amount of energy, called energy gap. The electrons are placed in the band at lower energy, called valence band, while the other band is called conduction band. In this situation, if an amount of energy at least equal to the energy gap is provided, an electron can be promoted from the valence to the conduction band and conduction is therefore achieved; this is the case of semiconductors.

If the energy gap is high, thus a really high amount of energy is needed to promote the electron to the conduction band, the resulting material is an insulator. See Figure 1.3.

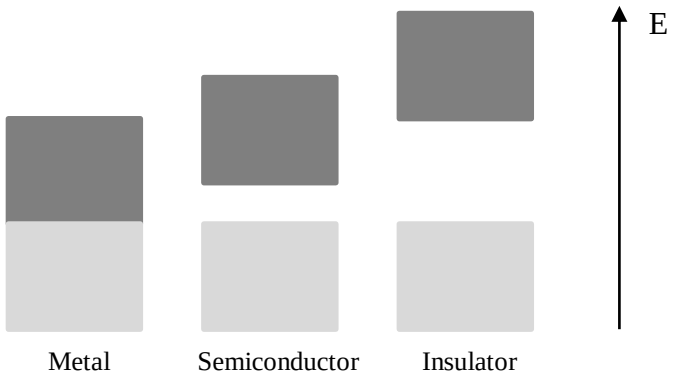

Figure 1.3: Band structure of metallic, semiconductive and insulating materials. Dark grey is the conduction band, light grey is the valence band.

1.2.2 Inorganic semiconductors

Classical semiconductors are inorganic, one of the most used one is silicon (Energy gap ~ 1.1eV). Indeed, currently the electronic industry is based on silicon technologies, and classical photovoltaic cells are manufactured with silicon. These materials can be intrinsic semiconductors, where conduction happens without adding any other impurity, exploiting the conductive mechanism explained before. For example, a photon with

enough energy can promote an electron in the conduction band creating a hole in the valence band, free charges are therefore generated. Inorganic semiconductors can also be extrinsic, in this case impurities are added with a process called doping, this consists in adding an element that has got one more valence electron than the semiconductor (n-doping), or one less (p-doping).

Silicon can be either an intrinsic or an extrinsic semiconductor, it is used pristine or doped depending on the applications. It has got four valence electrons, thus n-doping can be obtained adding an element of the V group (As, P, Sb), a free electron is now present in the lattice and this will be mobile if an electric field is applied. In the case of p-doping an element of III group (B, Al, Ge) is used and this lead to the presence of a hole in the lattice, see Figure 1.4.

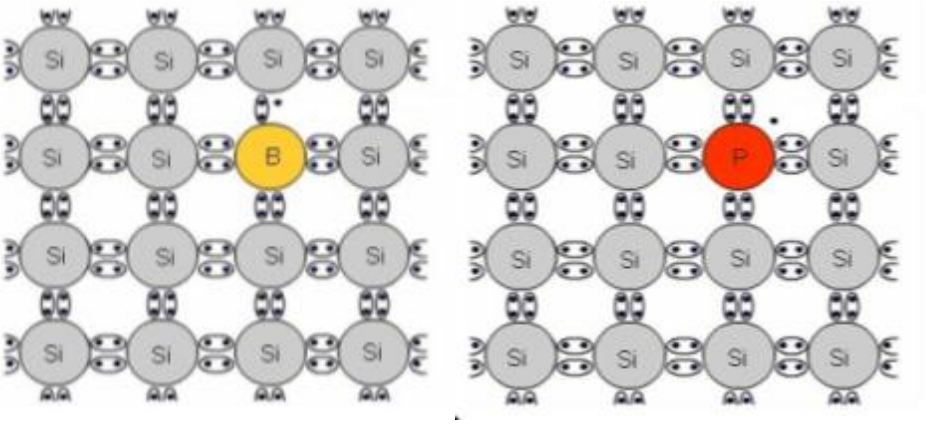

Figure 1.4: Doping of silicon, on the right an example of n-doping by adding a molecule of phosphorous, on the left an example of p-doping by adding boron.

If a sufficient amount of dopant is used, a new band will appear inside the energy gap, for n-doping this band is placed close to the conduction band and is called donor state, this new level enables the excitation of electrons to the conduction band very easily. For p-doping the band is close to the valence band and is called acceptor state, this new level makes possible an easy excitation of the electrons from the valence band to the acceptor state (Figure 1.5). Since the energy required to the excitation of the electrons in the new states is the ionization energy of the impurity, which is tipically between 10 and 50 meV, at room temperaturen (T = 300K) most of the impurities are ionizied.

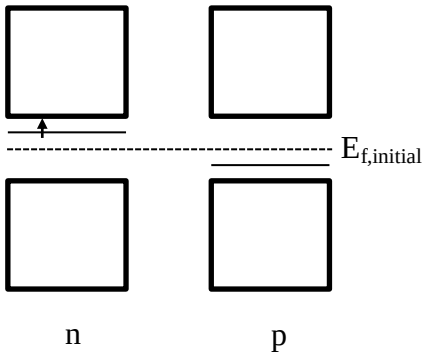

Figure 1.5: Illustration of acceptor level (on the right) and donor level (on the left)

In n-doping the electrons promoted to the valence band are responsible for the conduction, while in p-doping the holes created as a consequence of the promotion of electrons in the acceptor state, are responsible for conduction. It is important to note that the Fermi level, e.g. energy level in which the probability of finding an electron in that level is equal to ½), will swift to higher energy for n-doping and to lower energy for p-doping.

1.2.3 Semiconductive polymers

The conductivity of inorganic materials described till now is related to the solid-state structure, i.e. the lattice rigidity and three-dimensionality of covalent bonds that ensure the formation of valence and conduction bands; for organic semiconductors this does not fully apply. In conjugated polymers for instance, the carbon atoms are hybridized sp^2. This means that three of the valence electrons (2s, $2p_x$, $2p_y$) undergo hybridisation giving three identical hybrid orbitals which lie in the same plane each containing an electron, whilst the fourth electron resides in a p_z orbital orthogonal to the plane of the hybrid orbitals, see Figure 1.6.

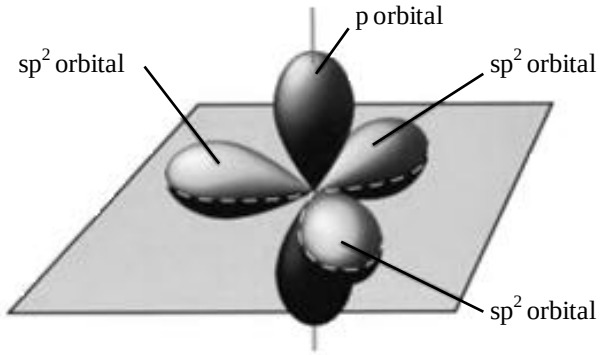

Figure 1.6: Illustration of sp^2 hybridisation, adapted from Steven S. Zumdahl, *Cheminstry*, Third Edition, © 1993 by D.C. Health and Company

The bond between two sp^2-hybridised carbon atoms is given by a σ-type bond. In addition, a π-type bond is formed between two p_z orbitals from a side-to-side interaction. These π-orbitals are delocalized along the backbone due to their conjugation (overlap) and are the responsible of conduction in polymer semiconductors. The delocalization however is not complete. Indeed, polymers are not metal-like conductors and this is explainable taking into account a phenomenon called Peierls distortion. The π-orbitals could be expected to contribute equally to bind carbon atoms, however it is energetically more favorable to form a dimerized structure with alternation of single and double bonds. [5]

An explanation of the semiconductive properties given by π-orbitals can be explained focusing on the electronic structure. The latter can be studied using the Linear Combination of Atomic Orbitals (LCAO) model, which describes how atomic orbitals combine forming molecular orbitals and how electrons arrange in the different energetic levels.

Molecular Orbital diagrams (MO) are used to illustrate the final structure, energy levels are represented via horizontal lines and are connected to the respective atomic orbitals via diagonal dashed lines (e.g. Figure 1.9). The energy of the molecular orbital depends on the kind of bond formed, therefore a σ bond will have an higher energy than a π-bond in absolute value. This happens because in σ-bond there is a strong head-on overlapping of the atomic orbital, while in π-bond there is a parallel weaker overlapping (Figure 1.7).

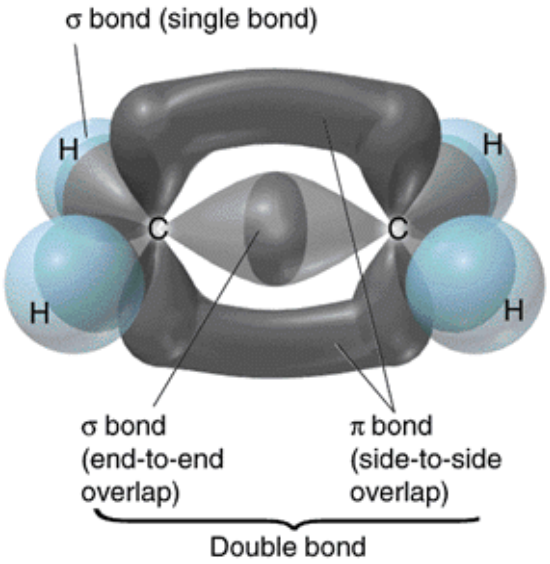

Figure 1.7: Illustration of σ and π orbitals. Adapted from syllabus of the Doctoral Training Center (DTC), Prof. Ji-Seon Kim.

Moreover each energy level of isolated atom splits in two energy levels due to the Pauli principle. Thus, associated to the bonding orbital, there is always an antibonding orbital (normally expressed with an *). Bonding orbitals are more stable, with high electron density between nuclei as a consequence of an in phase constructive overlap, antibonding orbitals are formed by out of phase overlap that induces a destructive interference, a low density between nuclei and thus a higher repulsion between nuclei. Bonding orbitals have always energy lower to the originating atomic orbitals, while for the antibonding happen the opposite and a nodal plane between the atoms is present. For these reasons the energetic order of different MO is the following (Figure 1.8):

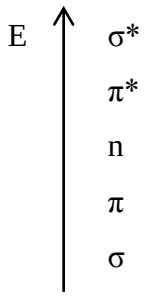

Figure 1.8: Energy of different orbitals

The σ-bonding will lead to the maximum stabilization of the system and so it is the first bond formed. Consequently a formation of a π-bonding involves at least a double bond.
Taking for example a system with four molecules, e.g. butadiene (C_4H_6), and concentrating on the π-orbitals forming, the MO diagram is that one presented in Figure 1.9. There are four energy levels and each level can contain just two electrons with opposite spin and lower energy levels are firstly occupied. The highest occupied molecular orbital is called HOMO, while the lowest unoccupied molecular orbital is called LUMO; an electron can be excited from the HOMO level to the LUMO level if an energy at least equal to the energy gap between the two is provided. When this happens a certain absorption spectrum can be measured. HOMO is related to the ionization potential, while LUMO is related to the electronic affinity of the molecule.
When more than one double bond is present, the molecular orbital is approximated via linear combination of atomic orbitals (in the example of butadiene combining two π-bonding and two π* antibonding). This combination minimizes the total energy of the system and the energy will increase, increasing the antibonding character (number of nodes).
A transition that would be theoretically easy to achieve, if we look at the energetic levels in Figure 1.8, is the n-π^*; the energy gap between the relative energy levels is

indeed lower than the π-π^*. The transition is however not favorable in terms of molar extinction coefficient, this has to do with the poor overlap between a π and a n orbital.

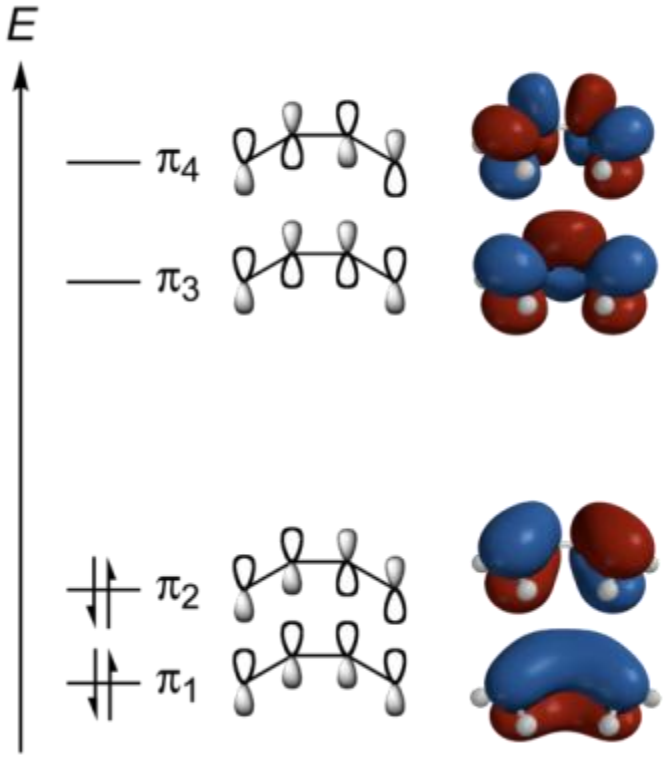

Figure 1.9: Illustration of LCAO of Butadiene. Adapted from syllabus of the Doctoral Training Center (DTC), Prof. Ji-Seon Kim.

In conjugated polymers, considering a certain double bond, the next-nearest bond is also a double bond, and therefore a system with "n" double bonds will lead to "2n" π-orbitals (n bonding, n antibonding) with an increasing number of nodes; this increase leads to a decrease of the energy gap and therefore to the semiconducting behaviour of these polymers. The decrease in the energy gap, associated to the increase in conjugation, is illustrated in Figure 1.10.

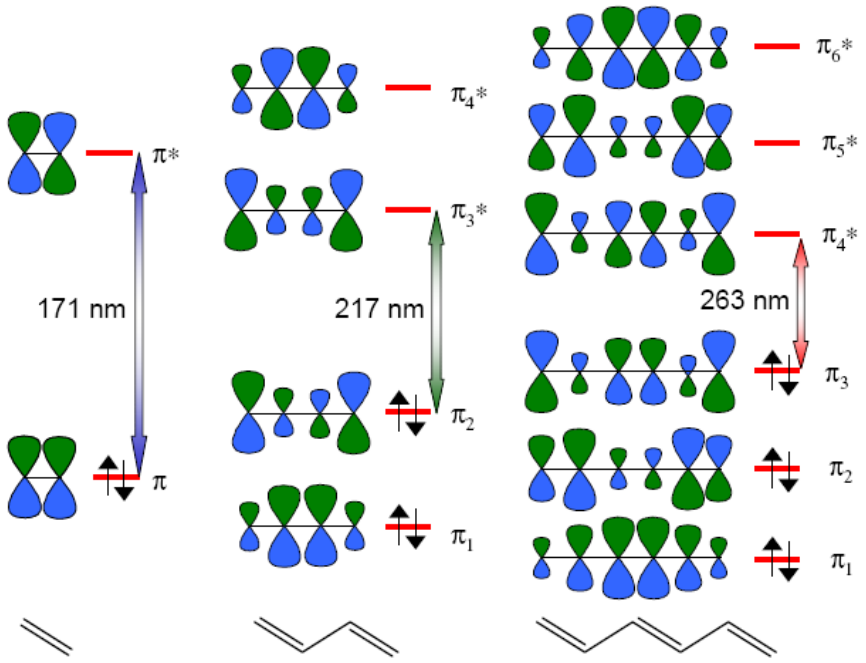

Figure 1.10: LCAO showing the decreasing of energy gap increasing the conjugation length. Adapted from syllabus of the Doctoral Training Center (DTC), Prof. Iain McCulloch.

A conjugated system with an infinite number of atoms (polyacetylene) should as a consequence theoretically lead to a system without energy gap and thus to the formation of a continuous band, similar to metals. This does not happen because of the Peierls band distortion explained above, which opens the energy gap between the HOMO and LUMO.

If we now compare the electronic levels of inorganic and organic semiconductors, there is a clear association between HOMO/LUMO and valence band/conduction band. Therefore a similar conductive behavior could be expected, however as stated before, in organic semiconductors a good conductivity is achieved only after a strong doping. This is caused by the absence of a rigid 3-D lattice (with covalent bonds) that prevents a strong electronic coupling between the chains. Different chains are coupled via weak bonds (Van der Waals). Another reason is the higher disorder present in these materials that induces differences in energy between the levels, resulting in a Gaussian distribution of states (DOS) (Figure 1.11).

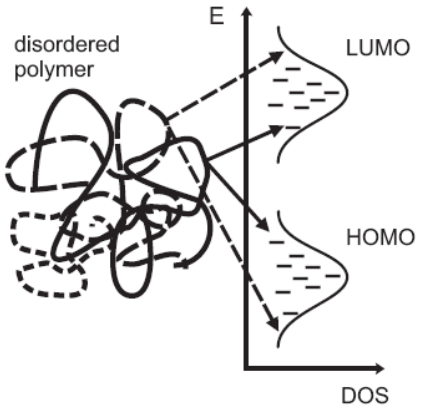

Figure 1.11: DOS of HOMO and LUMO in disordered organic semiconductors, adapted from syllabus of the Doctoral Training Center (DTC), Prof. Ji-Seon Kim.

The charge transfer between chains happens via a mechanism called hopping, in which charges jump from chain to chain. The transfer rate is a function of the electronic coupling between chains (J), the reorganization energy (λ) originated from a change in the nuclei coordinates as a consequence of the excitation and the final state energy difference (ΔE). The rate of transfer is modeled using the Marcus theory, according to:

$$\Gamma_{if} = \frac{2\pi}{\hbar}\left|J_{if}\right|^2 \frac{1}{\sqrt{4\pi\lambda kT}} e^{-(\Delta E+\lambda)^2/4\lambda kT} \qquad (1)$$

where Γ_{if} is the transfer rate, $\hbar$ is the reduced Plank constant and k is the Boltzmann constant. A schematic explanation of the charge transfer in an ideal system is given in Figure 1.12, in which a constant field is applied and the electron transfer is showed; the chain n+1 has a negative difference in energy (ΔE) in respect with chain n, equal to:
$\Delta E = E_{LUMO,n+1} - E_{LUMO,n} = -eaF$, where e is the electron charge and a is the intermolecular separation.

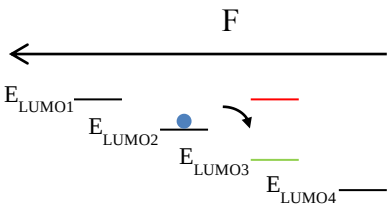

Figure 1.12: Schematic explanation of transfer of electrons, if the energy of $LUMO_{n+1}$ is lower than energy of $LUMO_n$, the electron can hop (green line), in the opposite case it cannot (red line)

If now we take into account a Gaussian distribution of the states due to the intrinsic disorder of the system, at low electron densities, most of the electrons lie in low energy of LUMO. In this situation E_n is lower than E_{n+1}, their difference ΔE is positive (red line in Figure 1.12) and can be high enough to prevent the charge transfer. This phenomenon is called trap filling effect and it's the reason of the carrier localization in organic semiconductors. The same process can be explained if we consider the interaction between charges in the DOS. Electrons at low energies are closer to the holes and therefore the coulombic interaction between charges is higher. When this energy is high, obviously the transport of the charges is affected. In this configuration it is clearly evident how low lying electrons or high lying holes can act as energy traps.

For this reason increasing the number of charges, higher levels of DOS are populated and the ΔE is less positive and the hopping process is more probable. For doped conjugated polymers charge mobilities are in the range of 10^{-6} to 1 cm^2/Vs. Increasing the order, providing for example anisotropy to the chains by mechanical deformation along one direction, can also slightly improve the mobility.

The doping of polymer semiconductors is different from the inorganic one, in this case no impurities are inserted in the active material and the role of dopant is either to remove or to add electrons to the polymer. Using iodine for example, causes the extraction of an electron and a formation of a counterion I_3^- (a salt is thus formed) plus the formation of a distortion in the surrounding as a consequence of the non-rigid structure, the specie forming is called positive polaron. If another electron is abstracted two things can happen: the formation of another positive polaron or the formation of a positive bipolaron via removal of the unpaired electron of the already existing polaron, the second process is favored. Similarly, if a reducing agent is used a negative polaron and bipolaron respectively are formed.

From an energetic point of view, the formation of polarons and bipolarons is associated with the formation of new levels inside the HOMO-LUMO gap, see Figure 1.13. Each polaron has got a charge equal to ± 1 and the spin is equal to ½, while a bipolaron has got a charge equal to ± 2 and a spin equal to zero.

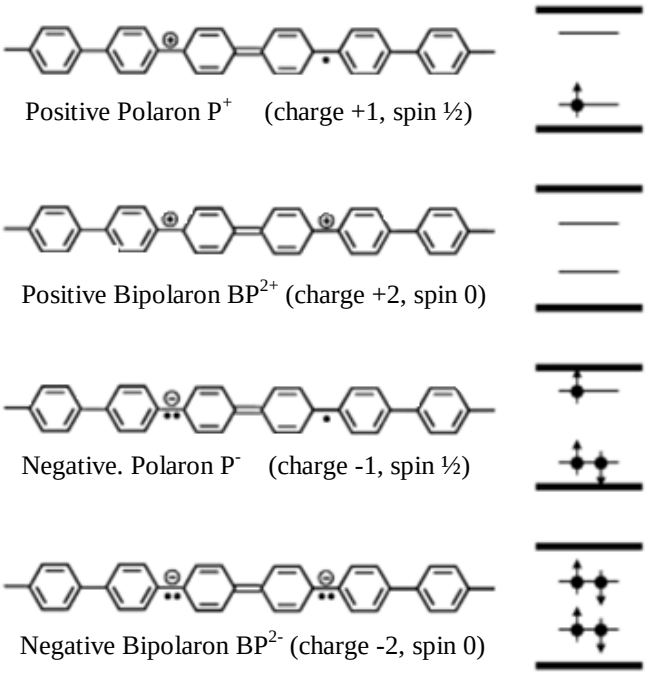

Figure 1.13: Polarons and bipolarons energy levels, example for Poly-Para-Phenilene (PPP), adapted from syllabus of the Doctoral Training Center (DTC), Prof. Ji-Seon Kim.

Another issue important to introduce is the behaviour of organic polymers once a photon is absorbed. As explained before, in inorganic semiconductors the excitation leads immediately to the formation of free charges. In organic materials the consequence of the excitation is the formation of an exciton, i.e. a bound electron-hole pair. They resides very closely together on the molecular chain, and are separated by few repeat units, therefore this excited species are localised. The electron forms in the LUMO, while the hole in the HOMO. The binding energy is around 500 meV, more than twenty times the thermal energy at room temperature. The coulombic interaction between the two induces excitonic levels in the band gap. (Figure 1.14).

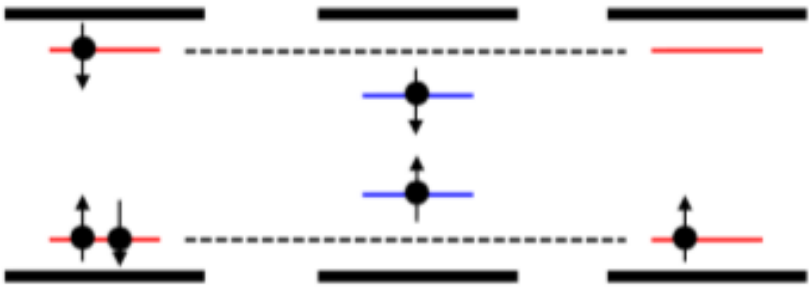

Figure 1.14: Energy levels of exciton (center) and polarons (left/right)

Excitons have a certain diffusion length (around 10nm for a wide range of conjugated polymers), their diffusion is a consequence of the Gaussian distribution of the energetic levels, if an exciton is formed in a chain with higher energy gap, it will diffuse to another chain with lower energy gap.

It is important to state that conjugated polymers for photovoltaic application are non-doped polymers. The purity is indeed very important and free charges already present in the chains have got a detrimental effect on the efficiency. Excitons are in fact strongly quenched by bulk charges. The electric field around an ion may overcome the exciton binding energy, resulting in dissociation and non-radiative recombination.

The charge transfer is possible for organic photovoltaics firstly because free charges are generated, therefore higher levels of the DOS are populated and the trap filling effect can be overcame. Secondly because polymers with strong π-stacking are employed, in this way the charge hopping distance is decreased and the charge-transfer process is facilitated.

1.2.4 Small molecules

Small-molecule materials have the same behaviour of conjugated polymers described above. They offer advantages over polymeric materials in terms of ease of synthesis and purification, which improve the reproducibility and avoid the problems of, among other things, batch to batch variations, or broad molecular-weight distributions. They normally have better charge-carrier mobilities than the polymers, however they are often characterized by a very low solubility in common organic solvents and very low viscosity, therefore vacuum deposition procedures are in many cases necessary for their processability.

1.2.5 Photophysics

In this thesis UV-vis spectroscopy is employed to determinate some important correlations between electronic behavior and polymer aggregation. This approach has been already used in different works. [6], [7]

The absorption spectrum of a material gives information on its energy gap. This can be controlled in different ways, as illustrated before, e.g. most prominently with adjusting the materials conjugation length. The latter depends on the regularity and planarity of the chains. Therefore the order of the system in terms of conformation, configuration or polydispersity is crucial. Conjugation length is also affected by chemical defects or conjugation blockers. Moreover, both HOMO and LUMO energy levels can be

manipulated changing the chemistry of the molecule, for instance adding electro donator/acceptor groups and using their different inductive and mesomeric effects. [8–10] For these reasons both chemistry and processing play a fundamental role. Considering a structure with a certain amount of disorder like in Figure 1.15, the polymer is composed of segments with different conjugation length. As a consequence the energy gap, and thus the absorption spectrum broadens.

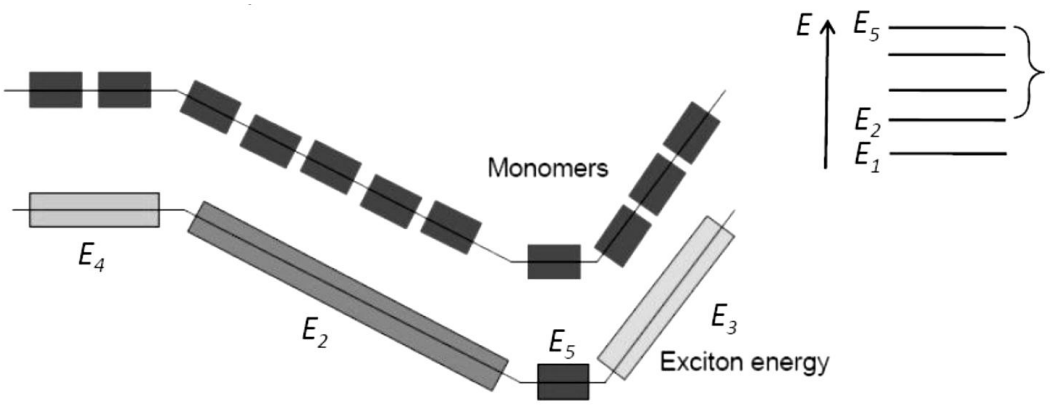

Figure 1.15: Conjugation lengths and energy gaps of a polymer resulting from disorder. Adapted from syllabus of the Doctoral Training Center (DTC), Prof. Ji-Seon Kim.

Each segment has got a certain energy gap E_1, E_2, E_3 and the overall spectrum is the sum of the three, see Figure 1.16

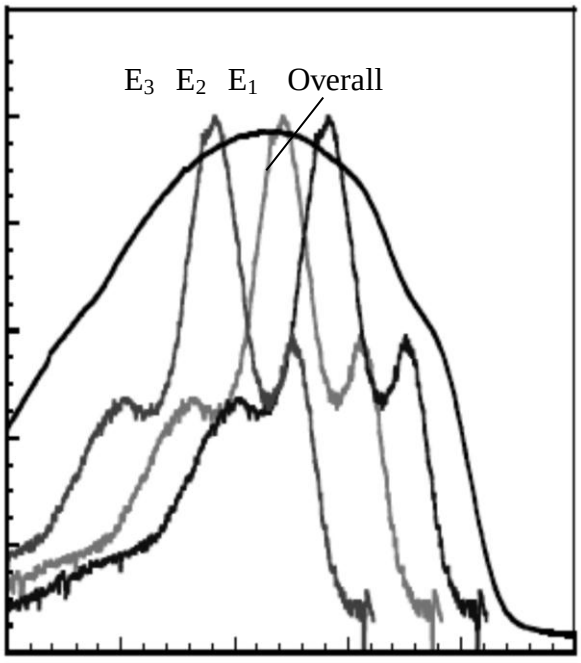

Figure 1.16: Illustration of a typical UV-vis absorption spectra of a disordered polymer. Adapted from syllabus of the Doctoral Training Center (DTC), Prof. Ji-Seon Kim.

Furthermore, for a certain energy gap, the absorption spectrum of a material is not well defined. The reason is that atoms in a molecule display always a vibration with a certain frequency *v* and associated to each vibrational mode, there is a certain vibrational energy level. Therefore for each electronic energy level, there is a certain number of vibrational levels depending to the molecular structure. The total energy is thus given by: *Et = Ee + Ev + Er* where *Ee* is electronic energy, *Ev* is the vibrational energy and the *Er* is the rotational energy. Typical vibrational quanta of polymers or small molecule are around 0.15 - 0.20 eV and lead to sub-bands such as those depicted in Figure 1.17. Thus excitation involves the simultaneous change of vibrational and electronic quantum number in molecules and the related transition is called vibronic transition.

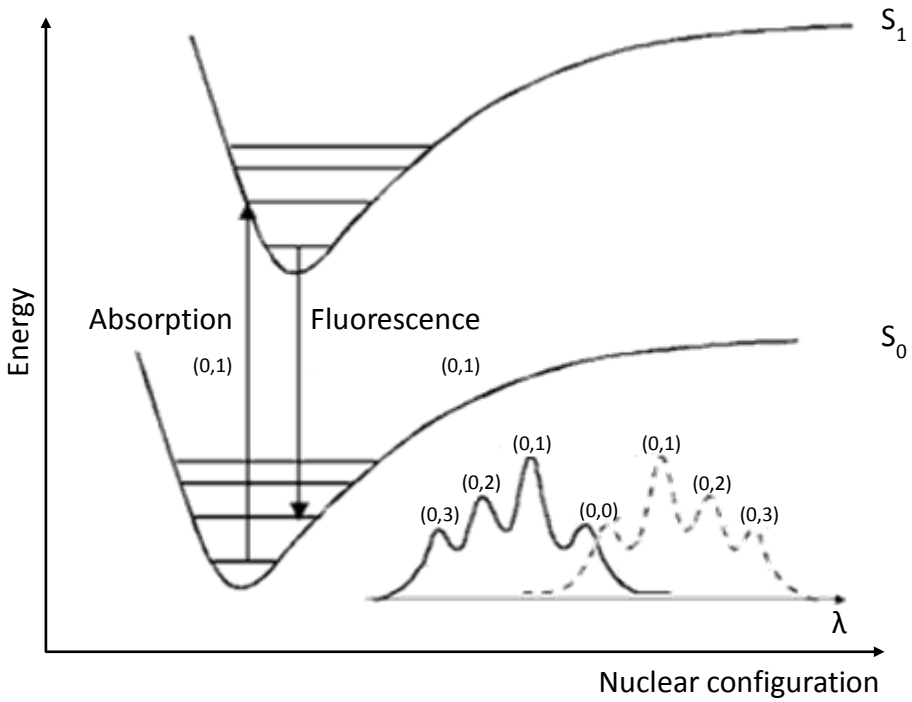

Figure 1.17: Schematic representation of vibronical coupling between energy levels and absorption and emission spectra.

Higher energy potential curves are displaced to the right as excitation introduces more antibonding character and thus equilibrium bond-length increases. Due to the Franck-Condon principle the vibronic transition (indicated by a vertical arrow in Figure 1.17) nuclei are assumed to be fix during the transition. When the electron is excited it will finish in a certain vibrational level of the excited state, with a probability proportional to the square of the overlap of the vibrational wavefunctions of the original and final state. After the excitation the electrons relax to the lowest vibrational level of the

excited state in agreement with Kasha's rule, [11] and from there they can decay to the lowest electronic state via photon emission (or via other non radiative decays). This last phenomenon is called fluorescence. Due to the relaxation to the lowest vibrational level the emitted photon will have a lower energy than the absorbed one. For the same reason the fluorescence spectrum is the mirror image of the absorption one.

This Franck-Condon (FC) progression is however not sufficient to explain the excitation and emissive processes especially when aggregates are formed. Indeed the molecular aggregation affects strongly the optical response. The reason for this is the fact that in certain conditions, an excited molecule within the aggregate can resonantly transfer its energy to another molecule via a so-called resonant excitonic coupling, *J*.

From an electronic perspective when the sign of the resonant electronic coupling is positive, there is a blue shift of the main absorption peak and a quenching in fluorescence. This behaviour is typical of the so-called H-aggregates, while for the J-aggregates the opposite happens. These aggregates derive from a supramolecular self-organization described for the first time by Scheibe et al. and Jelley; they observed independently the shift in the absorption bands of a pseudoisocyanine chloride. Different models have been then proposed to describe the aggregation of organic molecules [12].

To describe how strong the excitonic coupling is and therefore how free the exciton is to jump to another molecule it is useful to define the free excitonic bandwidth (W). This is the energy bandwidth of dispersed vibronic energy bands due purely to excitonic coupling, without taking into account the exciton-vibrational coupling. [7]

The free exciton bandwidth is related to the excitonic coupling by the relationship: $W = 4J$. Spano et al. [13] described how the absorption and emission spectra of an isolated molecule of a chromophore change when forming a J- or H- aggregate. This is based on the fact that it is possible to readily identify different peaks when the molecules are isolated. Then, for H-aggregate, as W increases the intensities of the A_0 and A_1 peaks decrease in both absorption and emission, with a progressive blue-shift of the main peak, as alluded to above.

Thus when W is low, the system is in the so-called weak excitonic coupling regime. There is still an interband coupling between vibronic excitons in different bands and the resonant coupling between molecules is low; in this configuration the sidebands remain visible despite they are less intense. When the coupling between excitons of different molecules is strong, the absorption is due to a exciton that is able to jump to a

neighbour molecule. Therefore there is just one strong peak and the fluorescence is quenched. Moreover the 0-0 peak is absent in emission, as this transition is forbidden. In ideal H-aggregates, composed with rigid molecules, the oscillation strength is concentrated on the top of the excitonic band. The 0-0 transition turns to be partially allowed in real nonrigid molecules: one or more vibrational phonons can terminate on the ground state and that create a low intensity allowed 0-0 transition. The trend of the peak modification is shown in Figure 1.18.

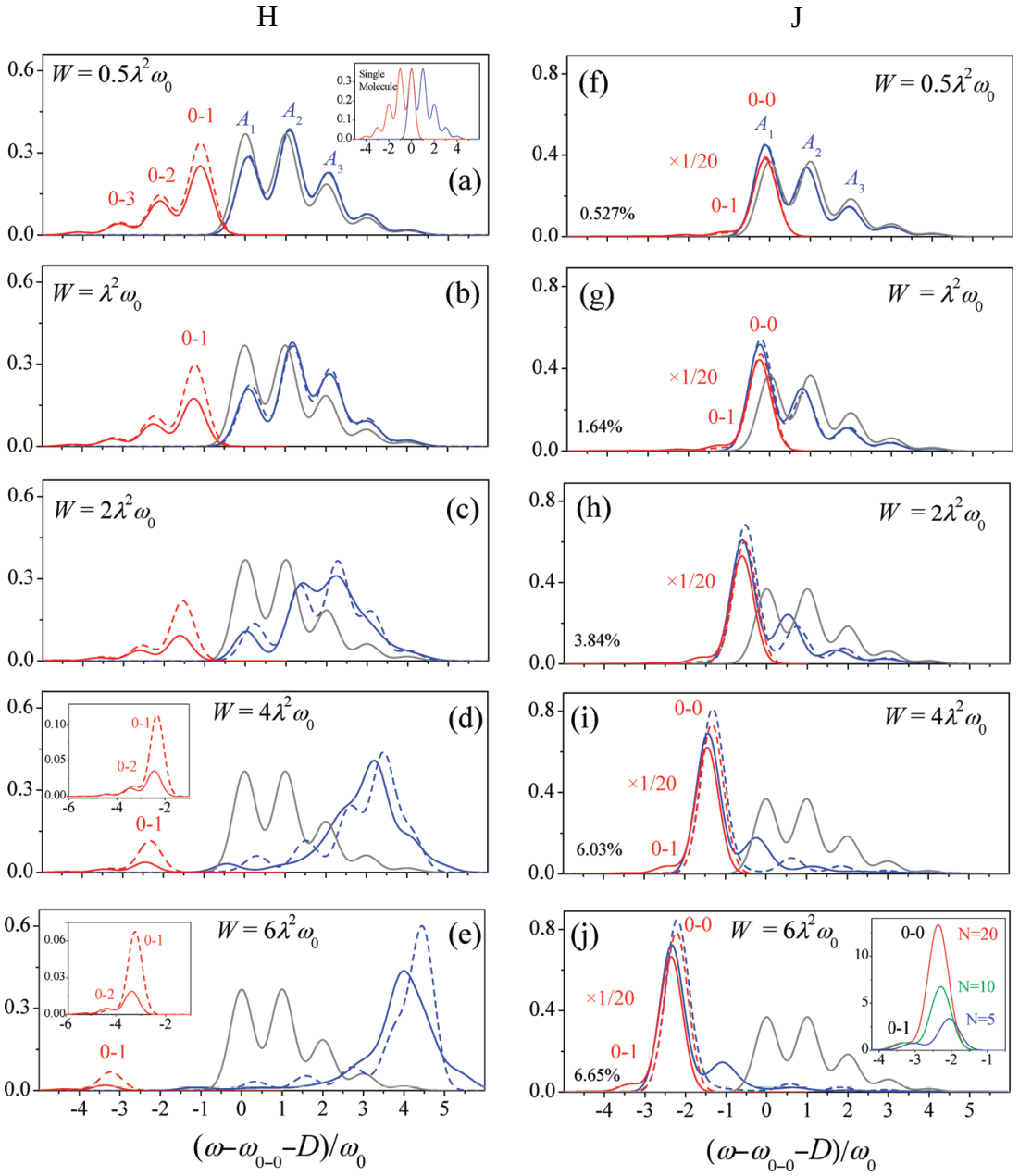

Figure 1.18: Absorption (blue) and emission (red) of H- aggregate (left) and J- aggregate (right). Adapted from [13]

If we now consider a conjugated polymer, such as regioregular poly-3-hexylthiophene (rrP3HT), that forms lamellar crystalline moieties with a 3.8 Å π-distance and a 16 Å separation between stacks, the inter-stack interactions are negligible and generally only a linear aggregation along the stacking axis is considered.

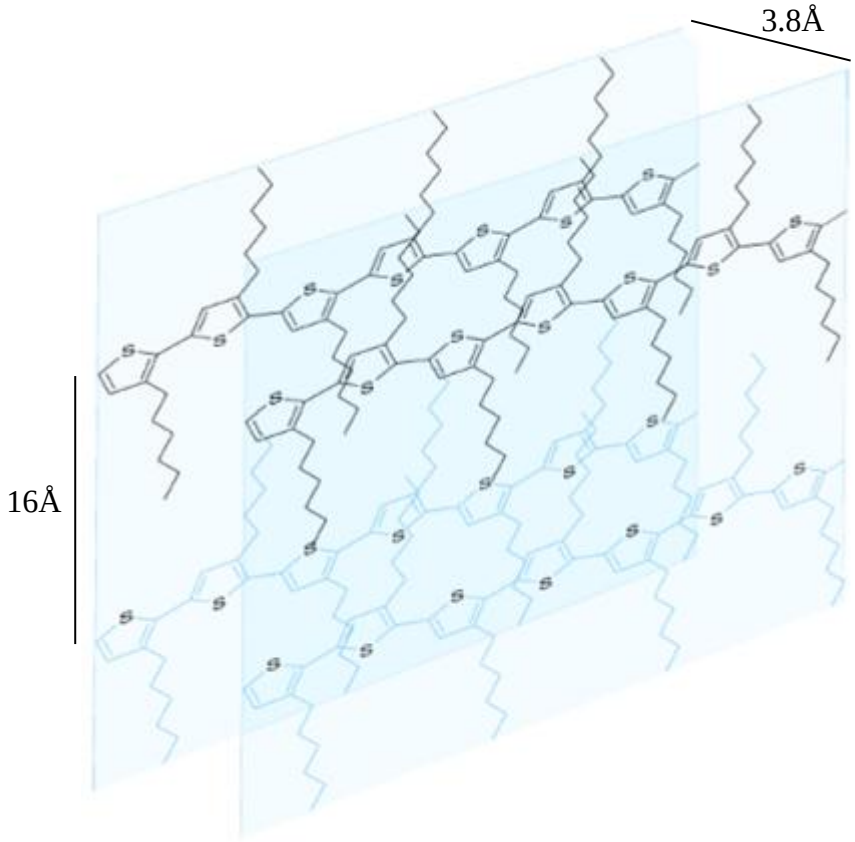

Figure 1.19: Interchains π-distance and stack distance in P3HT crystal. Adopted from CPE symposium on photophysics, Dr Jenny Clark.

Due to the small distance between the chains a strong resonant excitonic coupling (J) may be expected and therefore a high excitonic bandwidth (W), but this does not occur, possibly because of the relative extended conjugation along the chains.

The reason of this behaviour is related to the different interaction within the polymer lamellae in comparison with classical H- and J-aggregates. Normally there is a dipole-dipole interaction between molecules that causes the described optical shift from the Franck-Condon principle. In a polymer however, as a result of the increasing molecular weught, the dipole-dipole approximation is not valid anymore. [14]

If we plot for instance the average spectral shift of an aggregate in function of the chain length the trend depicted in Figure 1.20 is obtained:

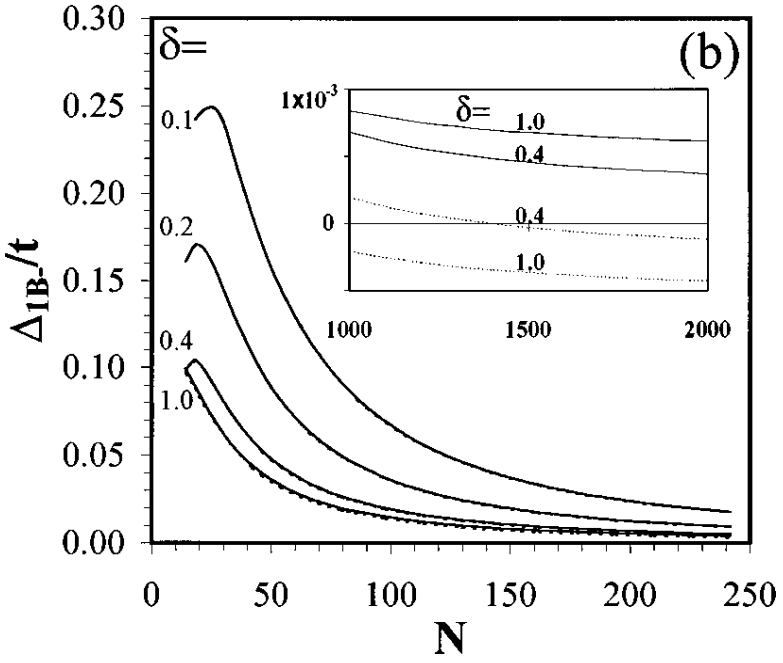

Figure 1.20: Exciton spectral shift as a function of the number of atoms N. Adopted from [15]

The initial increase in Figure 1.20 is explained by an intermolecular increase of polymers dipoles. Ones the polymer length exceeds the spacing between the chains the dipole-dipole approximation is not valid anymore and a rapid decrease is observed. In Figure 1.20, N has to be less than 10.

A further evidence that such a long chain dependence is valid for P3HT is given by Sebastian Westenhoff et al. [16] who measured the absorption and luminescence of different oligothiophenes with an intermediate electronic coupling, changing the number of thiophene rings. They showed how increasing the number of thiophenes from five to seven, a red shift of the maxima peaks is recorded, from 2.75, 2.82, to 2.90 eV for 5, 6 and 7 tiophenes oligomers respectively.

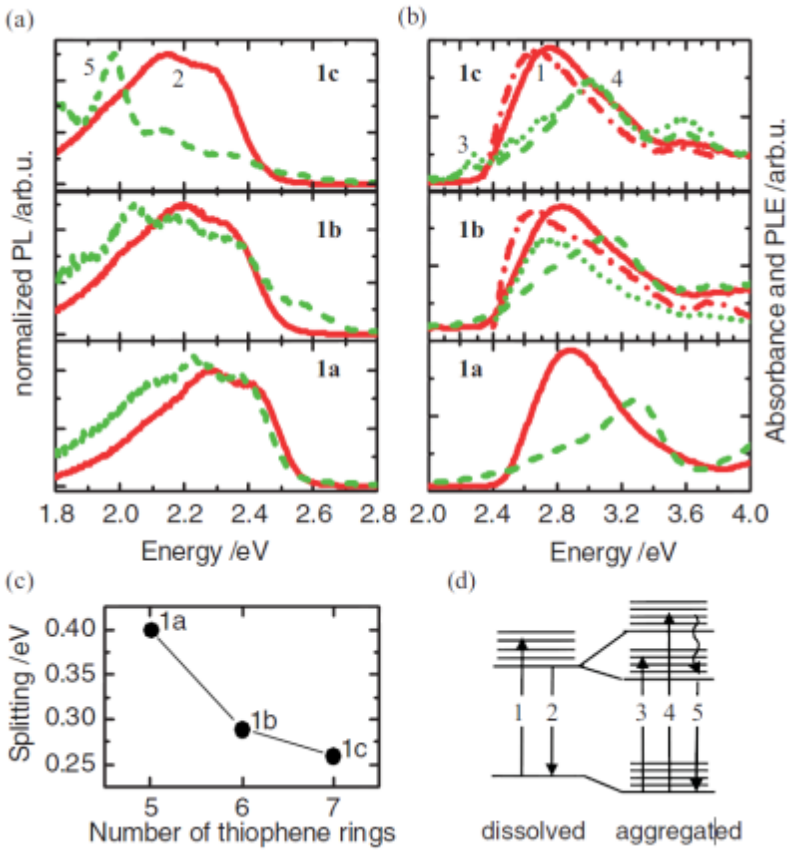

Figure 1.21: a) PL spectra of 7 (1c), 6 rings (1b), and 5 rings (1a) with excitation energy at 3.05 eV. b) The corresponding absorption and PL excitation spectra detected at 2.36 eV (1b) and 2.25 eV (1c). Red traces (dissolved conformation in hot solution) and green trace (the self-assembled phase recorded in cold solution) are depicted. The PL spectra are marked as dash-dotted and dotted for the dissolved and aggregated phase, respectively. The temperatures are 35 and 0 °C for 1a:, 75 and 10 °C for 1b, and 90 and 10 °C for 1c. Absorption spectra are raw data, PL spectra are normalized. c) Plots of the difference between the maximum of the absorption spectra for the three oligomers. d) Jablonski diagram depicting the electronic transitions involved in the spectra. Adopted from [16]

Hence since rrP3HT is a macromolecule, it is characterized by a weak excitonic coupling configuration. H-aggregates are the only emitting species in P3HT as deducted from the fluorescence data presented by Clark et al. [7]

First of all the absorption and emission spectra of P3HT differ for diluted and concentrated solutions and films. Fitting the data with a Franck-Condon approach is possible for the solution data, however it is not accurate for the film. Clark et al. hence concluded that most of the polymer chains self-organize to form aggregates (Figure 1.22).

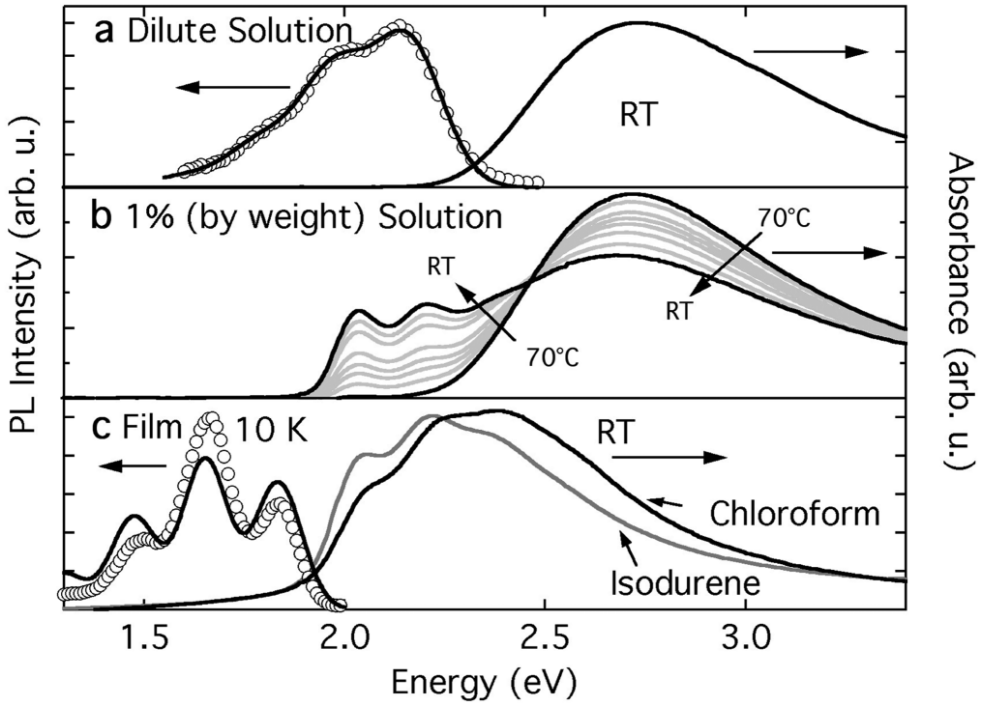

*Figure 1.22: (*a) Normalized room-temperature (RT) absorption and PL spectra of rrP3HT in a 0.0001 wt% isodurene solution. Solid line through PL is a Franck-Condon fit. (b) Temperature dependent absorption spectra of 1 wt % isodurene solution. (c) Normalized absorption spectra of a film obtained from 1wt % isodurene and chloroform solutions. The PL spectrum of a chloroform film is also shown (white circles) with a Franck-Condon best fit (solid curve). The PL spectrum was measured at 10 K whereas absorption spectra were measured at RT. Adopted from [7]

In order to find out which type of aggregate P3HT forms and to probe that it is the only specie that emits, temperature and time dependent PL spectra were reported. From this data it is possible to conclude that as the temperature increases the PL spectra blueshift and broaden because of the increased disorder. The 0–0 peak intensity originating from a less forbidden transition, as explained above using the model proposed by Spano et al. [7], [13–15], [17] also increases. In addition, Clark et al. noticed a redshift (even at 10 K) and loss of 0–0 peak intensity with time, as the system becomes more ordered. This behaviour is in agreement with a H-aggregate model, strongly indicating that this is the only emitting specie.

Focusing now on the absorption of P3HT: the vibronic transitions result from the symmetric ring-breathing and vinyl stretching mode, which is approximately at ω_0 = 1400 cm^{-1}. [6] Different peaks are thus visible in a UV-vis spectrum according with this progression and the relative intensities of these peaks can be related to the level of order in the chains. It is indeed possible to measure the magnitude of electronic coupling and the bandwidth from the eq. 2.

$$\frac{A_{0-0}}{A_{0-1}} \approx \frac{n_{0-1}}{n_{0-0}}\left(\frac{1-0.24W/E_p}{1+0.073W/E_p}\right)^2 \quad (2)$$

where n_{0-i} is the real part of the refractive index at the 0–i absorption and E_p is the phonon energy of the main oscillator coupled to the electronic transition.

The absorption spectra can be divided in two different parts: the first one at longer wavelengths is due to the weak excitonic coupling of H-aggregates, while at shorter wavelengths the absorbance is due to disordered unaggregated molecules. Speaking about disorder can however lead to some misunderstanding, this confusion comes from the different definition of disorder in oligomer aggregates and polymer aggregates. In oligomer aggregates disorder is of the type of molecular crystal one, including stacking faults, dislocations, grain-boundaries and point defects. By contrast, in polymer aggregates the disorder is linked to the intramolecular organization and therefore it manifests in torsional defects, kinks, and chemical defects that cause a decrease of conjugation. [14] Therefore in this work "improved order" and "aggregation" it is intended to describe the intrachain organization related that can result in improved conjugation. Indeed in the case of P3HT, in which the stacking distance remains fixed, a change in the absorption spectrum in terms of relative intensities of A_0, A_1 and A_2 peaks (as a consequence of the modification of the free excitonic bandwidth) can be related to the chain order. Clark et al. illustrated this relationship between change in absorption spectra and aggregation, measuring UV-vis and recording AFM images (Figure 1.24) of films spun from different solvents. Films obtained from high boiling point solvents featured a rougher surface and an increased A_0 peak, while the opposite was observed for structures obtained using a low boiling point solvent. [6]

It is important to point out that an increase in the A_2 peak can be related both to a higher content of molecular states associated to non-aggregated states and also to the presence of highly disordered aggregated small chains polymers that show a behaviour that is similar to the one of blueshifted olygothiophenes aggregate reported by Westenhoff et al.

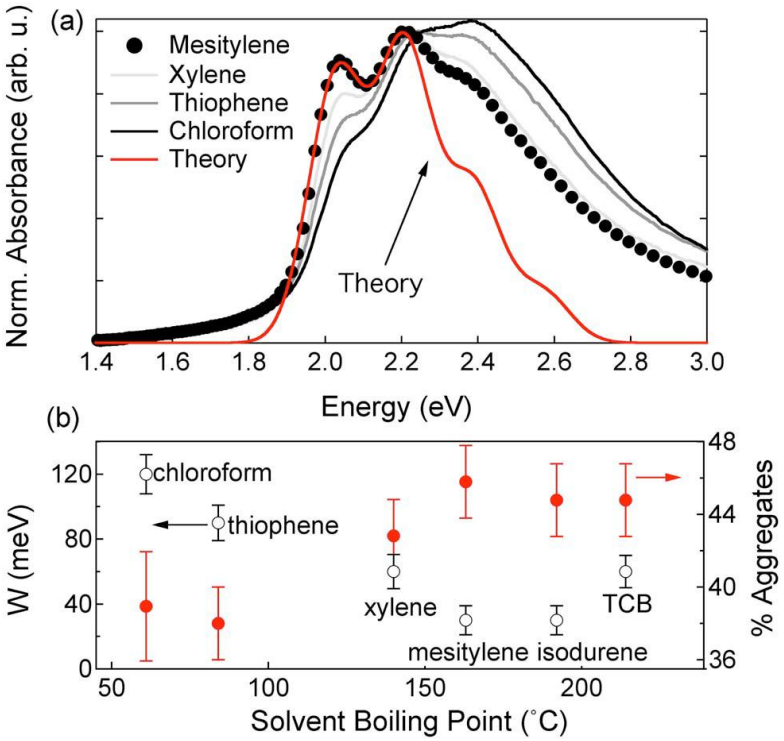

Figure 1.23 (a) Normalized absorbance spectra taken on P3HT films spun from different solvents. A theoretical spectrum for mesitylene using the equation proposed by Spano [14] is also shown (red line). (b) Relationship between exciton bandwidth W (white circles), left axis, and percentage of film made up of aggregates (full red circle), right axis. Adopted from [6]

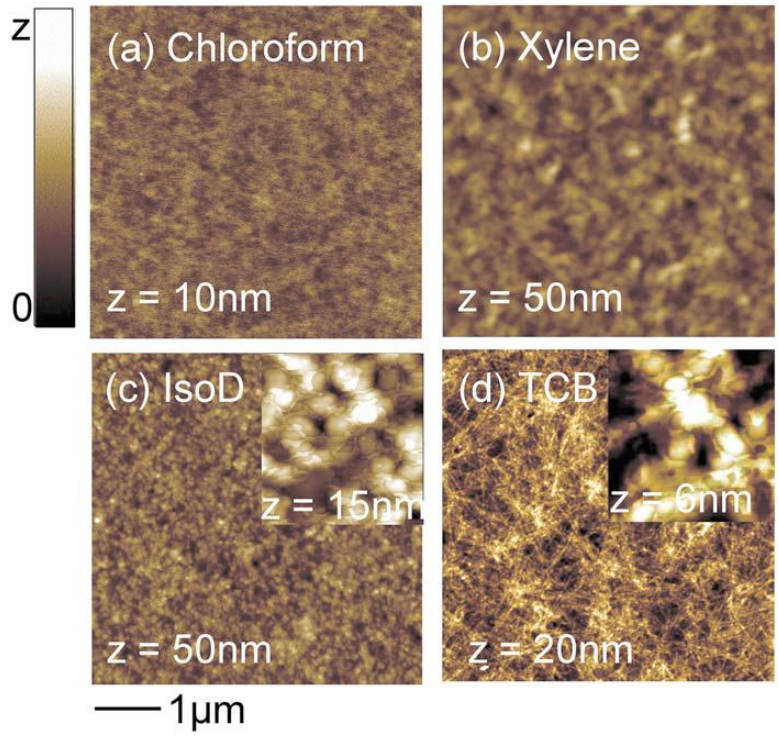

Figure 1.24: Tapping-mode AFM images of films spun from (a) chloroform, (b) xylene, (c) isodurene, and (d) 1,2,4-trichlorobenzene (TCB). Adopted from [7]

1.3 Working mechanism of OPV

1.3.1 Bulk heterojunction and differences with inorganic solar cells

Firstly it is useful to introduce the working mechanism of an inorganic solar cell based on p-n junctions. When a p- and a n-semiconductor are in contact, a charge flux starts at the interface between the two in order to equalize their Fermi levels: electrons tend to diffuse from the n-side to the p-side and an opposite flux of holes is observed. These charges are the majority carriers of the respective materials; the associated electric current is called diffusion current (I_{dif}). Thus, the regions nearby the p–n interface lose their neutrality and become charged as a consequence of the depletion of majority carriers. This part close to the interface is called depletion region and the carriers present are hence minority carriers. The latter will induce an electric field, E, as well as a counter flux of current, the drift current (I_{drift}). Increasing the concentration of minority carriers, due to the diffusion of majority carriers will increase the electric field E and therefore the drift current. When $I_{dif} = I_{drift}$ the flux stops, in this moment the Fermi levels of the two semiconductors become the same. At the equilibrium condition a certain voltage is present, called built in potential (ΔV), (Figure 1.25).

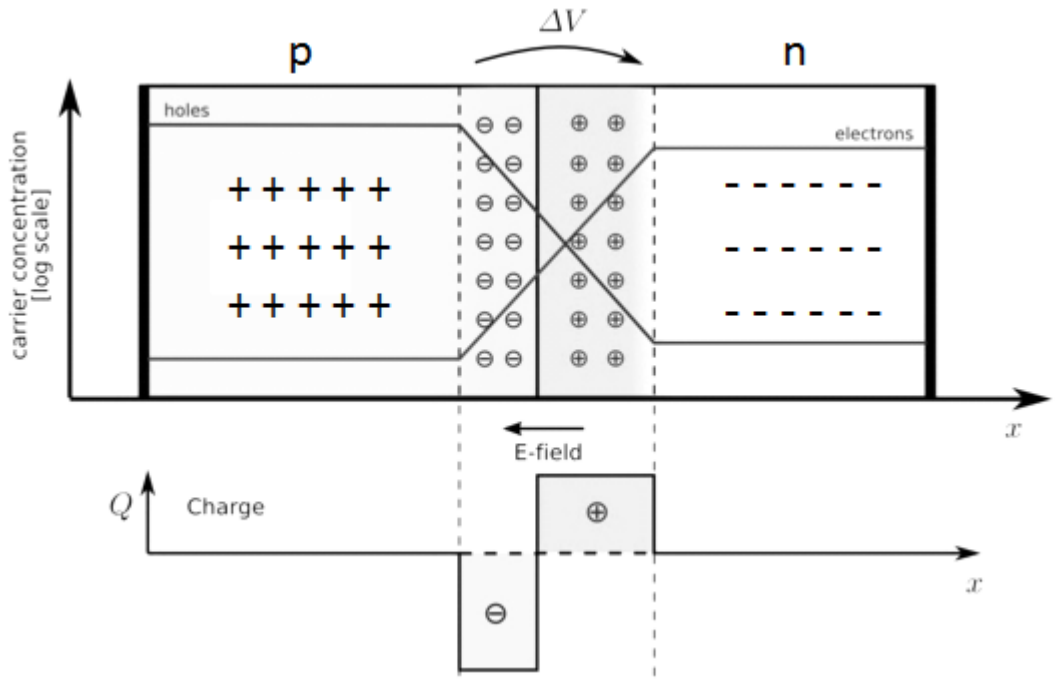

Figure 1.25 Illustration of a p-n junction.

Under illumination electrons are excited in the conduction band and holes are created in the valence band. The addition of photogenerated electrons and holes in the n-doped and p-doped respectively does not have any influence. In fact their concentration is already high, them being the majority carriers. On the other side, electron and hole photogeneration in the p-doped and n-doped semiconductors, respectively, are significant relative to the densities of minority carriers at equilibrium in the dark. For this reason an addition of minority carriers will increase the drift current: thus if electrodes are connected on both the sides of the cell, electrons created on the p-side are swept to the n-side and holes created on the n-side are swept to the p-side. The p-doped material is thus called donor, while the n-doped is called acceptor. As a consequence a flux of electrons holes is achieved and the the difference between the quasi-Fermi level energies determines the maximum open-circuit voltage (V_{OC}) (see Figure 1.26). It is important to specify that away from the junction, the transport of the charges is mainly governed by diffusion.

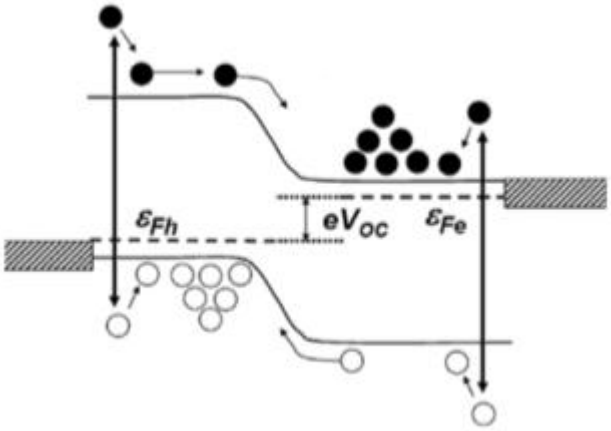

Figure 1.26: Illustration of the photovoltaic effect in a inorganic solar cell, adapted from [18].

Organic solar cells working principle is different from that one explained above. Some similarities are however present. As explained before, photon absorption generates an exciton in an organic material and not free charges. Thus the preliminary step has to be the dissociation of the exciton. For achieving this separation at least two materials have to be used, one donor material with an electron-donor character and one acceptor material with an electron-acceptor character. At their interface the difference in free energies (ΔG) between the exciton and the charge-separated state will provide the energy for the dissociation. The donor material exhibit a low ionization potential (and thus a high-lying HOMO energy), while the acceptor material possesses a high electron affinity (and thus a low-lying LUMO energy). The latter attracts the electron of the

exciton to the interface. Moreover it is fundamental that the donor and acceptor materials have an efficient hole and electron transport, respectively (Figure 1.27).

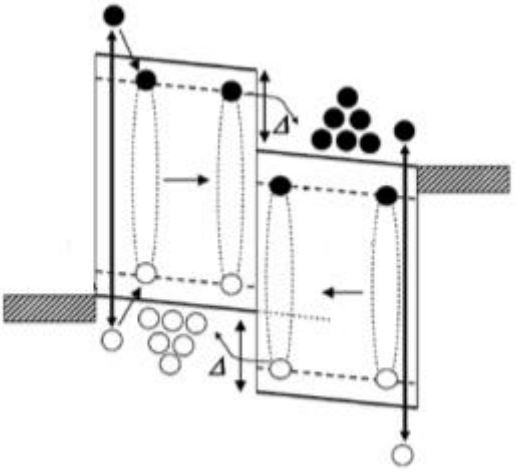

Figure 1.27: Illustration of the OPV working principle. Δ is the difference in energy between HOMO and LUMO of acceptor and donor material. Adapted from [18]

Note that in addition to the above description, there is evidence of the presence of charge-transfer states (CT) between the excited and charge-separate (CS) state. [18–20]. This state from a physical point of view consists of partially separated, but still Coulombically bound (E_b = 0.1 – 0.5 eV >> k_BT). The wave functions of the two charges will have an overlap creating a state lying within the optical gap of the two materials. To describe such an intermediated state, different nomenclatures are often used such as bound polaron pair, bound electron hole pair, geminate pair, and CTS. Charge pairs (and so the charge-separate state) can be formed only if the energy of the exciton is higher than the energy of the CT state.

1.3.2 Influence of the microstructure of the active layer

From a structural point of view, in the inorganic solar cell there is a bilayer structure that forms the p-n junction. In the organic case, bilayers generally do not produce good efficiencies. In fact the exciton needs to diffuse to the interface between the acceptor and donor material. This process is limited by the short diffusion length of ~10 nm in organics. As a consequence in bilayer structures most of the excitons do not separate in charges. For this reason a maximization of the interfaces is essential, a solution is given by the so-called bulk heterojunction (BHJ), in which the donor and acceptor components are intimately mixed in the bulk. A classical illustration of a BHJ is presented in Figure 1.28:

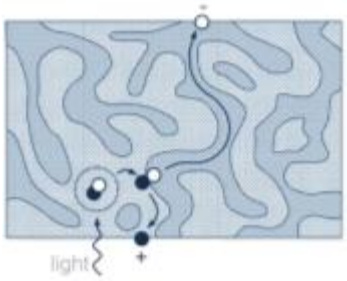

Figure 1.28: Schematic of a bulk heterojunction made of an electron acceptor and an electron donor.

Important in this structure is that the intermixing of the two components forming the active layer does not winder the charge collection, indeed it is essential that percolation pathways are created. As a consequence, the microstructure of the active layer is of paramount importance and strongly influences device performance. This is challenging as often more than two phases are present. The reason is that a bulk polymer features crystalline moieties as well as an amorphous phase depending on the molecular weight (M_w) (Figure 1.29). It is well estabilished that low molecular weight polymers form extended chain crystals, due to noentangled chains. This results in a polychristalline morphology with just one phase. However at a critical length of the chains, the macromolecules entangle inducing a semi-crystalline microstructure with two distinct phases: a lamellar structure given by the ordered chains and disordered amorphous structure.

Evidence is reported recently [21–24] that the presence of amorphous phases play an important role in the exciton dissociation. For example Reid et al. illustrated the relationship between molecular weight and yield of free photogenerated charges for P3HT. [24] As the molecular weight of P3HT was increased, there was a reduction of the free excitonic bandwidth. This reduction was correlated to the evolution from a chain extended to a semicrystalline microstructure. Related to this morphology change, there was a strong increase of the yield of free charges generation, confirming the hypothesis. The presence of the crystalline phase is also important. Reid et al. proposed a model to explain this issue: the separation of charge-pairs is favourable at the interphase between the amorphous and the crystalline phases. In fact in this case holes are preferentially transferred to the crystalline domain, while electrons are trapped by their lower mobility. If just one phase is present, purely crystalline or amorphous, there is not energetic gain. Charges are trapped and recombine quickly.

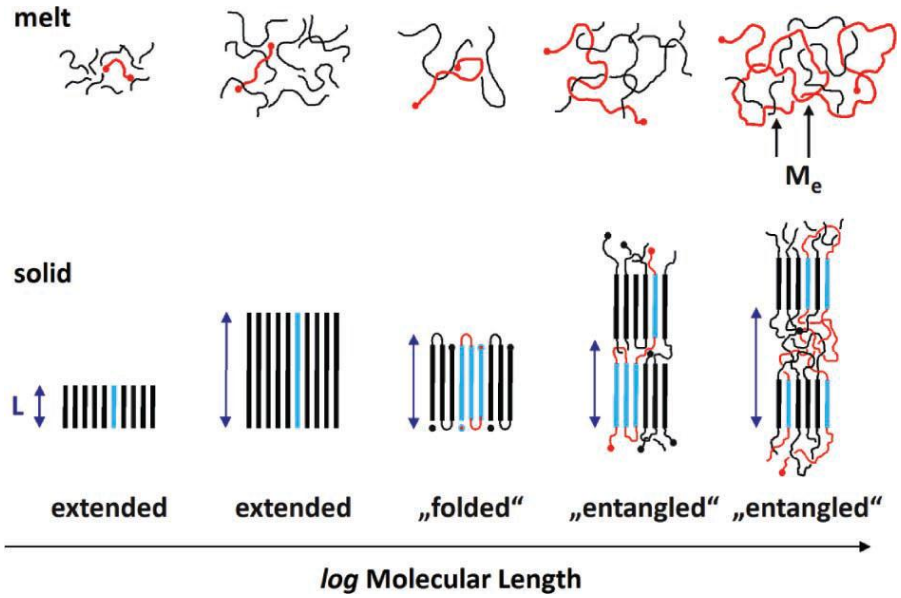

Figure 1.29: Illustration of the influence of molecular weight on the structure of a (semi)flexible polymer in the melt (top panel) and in the solid state (bottom panel). Adapted from [25].

1.3.3 Electrical characteristic of organic solar cells

It is useful to introduce the electrical characteristic of a solar cell; the model used is the same both for inorganic and organic photovoltaics. In the dark a solar cell works as a diode: if a forward bias is applied, an electric current is created, while a blocking current in the opposite (reverse) bias no current flows. Considering the p-n junction depicted in Figure 1.25, if the p-type is connected with the positive terminal and the n-type is connected with the negative terminal a forward bias is obtained: electrons from the n-region and holes from the p-region are attracted towards the junction and the junction becomes thinner, as a consequence the I_{diff} increases and a neat current is measured:

$$J_d = J_0 \left[exp\left(\frac{eV}{\beta kT}\right) - 1 \right] \quad (3)$$

Where J_d is the current measured, J_0 is the saturation current, $1<\beta<2$ is the diode ideality factor, V is the tension applied, k is the Boltzmann constant and T is the temperature.

In contrast, if the p-type is connected with the negative terminal and the n-type with the positive, in the reverse bias regime, the depletion mode becomes wider and act as an insulator. Hence, the resistance is increased and in the ideal case there is no flux of charges (Figure 1.30).

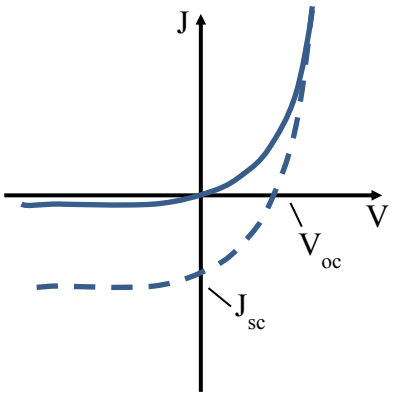

Figure 1.30: Schematic of a typical diode characteristic. Solid line: forward bias in I quadrant, reverse bias in III quadrant. Dashed line: the photovoltaic characteristic. J_{sc} and V_{oc} are the short-circuit current and the open-circuit tension respectively.

Under illumination a photocurrent is generated and therefore the total current produced is equal to

$$J = J_{ph} - J_d - J_r \tag{4}$$

where J_{ph} is the photocurrent, J_d is the diode current, J_r is the current loss by the resistances. Therefore a solar cell acts as a diode in the reverse regime in which the current is implemented due to the photocurrent (dashed line in Figure 1.30). Moreover a solar cell can be approximated with an electric circuit composed by a diode with reverse saturation current density (J_d), an ideality factor (β), a photocurrent source (J_{ph}), a series resistance (R_S), that takes into account the losses caused by the finite conductivity of the semiconducting material, the contact resistance between the semiconductors and the adjacent electrodes and the resistance associated with electrodes and interconnections; and a parallel resistance (R_p), which takes into account the loss of carriers during the conduction (Figure 1.31).

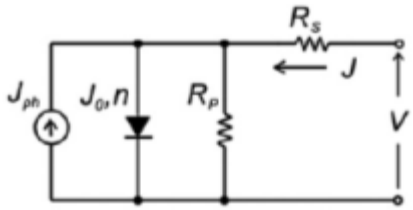

Figure 1.31: Equivalent circuit of a solar cell.

Solving the circuit provides the equations of the short-circuit current (J_{sc}) and the open-circuit voltage (V_{oc}):

$$J_{sc} = -\frac{1}{1+Rs/Rp}\left\{J_{ph} - J_0\left(\exp\left(\frac{|J_{sc}|R_sA}{\beta kT/e}\right) - 1\right)\right\} \tag{5}$$

$$V_{oc} = {\beta kT}/{e} \ln\left(1 + \frac{J_{ph}}{J_0}\right) \quad (6)$$

Now, for organic photovoltaics, studies [18] show that the J_0 can be approximated by:

$$J_0 = B\exp\left(\frac{-Efinal}{\beta' kT}\right) \quad (7)$$

where B is a coefficient with a value in the range of 1000 A cm^{-2}, β' is a correction factor and $E_{final} = LUMO_{acceptor} - HOMO_{donator}$. If now we combine equations (5) (6) (7) we obtain the relationship between J_{sc} and V_{oc} for organic solar cells:

$$V_{oc} = \frac{1}{e}\left(\frac{\beta}{\beta'}E_{final} - \beta kT\ ln\left(\frac{B}{J_{sc}}\right)\right) \quad (8)$$

The maximum power (P_{max}) is given by $P_{max} = I_{max} \cdot V_{max}$, which is the maximum area produced by the current and voltage (Figure 1.30). An ideal solar cell would have a maximum power equal to $I_{sc} \cdot V_{oc}$, this means that the entire area under the line produces power. The ratio between $I_{max} \cdot V_{max}$ and $I_{sc} \cdot V_{oc}$ is defined as the fill factor (FF):

$$FF = \frac{Imax \cdot Vmax}{Isc \cdot Voc} \quad (9)$$

The efficiency of the cell can be expressed by

$$\eta = \frac{J_{sc}V_{oc}FF}{P_{ph}} \quad (10)$$

where P_{ph} is the power density of illumination. Therefore from eq. (8) it is evident that a maximization of the efficiency can be realized by the maximization of the difference between the LUMO of the acceptor material and the LOMO of the donor. Another factor has however to be taken into account: if this difference increase too high, the difference in free energies (ΔG) between the exciton and the charge-separated state is too low. As a consequence ΔG has to be on the order of ~0.3 – 0.5 eV to realise optimum device performance.

1.3.4 Organic photovoltaic device layer structure

A typical OPV has the layer structure schematically depicted in Figure 1.32: Glass; indium tin oxide (ITO); polyethylenedioxythiophene:polystyrene sulphonate (PEDOT:PSS); photoactive blend layer; cathode interlayer; back contact (Al).

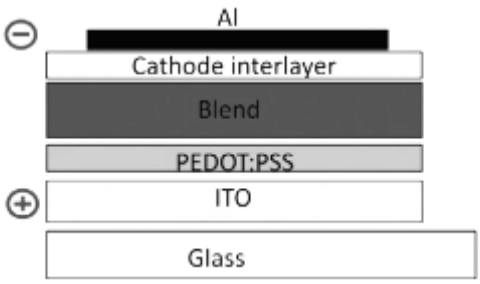

Figure 1.32: Typical device structure, adapted from [26].

PEDOT:PSS is a doped conducting polymer that is used to raise the work function of the bottom electrode in order to accept holes, and the cathode interlayer (usually a low work function metal) is used to lower the work function of the top electrode to accept electrons. The idea is to avoid any mismatch between energy levels in order to minimize losses. The photoactive layer thickness is normally around 100 – 200 nm while other layers are some 50 – 100 nm. Instead of using glass, a plastic flexible substrate can be used.

One of the most used blend for organic solar cells is composed by poly-3-hexylthiophene (p3HT) and the fullerene derivative [6,6]phenyl C_{61} butyric acid methyl ester (PCBM), (see Figure 2.1 for the chemical structures). In order to improve the efficiencies of the cells many groups are synthetizing polymers of varying HOMO and LUMO levels. The evolution of device efficiency obtained in recent years is summarised in Figure 1.33. Poly[2,1,3-benzothiadiazole-4,7-diyl[4,4-bis(2-ethylhexyl)-4H-cyclopenta[2,1-b:3,4-b']dithiophene-2,6-diyl]] PCPDTBT, poly[[9-(1-octylnonyl)-9H-carbazole-2,7-diyl]-2,5-thiophenediyl-2,1,3-benzothiadiazole-4,7-diyl-2,5-thiophenediyl] PCDTBT, Poly[[4,8-bis[(2-ethylhexyl)oxy] benzo[1,2-b:4,5-b']dithiophene-2,6-diyl][3-fluoro-2-[(2-ethylhexyl)carbonyl]thieno[3,4-b]thiophenediyl]] PTB7 are thiophene derivatives, characterized by long and more complicated monomer units.

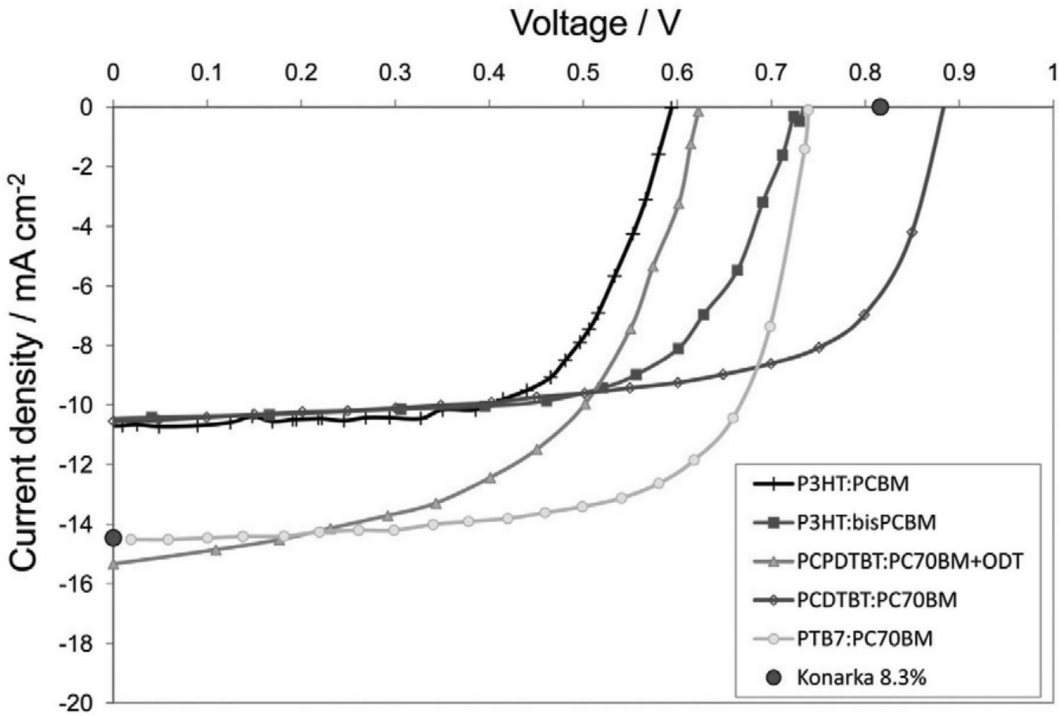

Figure 1.33 Evolution of efficiencies of OPV. Adapted from [26]

Compared to silicon solar cells, OPV feature a lower J_{sc} and FF but V_{oc} is comparable. An explanation of the low current, that is realised with OPVs compared to silicon devices is given by the larger band gap of organic semiconductors. The latter is typically around 2eV, while that one of silicon is around 1.1eV. FF is controlled by charge recombination, which can be divided in geminative and non-geminative processes. Geminative recombination is referred to processes between charges deriving from the same exciton that recombine immediately after the separation in a timescale around 100ns. This is caused by the difficulties of separating the charges, which is characteristic for organic materials and is linked to the trapping-process related to the less ordered structure explained above and to the low dielectric permittivity ($\varepsilon \approx 3 - 4$). Non-geminative recombination is referred processes that involve already separated charges during transportation towards the electrodes. This is due to the often low charge-carrier mobility rendering charge collection difficult. It is clear that the microstructure plays a really important role in cell processes, thus extensive research activities have been devoted to this aspect of OPV research.

Another source of efficiency losses are the contacts. A mismatching in energy levels is always present between active layer and electrodes resulting in a drop in the V_{oc}. This is particularly important for conjugated polymers, because of the impossibility of an easy doping. Therefore the HOMO and LUMO energies are not the only parameters

influencing the electrochemical potential at the electrode. The electrode work function and the degree of charge transfer with the organic play thus an important role.

Another important issue is the durability of the cells. Clearly it is important for competitiveness in the market to assure a product with sufficient long lifetime. Si-based photovoltaic modules have a durability of above twenty years. OPVs display significantly lower lifetimes. The problem originates mainly from the intrinsic tendency to photodegradation of organics, As a consequence OPVs require encapsulation with flexible or rigid materials.

Even if many problems have still to be solved, OPVs are progressively improving with respect to performance and lifetimes, with record devices reaching now 10% (Figure 1.34).

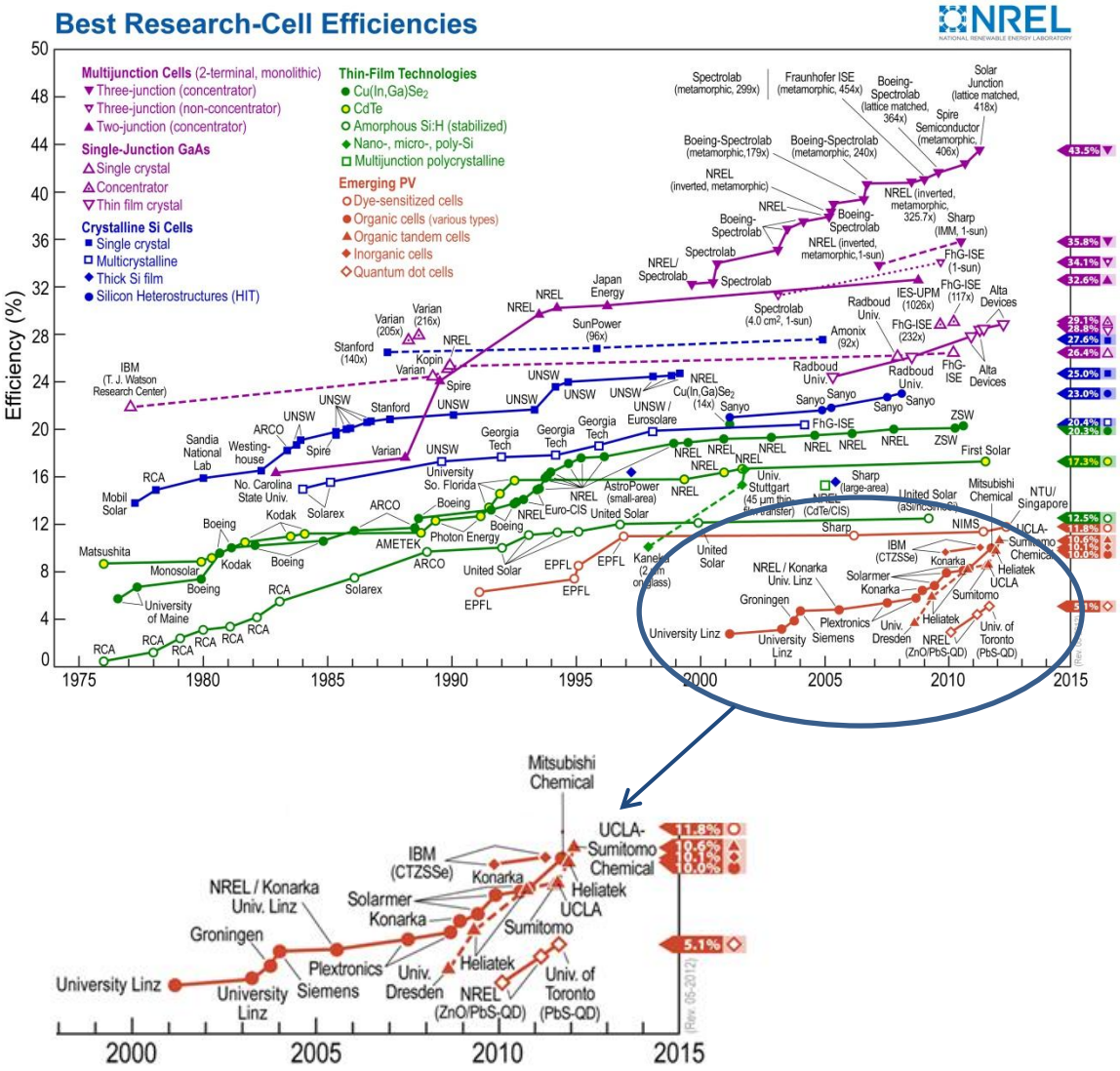

Figure 1.34: *Efficiency* records in photovoltaics, in red is the data collected for OPVs, which are highlighted in inset.

1.3.5 Ternary blend

In the bulk polymer industry blending of different polymers or use of additives is a widely applied strategy to obtain the required properties for a given application, e.g. to improve the processability of the critical component, or to reduce costs. Blending is so often used for this purpose as it is often easier to follow this approach than synthetize new polymers. The compounding industry is thus progressively reaching more importance. Furthermore extensive literature exists on this topic [27].

In the plastic electronics area, blending may lead to additional processing optimization. OPV devices are normally produced with an active layer thickness of around 100 - 200 nm depending on different parameters (i.e. selection materials, solvent, coating technique). Above ~200 nm, film absorption is high enough to capture the majority of the available light but V_{OC} starts to decrease, especially when very large thicknesses are reached: there is a large loss due to the fact that high carrier density cannot be maintained, meaning that non-geminate recombination dominate. [28] This restriction can create some technological problems. For instance many coating techniques require deposition of hundreds of nanometres of thickness [29]. Moreover, thin films are mechanically weak. P3HT exhibits e.g. a Young Modulus of 0.252 ± 0.057 GPa, measured using a buckling-based metrology. [30] This is low compared to normally bulk commodity. In addition the viscosity of P3HT:PCBM is low, (1-5 mPa s depending on the solvent and on the concentration), which is too low for printing techniques. [31]

For this reason use of ternary blends has been recently proposed to improve the above discussed properties. Different electrically inactive polymers including i-PS, a-PS, PE have been tested as a third component in the classical donor:acceptor. [1], [32–36] As a first step field-effect transistors were made to measure their charge transport; [1] different polymers, concentrations and process parameter have been studied. As a result it has been shown how the use of semicrystalline polymers leads to an improved charge mobility (μ_{FET}), than when using amorphous additives. High concentrations of insulating polymers up to ~90-95 wt% did not deteriorate the device performances, above these concentrations a significant decrease in performance is found.

XRD data showed intense h00 diffraction for P3HT (attributes to lamellar stacking) in HDPE blends (Figure 1.35) and i-PS systems, while diffraction peaks were weak for blends with a-PS and more amorphous polymers like LLDPE and ULDPE. Furthermore

the h00 diffractions in blends with semicrystalline polymers displayed high intensity out of plane, indicative of a preferential order of the lamellae in the plane of the film.

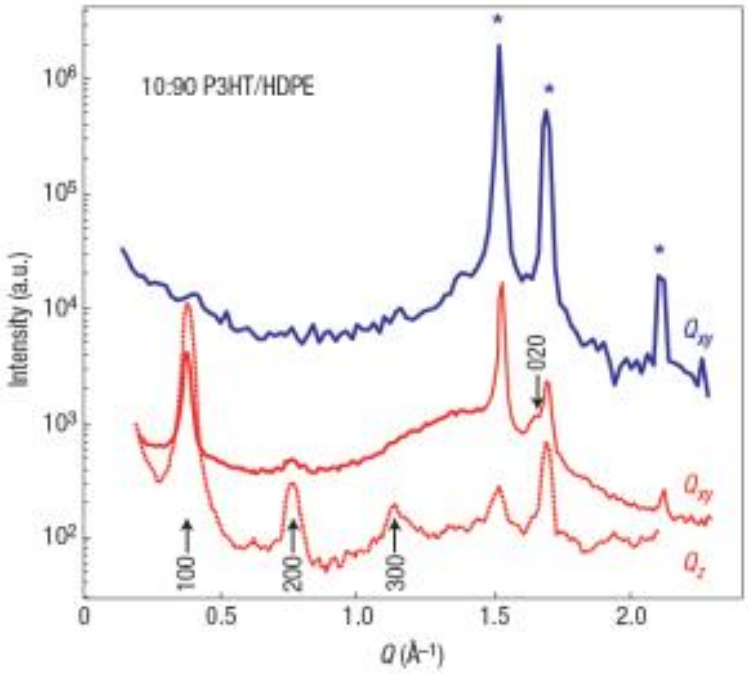

Figure 1.35: GIXD diffractograms of 10:90 P3HT/HDPE Mw=120 kDa films. Blends processed under conditions for which P3HT crystallizes before the insulating polymer showed well-defined P3HT diffractions both out of plane (red, dotted line) and in plane (red, solid line). Diffraction are not present from films in which the insulator crystallized before the P3HT (in-plane diffraction for P3HT-HDPE: blue, solid line). The main HDPE reflections are indicated with asterisks (110 at Q = 1.52 $A^{\circ -1}$, 200 at Q = 1.69 $A^{\circ -1}$ and 210 at Q = 2.11 $A^{\circ -1}$). Adopted from [1]

The different behaviour between amorphous and crystalline polymers was explained by the different solidification process for the different systems: during cooling of blends comprising amorphous polymers (i.e. a-PS), vitrification occurs, affecting P3HT crystallization. On the other hand when multicomponent systems containing a semicrystalline polymer is cooled, crystallization of the insulator can lead to a pronounced crystallization of P3HT, depending on the relative concentration and deposition temperature. These last two parameters thus play a fundamental role in the crystallization process of the blend. Considering for instance HDPE:P3HT and looking to the phase diagram (Figure 1.36) it is possible to identify a concentration ($c_{threshold}$ red shaded circle) below which the polymers in the liquid phase are miscible. At $c > c_{threshold}$, there is phase separation in the liquid phase and crystallization of P3HT is followed by segregation due to crystallization of HDPE. If $c < c_{threshold}$ and $T > T_{eutectic}$, P3HT/HDPE are miscible seemingly preventing crystallization of P3HT. For this reason lowering the MW of PE and using a LLDPE, which will be more miscible with

P3HT, lowers the $c_{threshold}$. This concentration coincides with the threshold observed in device performances. [1] It is important to note that these studies were possible thanks to the wide range of polyethylene existing. In this thesis, we therefore continue to work with this bulk commodity polymer.

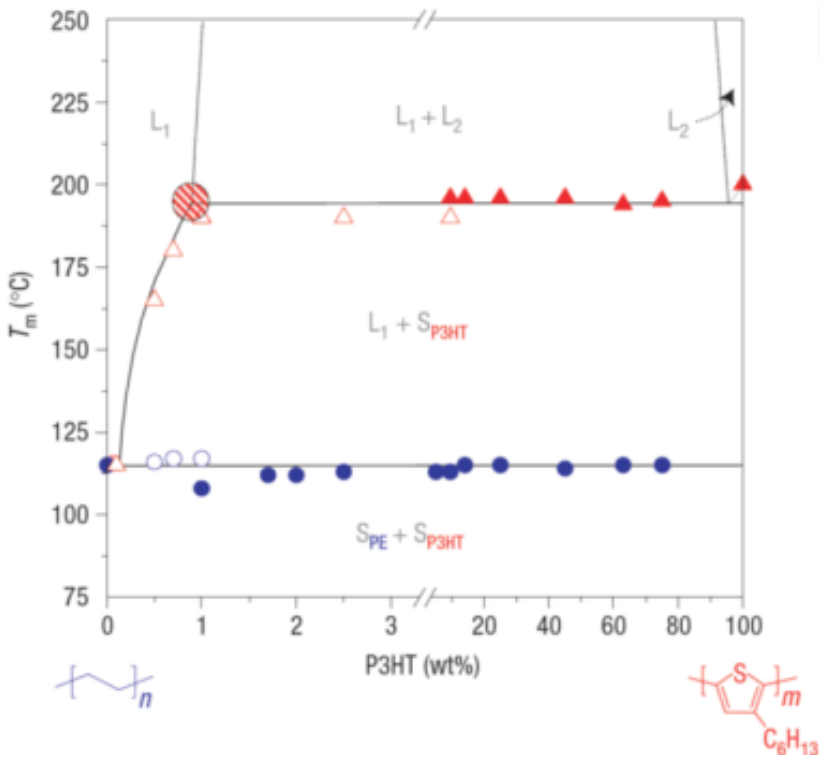

Figure 1.36: Binary non-equilibrium composition–temperature diagram of P3HT/HDPE$_{Mw=221}$ kDa binary deduced from DSC peak cooling temperatures (filled symbols) and optical microscopy (open symbols). HDPE, circles; P3HT, triangles. Lines are guides to the eye. The P3HT/HDPE composition of minimum P3HT content at which liquid–liquid phase separation occurred (L_1+L_2 regime; minimum c_{P3HT} is indicated with a red shaded circle). Adopted from [1]

As in the above, the most critical criteria is that P3HT crystallizes prior to HDPE. This is realized by selecting the appropriate deposition temperature, following for instance the solidification process named I in the phase diagram displayed in Figure 1.37.

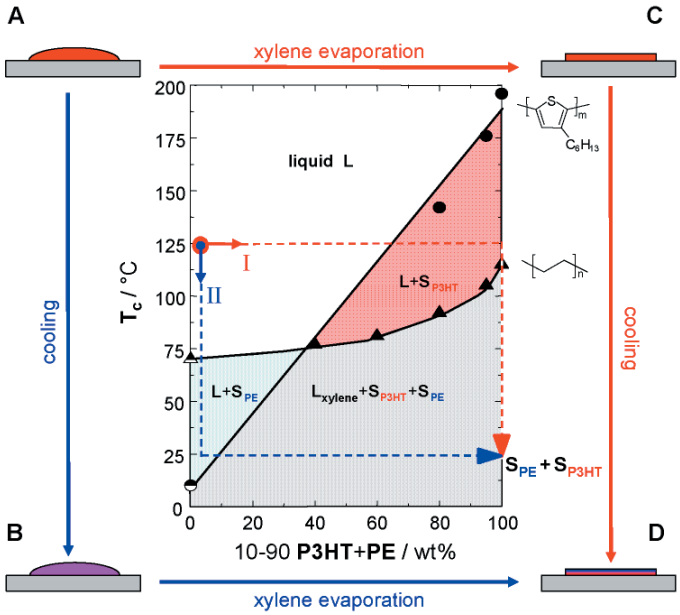

Figure 1.37: I) solidification process in which P3HT crystallizes before HDPE and that lead to optimal microstructure and performances, II) opposite case. Adopted from [1]

Summarizing, in order to achieve high charge-carrier mobility and an optimal P3HT crystallization, the concentration of P3HT has to be selected such that it is above $c_{threshold}$ and the temperature has to be sufficiently high (i.e. 125°C) to prevent the HDPE crystallizing prior to the semiconductor. In these conditions $\mu_{FET} = 6 \times 10^{-2}$ $cm^2V^{-1}s^{-1}$ is measured for the insulating semiconductor blend, which is comparable to the mobility of neat P3HT. HDPE is thus a perfect candidate for producing robust OPV ternary blends.

In order to quantify how the mechanical behaviour of the films is improved by addition of the HDPE, it is useful to notice how the stress-strain curve changes when this insulating polymer is added to P3HT. The Young modulus and the elongation at brake increase significantly with blending (Figure 1.38).

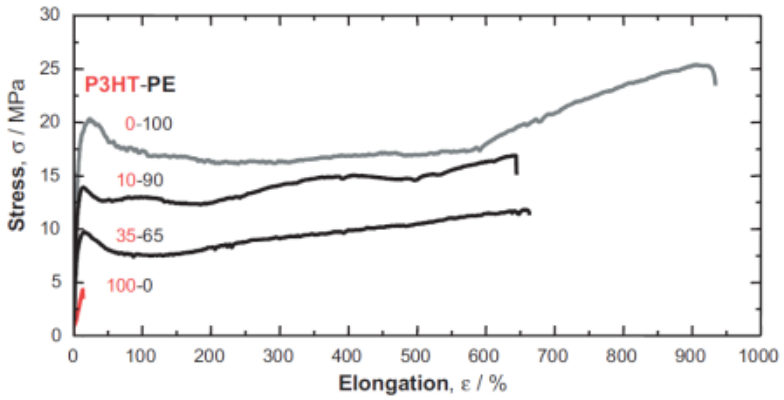

Figure 1.38: Stress-strain curve of different ratio of P3HT:PCBM. Adopted from [36]

Blending may also offer other advantages in OPV applications, for instance one challenge is to dissociate excitons efficiently. For this process the interface between donor and acceptor material play an important rule. Moreover the charges have to be able to reach the electrodes, this requires a percolating structure. Clearly the addition of a third material can be challenging for the efficiency of these processes and the photophysics properties of the film in general can be affected.

Ferenczi et al. demonstrated however that a ternary blend P3HT:PCBM:HDPE with a content up to ~50 wt% of HDPE showed performances comparable with those ones of the binary donor:acceptor blend. [2] In their work they analysed the influence of insulating polymer content, thickness, and annealing temperature: for a HDPE content of 40 wt% and a thickness ~300 nm. They found that the best device performance for an annealing temperature below the melting temperature of HDPE. Comparing now the J-V curve of the binary blend with that of the ternary blend (at a thickness of 100 nm), a decrease of J_{sc} is reported to the decreased optical density in the ternary blend. If the thickness was increased the photocurrent generation efficiency (ratio between the actual J_{sc} and the maximum J_{sc} available due to the semiconductor component alone) decreased, but the J_{sc} stayed comparable to the binary. Basically the current is maximised at larger thicknesses (despite the photocurrent efficiency decreases) which renders it possible to produce thick ternary blend solar cells. However increasing the content of HDPE above 50% led to decrease in the performance indicating that percolation was lost. Similar observations were made for transistors. [1]

Comparing the efficiency of a ternary blend with a-PS with that one with i-PS, both a decrease in Jsc and a decrease on the content threshold of insulator is found. This is due to the smaller crystallinity of P3HT and to the limited percolation network in such blends.

2. Experimental Methods

2.1 Materials

The donor materials used in this work are poly(3-hexylthiophene) (P3HT) and a diketopyrrolopyrrole (DPP)-based copolymer, DPP-TT-T. In the nomenclature, TT is used for the thieno[3,2-b]thiophene while T stands for the thiophene. The acceptor materials used are [6,6]-phenyl-C_{61}-butyric acid methyl ester ($PC_{61}BM$) and [6,6]-phenyl-C_{71}-butyric acid methyl ester ($PC_{71}BM$). For the insulating component we selected high-density polyethylene (HDPE). The chemical structures and of these materials are listed in Figure 2.1.

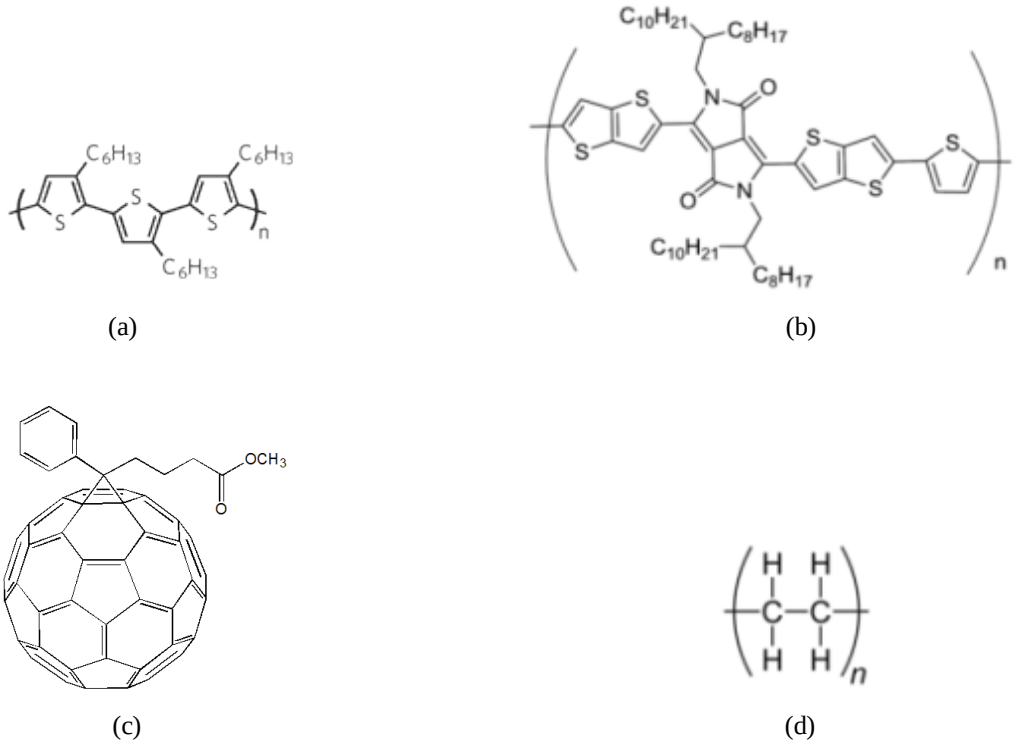

(a) (b)

(c) (d)

Figure 2.1: Chemical structures of (a) rrP3HT, (b) DPP-TTT, (c) $PC_{61}BM$, (d) HDPE

In table 2.1: Weight-average and number-average molecular weight (M_w and M_n, respectively) deduced from gel permeation chromatography. The dispersity (PDI) and the suppliers are also listed.

Material	Company	MW (kDa)	Mn (kDa)	PDI
rrP3HT	Merck	47.81	26.20	1.83
DPP-TTT	Imperial College, Prof. Iain McCulloch's group	102	14	7.28
HDPE	Sigma-Aldrich	125	-	

Table 2.1

Both P3HT and HDPE are semicrystalline polymers. From differential scanning calorimetry (DSC) it is possible to determine the melting temperature, T_m, and the crystallization temperature, T_c. A T_m~210°C and a T_c~189°C is measured for P3HT and a T_m~122°C and T_c~116°C for HDPE when a cooling rate 10°C/min was used.
DPPTTT is a diketopyrrolopyrrole (DPP)-based copolymer. These class of polymers are attractive materials in which the DPP core is electrondeficient leading to a narrow band gap. Furthermore, the planarity of the DPP skeleton and its ability to accept hydrogen bonds result in an increased π-π stacking. The substitution of thiophenes with larger thieno[3,2-b]thiophene units extends the polymer's coplanarity and also promotes a more delocalized HOMO distribution along the backbone. This is expected to enhance intermolecular charge-carrier hopping. [10]

2.2 Film preparation

Thin films were prepared by solution-processing methods. Materials were first weighed with a balance (Mettler Toledo XS205), then transferred in a vial. After adding the appropriate solvent they were stirred on a hot plate till complete dissolution is achieved. Films were produced via wire bar coating at appropriate temperatures on glass slides. Other methods used were drop casting and spin coating. For the P3HT:PCBM:HDPE ternary blend a deposition temperature above 115° was needed, as explained before, in order to prevent HDPE to crystallize before P3HT. The solutions were prepared using a concentration of 18 mg/ml, these were quite viscose, especially those ones comprising a high HDPE content. Therefore Pasteur pipettes, substrates and the bar were pre-heated to avoid solidification of the solution before the deposition. The solvent used for these blends was 1,2,4-trichlorobenzene. This is a solvent commonly used for organic semiconductors with high boiling point (214,4°C). Other solvents such as xylene and

decalin were tested but with the first one a perfect dissolution of HDPE was difficult to achieve due to the law boiling point (138°C), while with the second one problems occurred with the dissolution of PCBM. Moreover TCB is the same solvent used in previous studies of this blend. [1], [2] So its employment allowed a better correlation with already existing data. For DPP-TTT and blends comprising this polymer both TCB and CB were used.

2.2.1 Wire bar coating

A wire bar coater (Figure 2.2) consisting of a heating bed and the coating bar, was employed for most film fabrication as this methods allows the coating of polymeric films on flexible or rigid substrates with a high reproducibility, excellent control of rate, temperature and thickness of deposition, compatibility with different dimensions of substrates and low material losses. It is also a scalable technique that could possibly be used in an industrial production and is compatible with roll to roll manufacture.

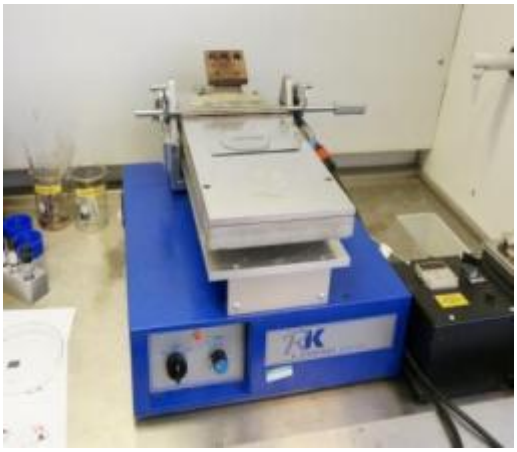

Figure 2.2: Wire-bar coater

The bar is comprised of wires (Figure 2.3) of a certain diameter (D) that influences the wet layer thickness and therefore the final thickness of the film (T): the thicker the wires the thicker will be the resulting dried film (Figure 2.4).

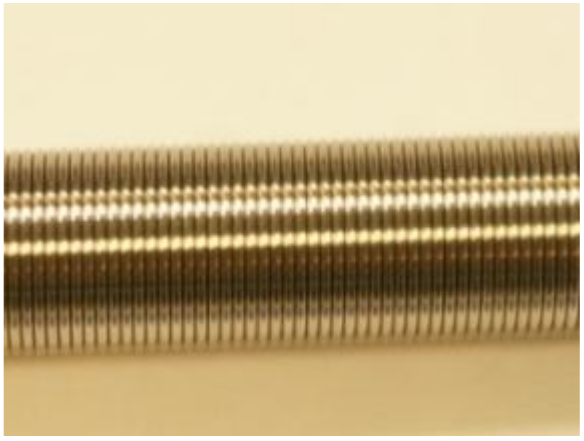

Figure 2.3: Wire-bar detail

This can be calculated from equation 11:

$$T = 0.107D \tag{11}$$

If are takes into account the losses due to friction, to be ~25%, relationship becomes:

$$T = 0.08D \tag{12}$$

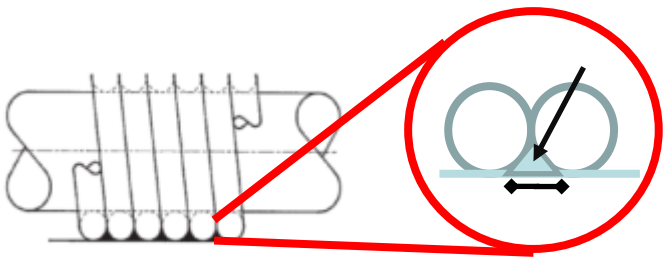

Figure 2.4: Wire-bar coating volume.

Note though that the thickness varies also with bar speed, temperature, quantity of material used, gap between bar and substrate. However once a certain set up is chosen, the reproducibility and the quality of the films are excellent. A KControl Coater model 101 was used for this thesis.

2.2.2 Drop Casting

Drop Casting is probably the simplest processing method used to make a film of organic semiconductors. The solution is dropped on a surface and a film is formed as a consequence of the evaporation of the solvent. The concentration of the solution and the temperature of the substrate are the key factors that govern the film formation.

Although the quality of the film is generally not particularly good, this method is useful when a very thick film is needed. For this reason drop casting is used for materials characterization and usually not for devices preparation.

2.2.3 Spin coating

Spin coating is a common deposition technique in which the solution is dropped on a rotating substrate. An excess of solution is used and then removed by the centrifugal force. Good quality films can be obtained with this method, thus it is one of the most used procedures in processing of organic semiconductors. Note though that spin-coating leads to a high loss of material and allows limited of deposition temperature control. It is also incompatible with large substrates and it is also difficult to process small molecule semiconductors (because of the low viscosity) by spin-coating. Moreover rapid solidification can affect strongly the crystallization process of the polymer and the distribution of different phases within the film. Furthermore spin coating technique is not scalable and therefore is not compatible with an industrial production.

2.2.4 Ultraviolet-visible (UV-vis) spectroscopy:

Spectroscopic techniques are widely used in the characterization of organic semiconductors since they can give important information about the optoelectronical behaviour of semiconducting films and devices. The ultraviolet-visible (UV-vis) spectroscopy is an optical technique used to measure the absorbance of a given solution or thin film in the range of wavelength of ultraviolet, visible and infrared. The absorbance is then proportional to the transition from the ground state to the exited state and can therefore give information on the electronic properties of the material. As mentioned in the introduction it is then possible to correlate these measurements with different characteristics of the polymers, such as: order, aggregation and conjugation.
The absorption *A* is given by the Beer-Lambert Law:

$$A = -log_{10}\left(\frac{I}{I_0}\right) = \varepsilon c l \tag{13}$$

where *I* is the intensity of the transmitted light, *Io* is the intensity of the incident light, ε is the molar extinction coefficient, *c* is the molar concentration, *l* is the distance the light travels through the material.

A Perkin Elmer Lambda 25 spectrophotometer was employed for UV-vis spectroscopy measurements.

2.2.5 Photoluminescence spectroscopy (PL)

PL is another technique, similar to UV-vis spectroscopy, that measures the photon emission consequent to the return from the excited state to the ground state. As mentioned in the introduction the spectrum given by PL spectroscopy can be the mirror image of the UV-vis spectra, in absence of effects that prevent the excited species to return to the ground state in a radiative way. This is referred as PL quenching and can happen for instance when an acceptor material is present. In this conditions the exciton is separated in charges and the electron is transferred to the acceptor material. Exciton energy transfer to another state/ground state also leads to a non-radiative decay mechanism. The charge transfer is at the basis of the functioning of a photovoltaic cell, PL is thus an important tool to measure the charge transfer efficiency from the donor to the acceptor in the characterization of blends for these devices. Raw data of PL are corrected according to the formula below:

$$PL_{corr} = \frac{PL_{raw}}{1 - 10^{-A}} \tag{14}$$

where A is the absorbance at the pumping wavelength and remembering that $A=-log_{10}T$ then the formula becomes:

$$PL_{corr} = \frac{PL_{raw}}{1 - T} \tag{15}$$

Therefore this correction is used to consider the initial absorption of the film.
In my work an excitation wavelength of 520 nm was used with a steady state spectrofluorimeter Horiba Jobin Yvon, Spex Flouromax 1.

2.2.6 Differential scanning calorimetry (DSC)

DSC is one of the most important thermoanalytical techniques used in materials characterization. A certain heating cycle is applied to a reference and the sample. The heating flux required to keep the material at the same temperature of the reference is measured as a function of temperature. The reference should, therefore, have a well-

defined heat capacity and should not undergo any transition in the range of temperatures investigated.

DSC enables the investigation of any physical-chemical process that requires an exchange of heat, determining the nature (exothermic or endothermic) and intensity of the thermal event. This technique is really useful to study effects of polymer processing and can give information about melting, crystallization, glass transition temperatures, decomposition and crosslinking.

Depending on the purpose of the experiment, different numbers of cycles can be applied: the processing history (i.e. deposition temperature, annealing, quenching) is really important and influences strongly the thermal behaviour of the material For this reason the data from different cycles can be important to study the processing effects.

Here, DSC measurements were conducted under N_2 atmosphere at a scan rate of 10-20 °C/min with a Mettler Toledo STAR^e system DSC. Standard Mettler Aluminum crucibles were utilised. The sample weights were ~5 mg.

2.2.7 Optical microscopy (OM)

Optical microscopy is an easy, fast and direct method to analyse the microstructure of thin films. It is especially useful when you use blends of different polymers in order to detect how the phases are organized and evolve with time or temperature. OM can be thermally resolved when using a hot-stage. This last device consists of a heating cell connected with a processor that enables the controlled heating and cooling.

It is possible to use the microscope with crossed polarizer in order to distinguish crystalline from amorphous regions. A first polarizer is applied to the incoming light and a second polarizer (the analizer), perpendicular to the first one, is placed after the sample. Thus if the sample is amorphous all the light will be filtered and the image will be dark, in contrast if crystal regions are present then the light will be rotated according to the crystals orientation leading to birefringence. Such an analysis can be applied to polymer films to detect the amount, geometry of crystals and to study phase transitions.

Optical microscopy in this thesis is carried out with an Olympus BX51 polarising microscope equipped with a Q-imaging Go-3 camera. The hot-stage is a Mettler Toledo FP82HT connected with a Mettler Toledo FP90 Central Processor.

2.2.8 Wide-angle x-ray scattering (WAXS)

Wide-angle X-ray scattering (WAXS) was a diffractometry technique based on the elastic scattering phenomenon of an X-ray beam by crystal planes of a material allowing the determination of the molecular arrangements within a solid-state or liquid crystal structure. "Wide angle" defines scattering angles 2θ larger than 5°.

The basis of WAXS is the Bragg's law that states the conditions for obtaining a constructive interference between the waves reflected by the crystal planes (Figure 2.5). According to the law this only occurs if the difference in the optical path of the waves is an integer multiple of the wavelength:

$$n\lambda = 2dsin\theta \tag{16}$$

where n is an integer, λ is the wavelength of the incident X-ray, d is the distance between successive crystallographic planes, and θ is the angle between the incident X-ray beam and the scattering planes.

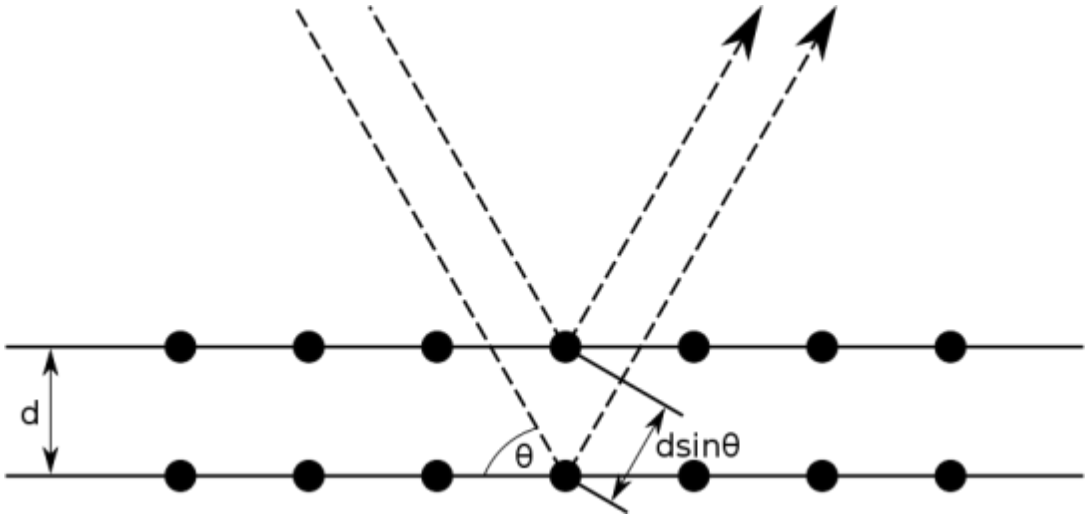

Figure 2.5: Waves reflected by crystal planes

X- ray diffraction (XRD) measurements were carried out with a PANALYTICAL X' PERT-PRO MRD diffractometer equipped with a nickel-filtered Cu-Kα1 beam and X' CELERATOR detector, using current I = 40 mA and accelerating voltage U = 40kv.

2.2.9 Transient absorption spectroscopy (TAS)

Transient absorption spectroscopy is a technique used to study the transient species that are formed as a result of photoexcitation. After a first excitation (pump) a series of weak probe pulses are sent through the sample with a certain delay with respect to the

pump pulse and a difference absorption spectrum is then calculated (Figure 2.6). Thus the absorption of an excited state is measured. Two types of measurements are then possible depending on the set-up: one possibility is studying the changing of absorption spectrum at a certain fix time; another one is measuring the evolution of the differential signal over time at a certain wavelength.

Hence depending on the timescale it is possible to determine which transient specie is formed and to detect its decay. In my work the analysis was performed investigating the microseconds to milliseconds timescale in order to study the geminate charges recombination. The pump pulse was produced by a LN1000 Megaplus nitrogen laser which pumps a PTI dye laser with excitation energy filtered in order to reach 3mJ/cm^{-2} for a wavelength of 520 nm, the pulse is directed in a quartz cuvette using a light guide. The probe was produced from a 150W tungsten lamp, which passes through two monochromators for the selection of probe wavelengths that in this work is 980 nm. The detection system consisted of a silicon photodetector and a Tektroniks TDS 220 oscilloscope, connected to a computer.

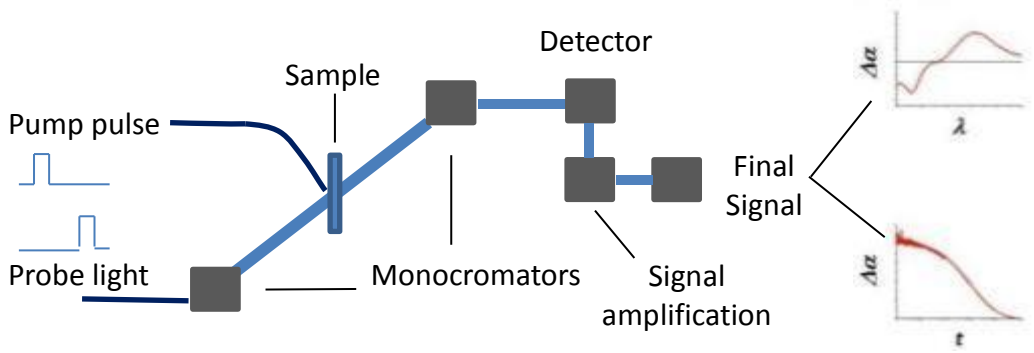

Figure 2.6: TAS layout

In this work the decay of the differential absorption signal over time was measured. The raw data were corrected according to the formula 17:

$$\Delta OD_{corr} = \frac{\Delta OD_{raw}}{1 - 10^{-A}} \qquad (17)$$

where A is the absorbance at the pumping wavelength and ΔOD is the different in absorption. Remembering that $A=-log_{10}T$, then the formula becomes:

$$\Delta OD_{corr} = \frac{\Delta OD_{raw}}{1 - T} \qquad (18)$$

This correction was used to consider the initial absorption of the film.

2.2.10 Dektak profilometer

A profilometer is a measuring instrument used in surface sciences. In the classical version of this device the sample is moved under a fix stylus. Different scan lengths and speeds are possible; nowadays other non-contact methods can be employed.

The Dektak is a contact profilometer for measuring step heights on a surface. Due to the very low force applied to the stylus it is a useful measuring instrument also for organic semiconductors. A video camera with variable magnification connected with a monitor allows for manual placement of the stylus. Normally a scratch is applied on the film and the difference in height between the top of it and the substrate is measured (Figure 2.7).

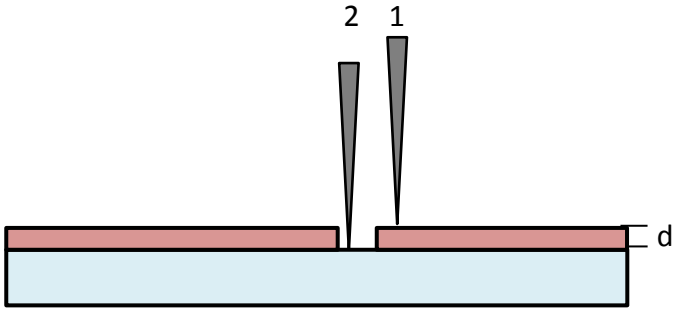

Figure 2.7: Dektak working principle, the tip moves from 1 to 2 and the gap is measured

Profilometry is fast and does not require complicated preparation of samples as e.g. needed in other more accurate techniques such as atomic force microscopy (AFM) and the accuracy is still sufficiently high for the purpose of characterization of organic semiconducting fils.

Measurements for this thesis were carried out with a Sloan Dektak surface profiler.

2.2.11 Evaporative deposition

Evaporation is a technique used in thin film deposition in which the material to be deposited is first evaporated in vacuum by electrically resistive heating and then condensed back to solid state on a given target. An evaporator consists of a vacuum pump and an energy source for the evaporation. This method is used in OPV fabrication to deposit the back contacts, normally made of aluminium. To this end the whole system is placed in a glove box. In this thesis, in order to achieve a good deposition, a current around 1mA was used and a deposition rate of ~0.1 $Ås^{-1}$ for the first nanometres which was then increased to ~0.3 $Ås^{-1}$. A vacuum in the order of $10^{\wedge-6}$ mbar was employed. The Al was deposited through a shadow mask of the design schematically

depicted in Figure 2.8 using an Edwards 307A evaporator. The active photovoltaic diode area defined by the overlap between orthogonal ITO and Al stripes was 1.5 mm×3 mm.

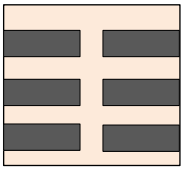

Figure 2.8: electrodes design

3. Results and discussion

3.1 P3HT:HDPE binary blend

A ternary blend is a complex system that involves different phases and interfaces. For this reason, firstly a binary blend P3HT:HDPE was analysed. Initially a blend ratio of 1:1 by weight was chosen and processed from TCB (18mg/ml total polymer content). The influence of relevant processing parameters on microstructure was then assessed with optical microscopy and UV-vis spectroscopy.

The effect of deposition temperature was first studied. Temperature were selected between 100°C and 150°C in order to ensure that P3HT crystallises first (see Figure 1.37). The deposition temperature seemed not to significantly affect microstructure as all films feature similar morphology. Analogous observations were made when annealing these thin film architecture. After annealing at different temperatures (between 120 and 150 °C) for 10-15 min no appreciable differences were seen in the film microstructure.

In a second set of experiments, we therefore elucidate if the thickness affects the solid-state microstructure. Thicknesses of binary films was changed from ~80 to ~500 nm. Again no difference was observed (see Figure 3.1

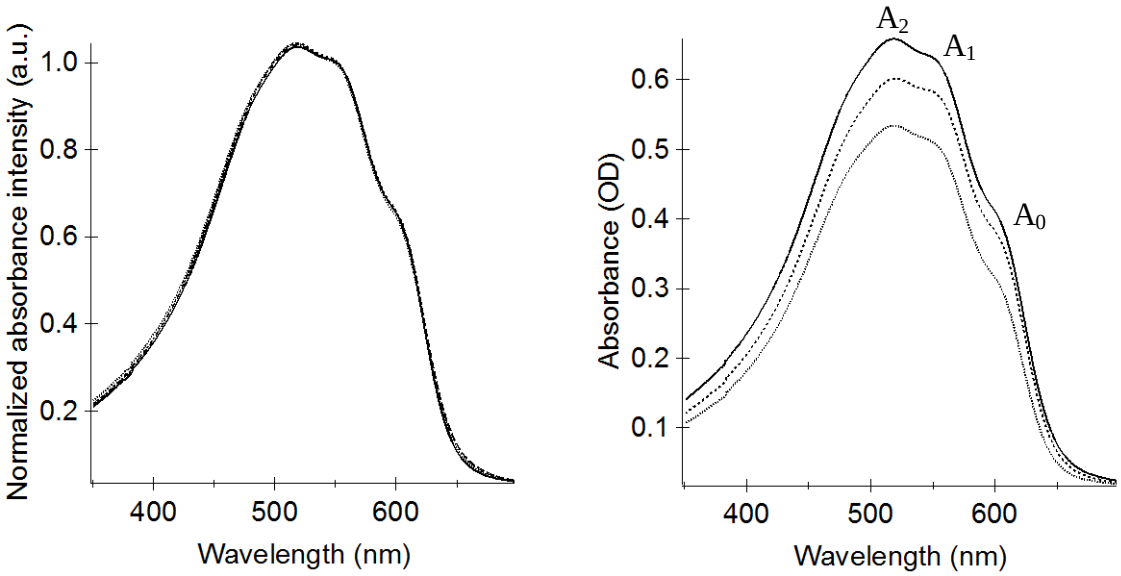

Figure 3.1: UV-vis spectra of films P3HT:HDPE 1:1: on the right the raw data, on the left the normalized ones.

Three absorption peaks are clearly visible, A_0~595 nm, A_1~547 nm, A_2~525 nm, each absorption is given by a Gaussian distribution and the spectrum is the overlap of the three.

The effect of solvents on blend microstructure was also studied, TCB and decalin were selected for this purpose. A small difference in the UV-vis spectra was observed for films cast from these two solvents (Figure 3.2). The films featured however very similar morphology as observed in optical microscopy.

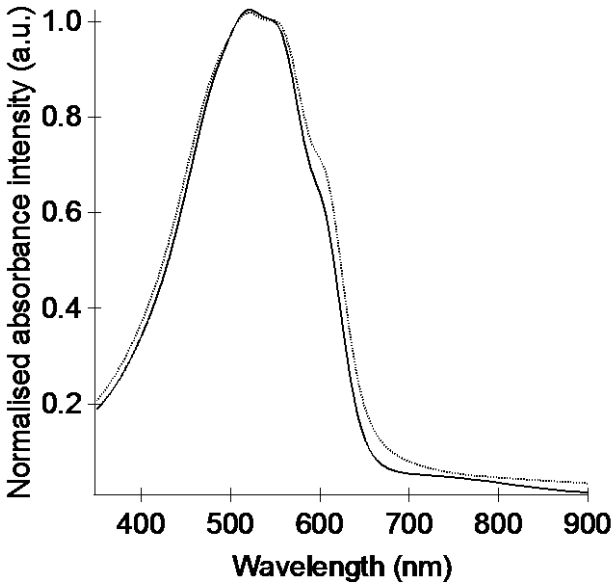

Figure 3.2: UV-vis spectra of 1:1 P3HT:HDPE blend films cast from decalin (dashed line) and TCB (solid line) respectively.

More specifically films obtained from TCB display a A_0 absorption at higher energy (dashed line) compared to those cast from decalin. This can be interpreted with a model explained in the introduction that demonstrate how such a shift is related to an increased aggregation of the polymer and an increased conjugation length intrachain. [6], [7], [12–17] We attribute this to the fact that TCB has a higher boiling point leading to a slower evaporation rate. Under these conditions the polymer is able to obtain a better organization and intrachain order.

We turn now the attention to the influence of different HDPE content which we varied from 0 wt% to 90 wt%. The blend composition seems to have an effect on microstructure. The UV-vis spectra of the individual blend films show a noticeable shift of the intensities of the absorption peaks. The data were normalized to the A_1 absorption in order to better distinguish the relative changes of A_0 and A_2. Introducing a content of HDPE up to 60 wt% leads to an increase in A_0 and a decrease in A_2 (Figure 3.6). At 70 wt% and more HDPE, an opposite trend is present. This shifts demonstrate

how an introduction of HDPE in the blend induces a better aggregation of the P3HT. This improvement is gradual, as the content of polyethylene increases. As described in the introduction, the crystallization of HDPE occurs after that of P3HT at the selected deposition temperature. During cooling, the solidified P3HT segregates from the crystallising HDPE which seems to lead to further aggregation of P3HT.

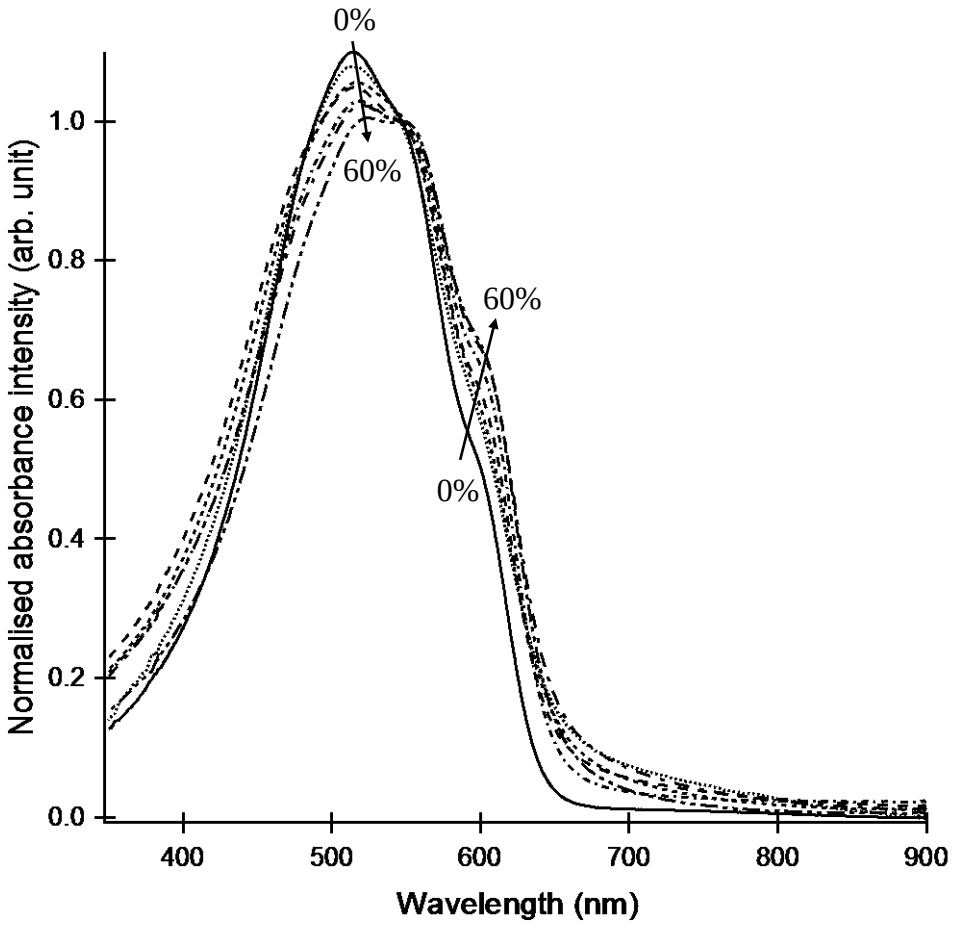

Figure 3.3: UV-vis spectra of different blends of P3HT:HDPE. The solid line is the reference P3HT (0 wt% HDPE). The content of HDPE is increased up to 60 wt% in 10 wt% steps. The films were cast from TCB (18 mg/ml).

In order to illustrate more clearly the observed changes in the UV-vis spectra of different blend films, in Figure 3.4 the enlargements of A_2 (on the right) and A_0 (on the left) is shown.

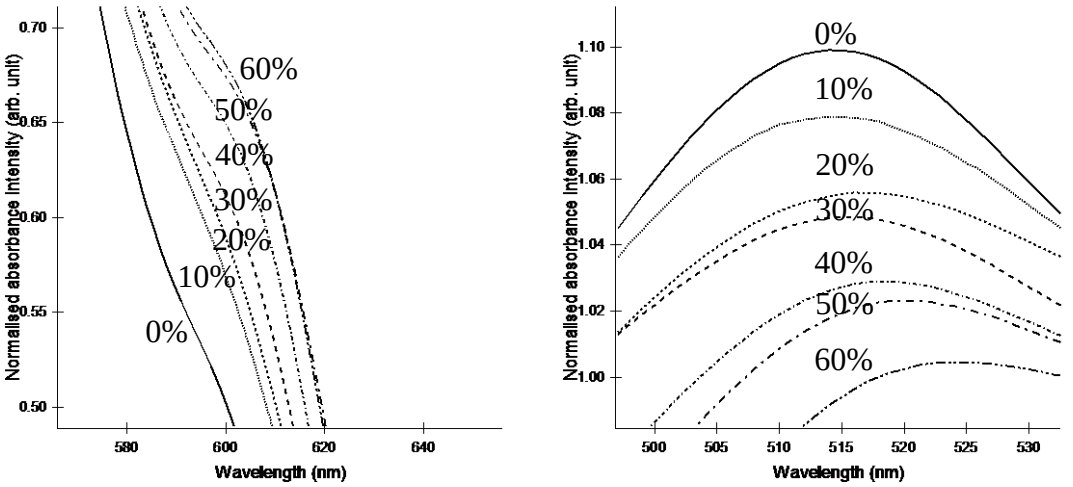

Figure 3.4: UV-vis spectra of different blends of P3HT:HDPE, with focus on the changes observed for A_2 (right) and A_0 (left).

When the content of HDPE was increased from 60 wt% to 90 wt% (Figure 3.5) the A_0 absorption become gradually less intense, while the opposite is observed for A_2. This suggests that with increasing HDPE (>60 wt%) content the P3HT aggregation is reduced. Note though that even for films with 80-90 wt% of HDPE the spectra are still comparable to those of neat P3HT.

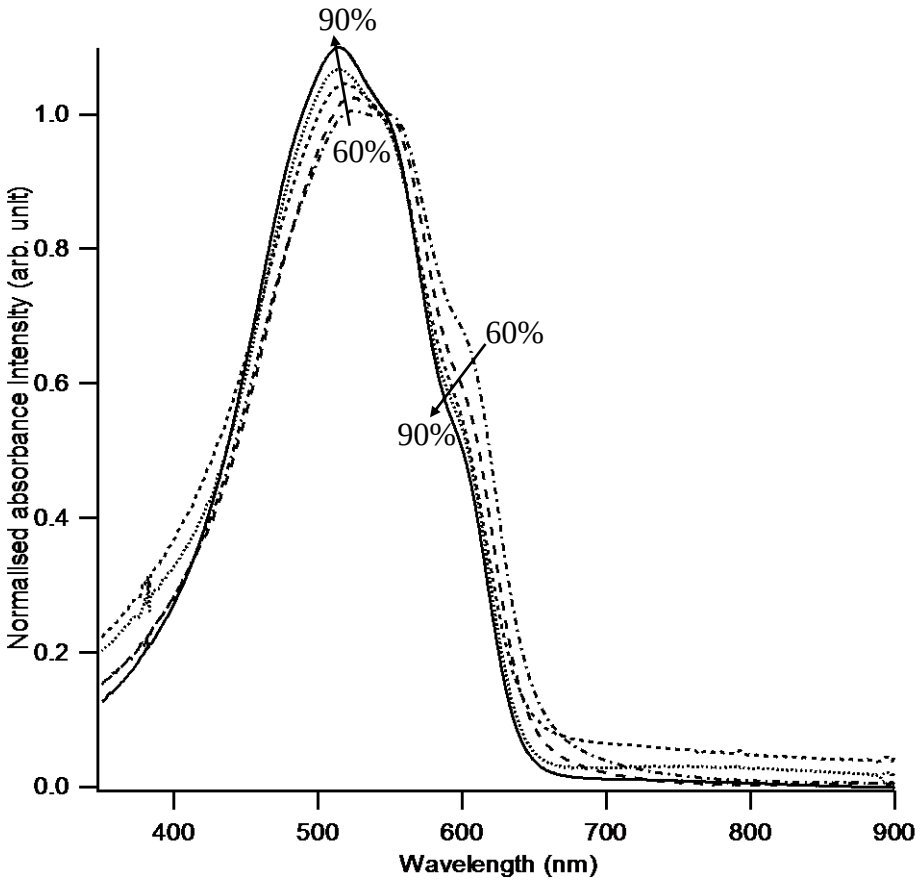

Figure 3.5: UV-vis spectra of different blends of P3HT:HDPE at an insulator content between 60 and 90 wt%. The solid line refers to the reference P3HT (0 wt % HDPE The films were cast fom TCB (18 mg/ml).

In Figure 3.6 it's shown the intensity of A_0 (left) and A_2 (right) as a function of HDPE content.

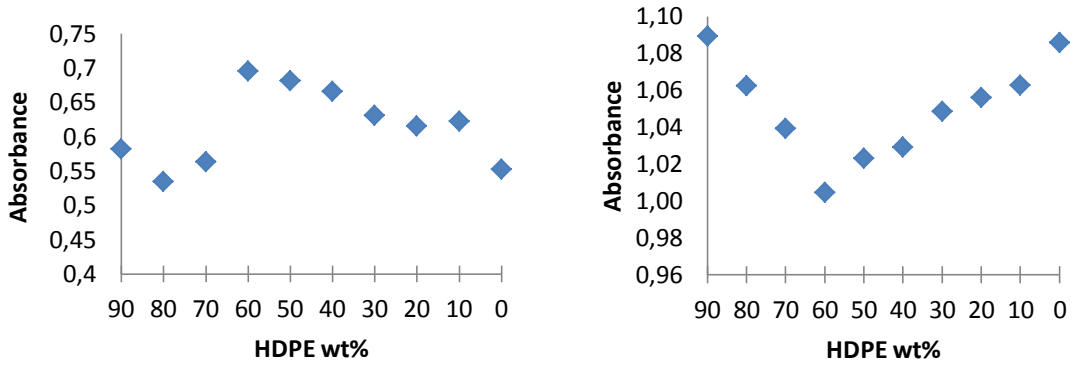

Figure 3.6: Normalised A_0 (left) and A_2 (right) absorbance as a function of HDPE content.

The microstructure of the films with different content of HDPE was also analysed via optical microscopy (Figure 3.7), for percentages close to 50 %wt different phases are visible, while if the concentration of one component is low it is difficult to distinguish them.

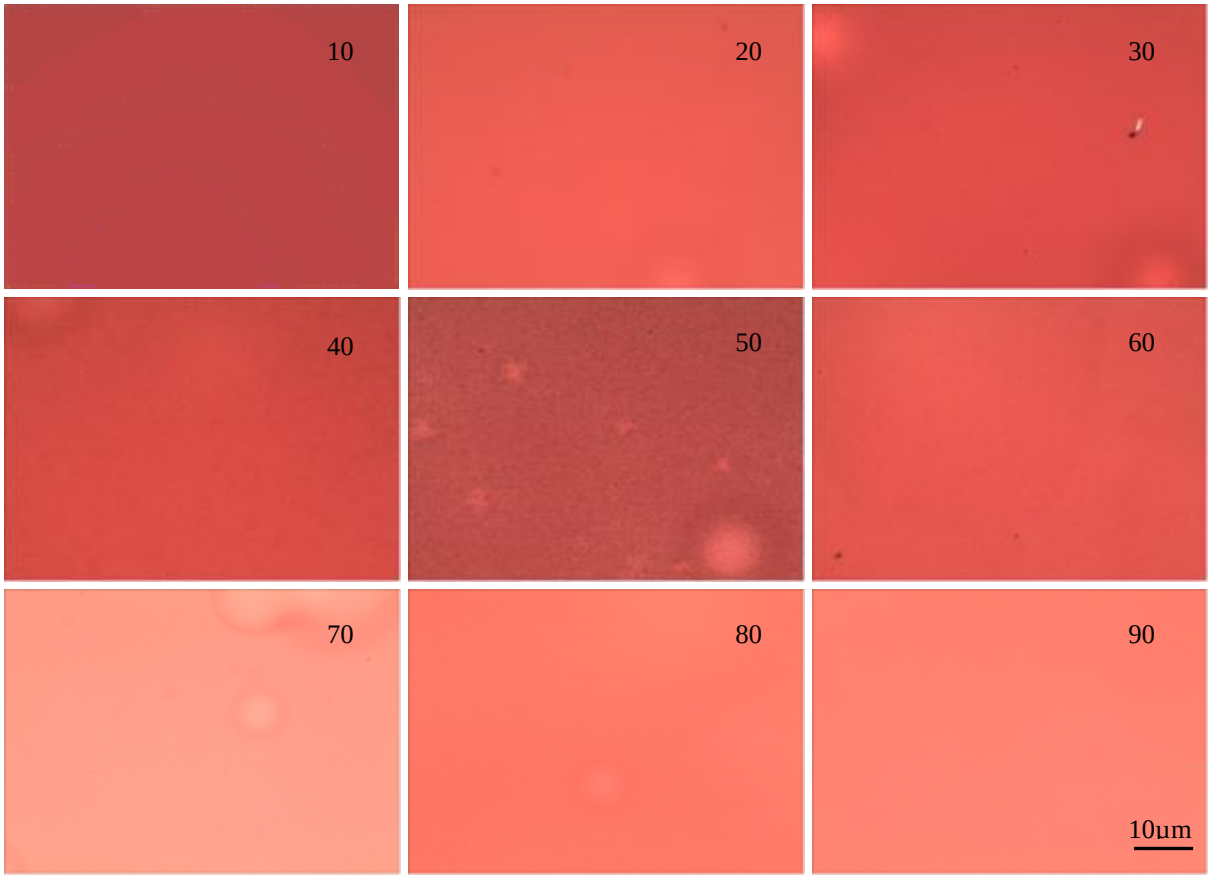

Figure 3.7: Optical microscopy images of binary blend P3HT:HDPE, in top corner is indicated the HDPE content in wt%, solution 18mg/ml in TCB.

In cross-polarised microscopy birefringent crystals were observed for blends comprising 60-100 wt% of HDPE. Polyethylene shows a lamellar structure, forming so-called spherulites. Each spherulite consists of fibrils growing in a radial direction and leading to the characteristic Maltese-cross pattern. This structure is visible via polarised microscopy because the crystallites within the spherulite have a constant orientation with respect to the radius vector. If a certain orientation is parallel to one of the polarizer, light can pass through the sample as shown in Figure 3.8 are visibile.

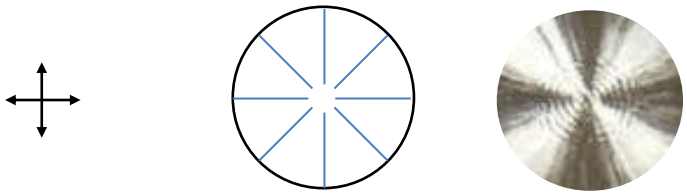

Figure 3.8: Illustration of the Maltese-cross formation. Left: orientation of the polarizer. Centre: analyser system. Right: appearance of the Maltese-cross.

In the films studied, spherulites were observed up to a P3HT content of ~40 wt% (see Figure 3.9). The dimensions of the spherulites were increasing in comparison to neat HDPE, in agreement with previous work. [1] (The difference in colour between micrographs taken of blends comprising 10wt% to 40wt% is due to image corrections that were applied to visualise better the microstructure.)

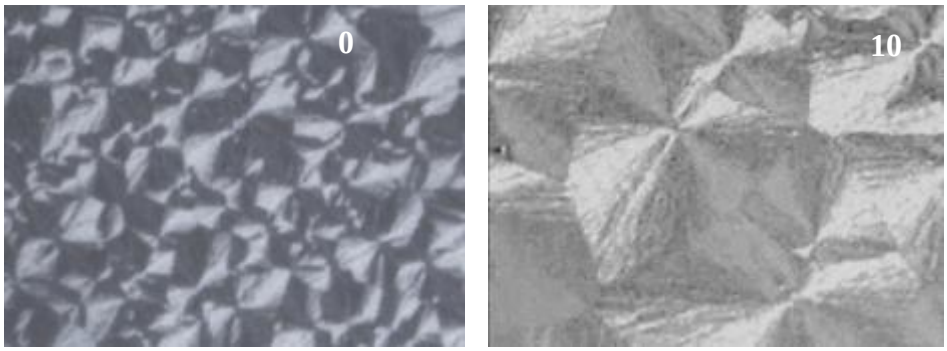

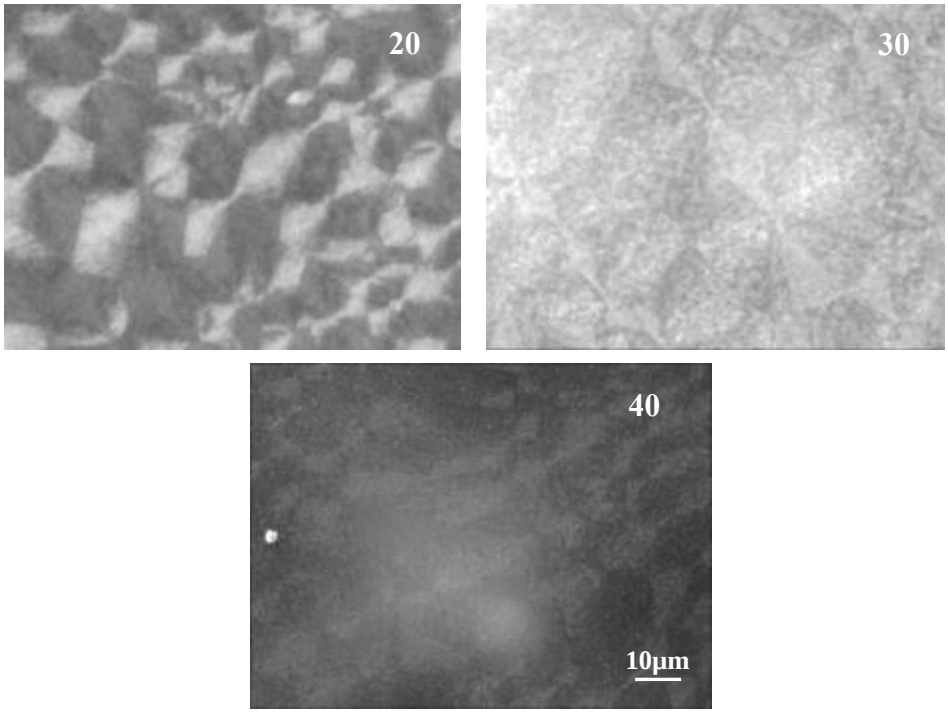

Figure 3.9: Set of images taken using polarized light with optical microscope, on top corner the HDPEwt%.

We turn now our attention on the photoluminescence of P3HT:HDPE blends. PL analysis was carried out at an excitation wavelength of 520 nm. The spectra in Figure 3.10 show how an addition of HDPE leads to an increase in the luminescence. Emission of P3HT is generally low due to the H-aggregate nature of this polymer. Addition of HDPE seems to reduce the molecules interactions leading to an enhanced luminescence. This observation is not in contradiction with the concept exposed above of a better aggregation in the presence of HDPE, indeed from normalization on the 0-1, the 0-0 emission peak is less intense compared to the 0-1 transition.

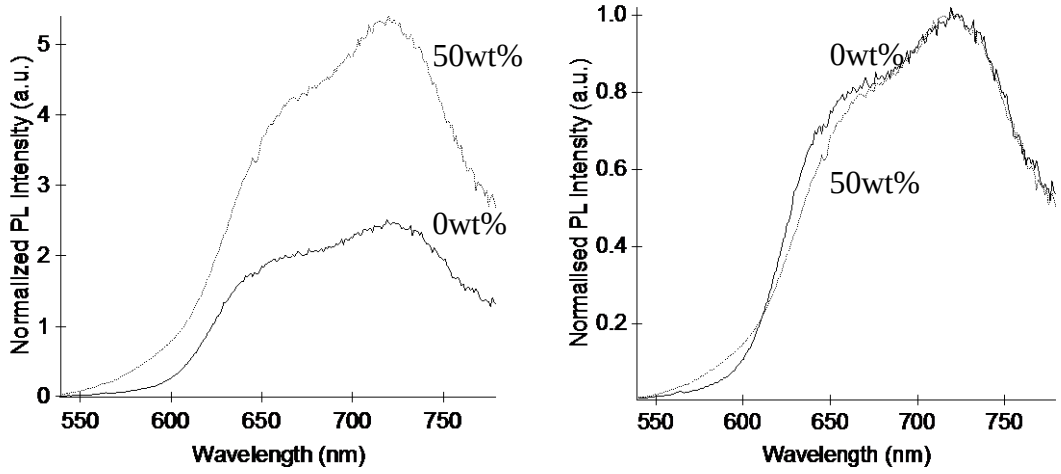

Figure 3.10: Left: photoluminescence spectra of P3HT (solid line) and P3HT:HDPE 1:1 (dashed line). Right: corresponding normalised spectra. Excitation wavelength was 520nm.

3.2 $PC_{61}BM$:HDPE binary blend

The microstructure of the active layer is of key importance for the working of organic solar cells. Therefore it is crucial to elucidate the tendency of PCBM to form aggregated domains e.g. through phase separation from HDPE.

To this end thermal behaviour of PCBM:HDPE binaries and the two neat components was performed using DSC. An amount of ~5 mg of material was used and the samples were heated and cooled at 10°C/min. For HDPE we observed a sharp melting endotherm with a maximum at ~130°C and an onset at ~122°C. During cooling an exotherm at ~116°C which is related to the crystallization (Figure 3.11).

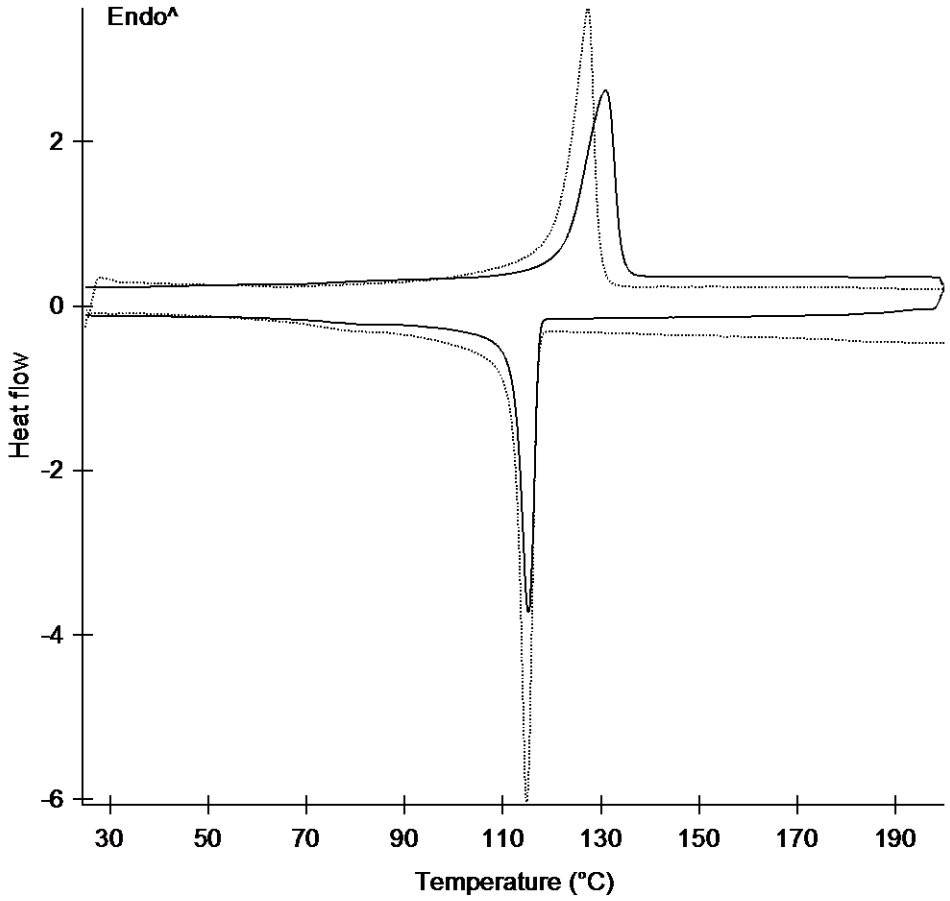

Figure 3.11: Thermogram of neat HDPE. ~5mg of material was used with (heating and cooling rate of 10°C/min) HDPE (solid curve) and HDPE:PCBM 1:1 (dashed line)

If the same analysis was performed on a blend of HDPE:PCBM 1:1 ratio by weight, a decrease in the HDPE melting point is found, with T_m ~126°C. Crystallization temperature was also affected by the addition of PCBM (T_c ~115°C). This decrease

may originate from an eutectic phase behaviour. However further investigations are required to fully elucidate the HDPE:PCBM phase behaviour.

The PCBM aggregation in such blends was assessed with optical microscopy in combination with a hot stage. Images of the evolution of aggregation with time and temperature were taken. The samples are annealed at different temperature for 15 minutes. At T_{ann} of 120°C, no effects on the microstructure were observed, but when the annealing temperature exceeded 125°C, visible aggregation of PCBM occurred with a small but distinct change of crystal size being found with annealing time. (Figure 3.12).

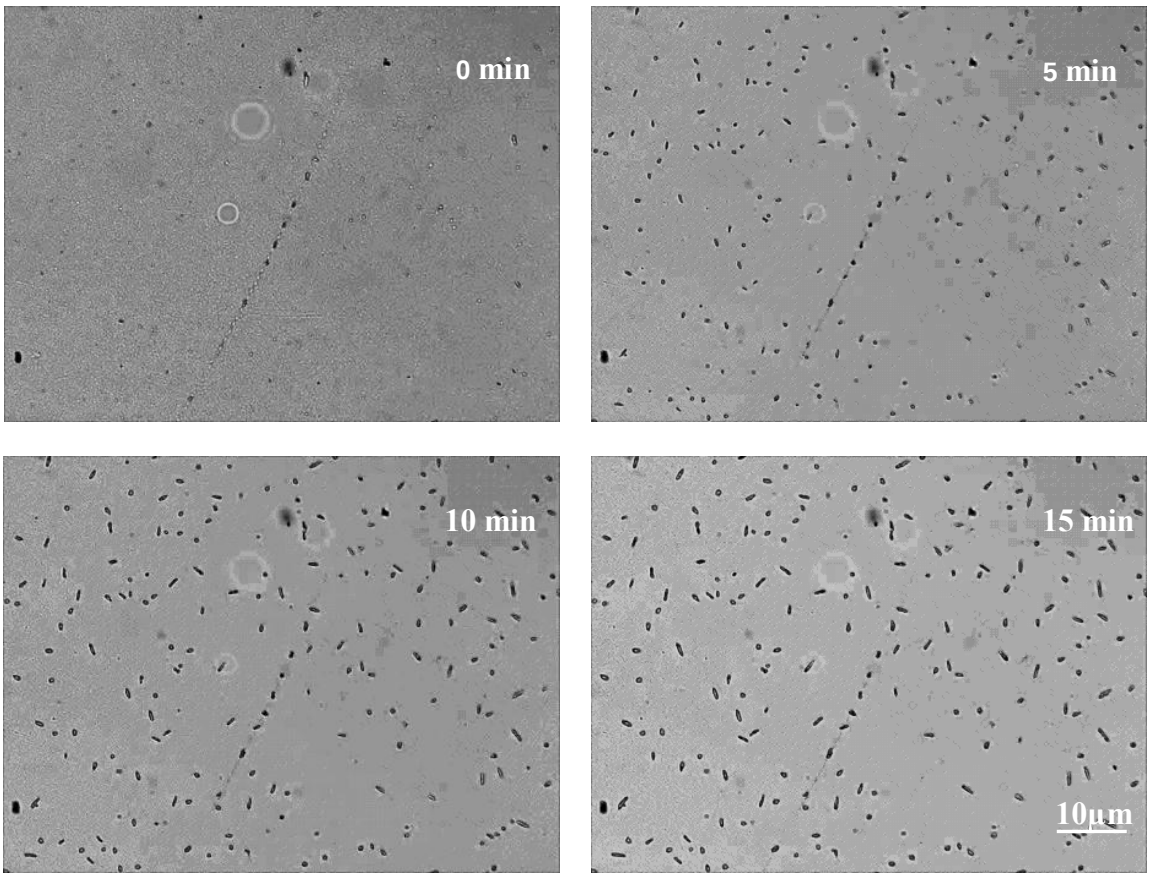

Figure 3.12: Optical micrographs of HDPE:$PC_{61}BM$ (1:1 ratio) annealed at 125°C, for the period of time indicated.

Thereby higher annealing temperatures led to PCBM aggregates of larger dimensions. For example at 170°C a rapid aggregation of relative large crystals of PCBM occurred, dimension and number of aggregates increase rapidly over time. Chrystal grow did however led to a depletion of the film wound the crystal, visible by the change of colour, which indeed is lighter (Figure 3.13).

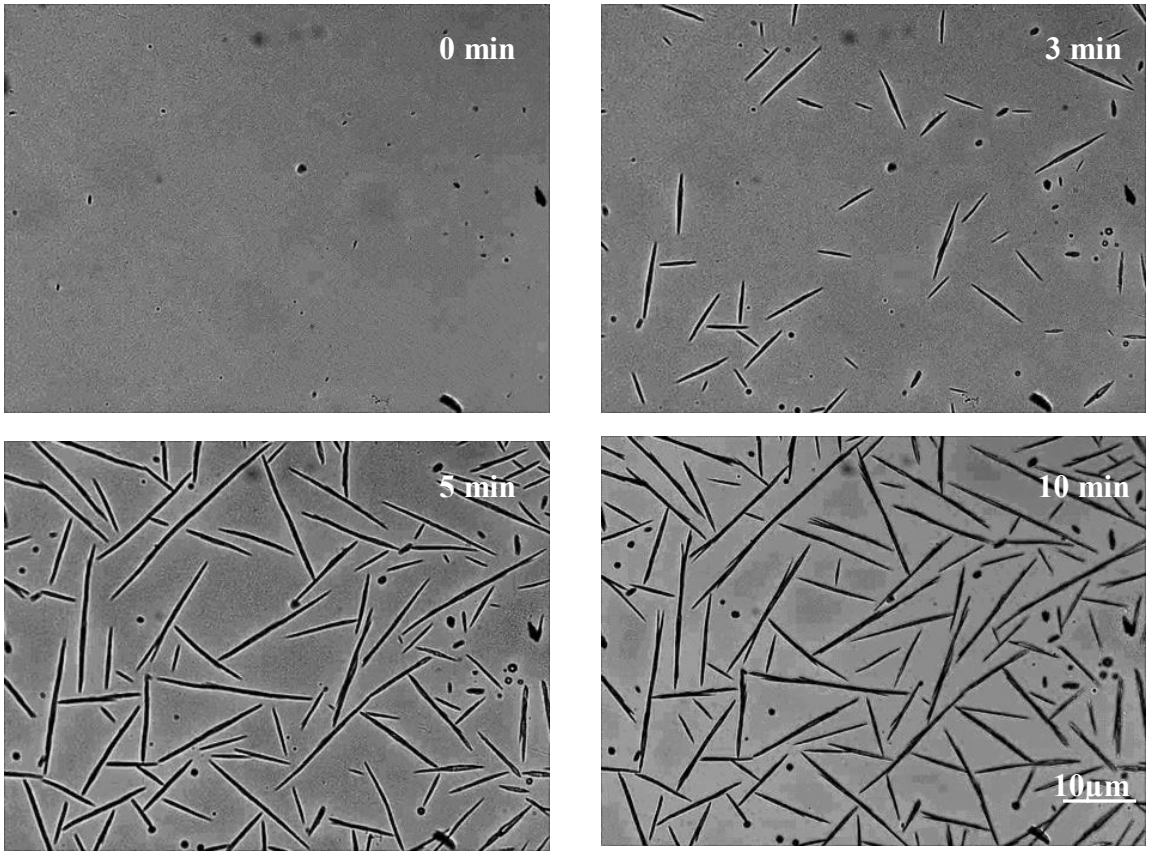

Figure 3.13: Optical micrographs of a 1:1 HDPE:PCBM blend annealed at 170°C. Annealing time is indicated in the top corner.

These results illustrate that an aggregation of PCBM is only possible once the HDPE melts.

UV-vis spectra of the blend were also measured in order to study the effect of HDPE on the absorption of PCBM, however no changes were observed in the PCBM spectra upon addition of HDPE.

3.3 Ternary blends

In order to evaluate the properties of the ternary P3HT:PCBM:HDPE blends, films of different compositions were prepared. Therefore, the P3HT:PCBM ratio was kept constant (1:1 by weight) while the HDPE content was varied over the range of 0 to 90 wt%. Initially we focused on a blend comprising 40 wt% HDPE content and the effect of processing was investigated. For this purpose we used UV-vis absorption spectroscopy.

First we varied the deposition temperature from 100°C to 150°C. No significant changes were observed in absorption and microstructure, this both for the ternary P3HT:PCBM:HDPE and the binary P3HT:PCBM system.

The effect of ternary blend thickness on aggregation of the P3HT was also studied. The UV-vis absorption of the binary blend shows a strong thickness dependence, with an increase of intensity of the A_2 absorption and decrease of A_0 as the thickness increases (Figure 3.14). This implies better aggregation is achieved for thin films. Different thicknesses are recognizable in the raw data since they absorb differently as described by the Beer-Lambert law (equation 13).

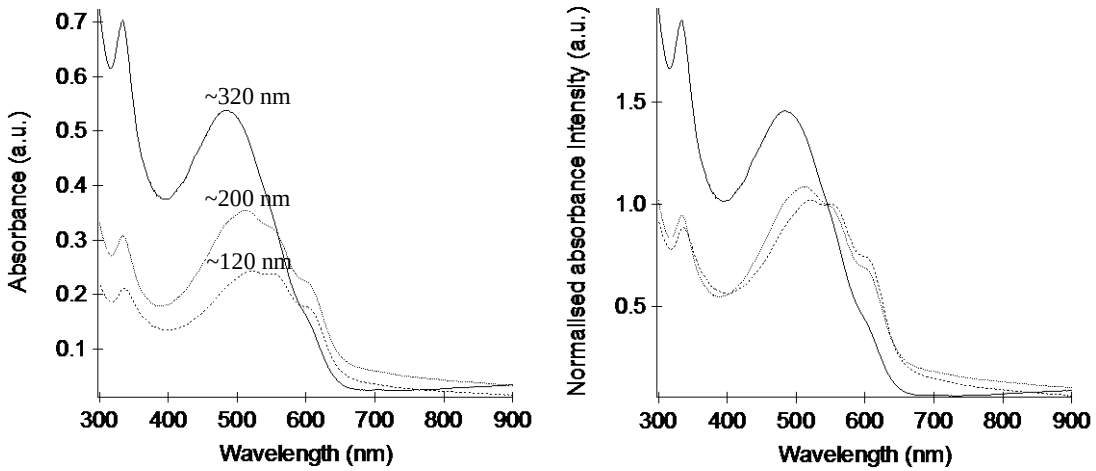

Figure 3.14: UV-vis absorption spectra of P3HT:PCBM as cast films, on the left the raw data and on the right the data normalized on the A_1 peak.

After annealing these blend films at 125°C and 140°C for 15 minutes, a similar trend as observable for the cast films is present, albeit less pronounced (Figure 3.15). Note though that annealing affects the shape of the spectra of thick films, while thinner films were less sensible to this post-treatment.

This observation suggest that annealing of thick films allow a reorganization of the macromolecules leading to molecularly more ordered system.

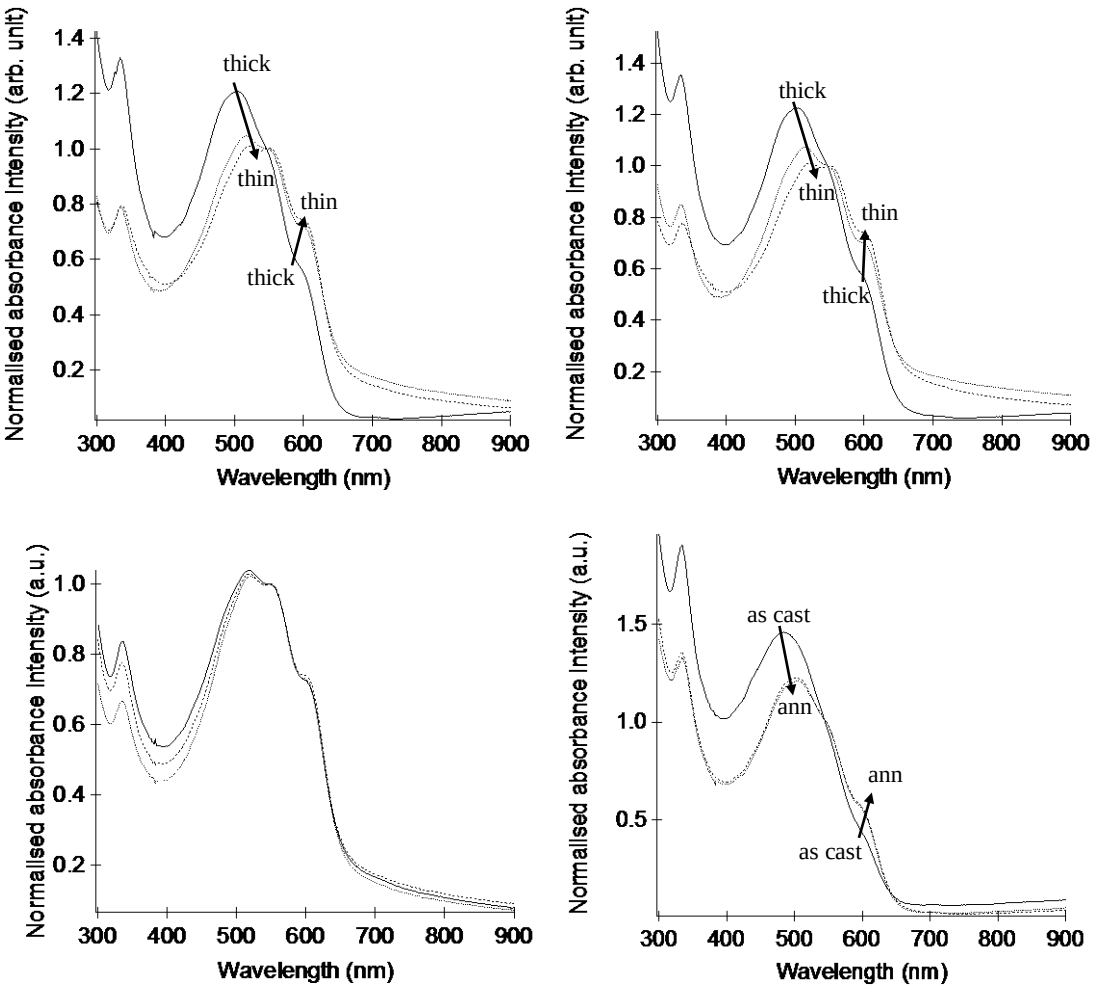

Figure 3.15: UV-vis absorption spectra of P3HT:PCBM films. Top panel: films of different thickness, (thicker film in solid line). Annealed at 125°C (top left), and at 140°C (top right) respectively. Same films used in Figure *3.14*. Bottom panel: annealing effect on the same film. Thin films (bottom left) and thick films (bottom right). The solid line refers to the as-cast film, the dashed lines are the annealed films.

This behaviour is in contrast to films prepared via spin-coating where it is found that thin films are less aggregated than thick films. [28] The explanation typically given is that for thick films the evaporation is slower and therefore the polymer is able to organize in a more ordered structure. This is definitely true for a deposition technique like spin-coating in which the fastness of rotation induces a quick solidification. However the films used in this work are obtained via wire-bar coating, for which the dynamics of crystallization are different. Apparently thin films have sufficient time to order and aggregate.

Similar observations were made on ternary blends of film thickness < 250 nm. There is a hyperchromic shift of the A_2 absorption as the thickness increases, while a hypochromic shift is found for $A_{0.}$ For thicker films (> 250 nm) (absorbance around 0.32 OD), no variations with film thickness was found (Figure 3.16).

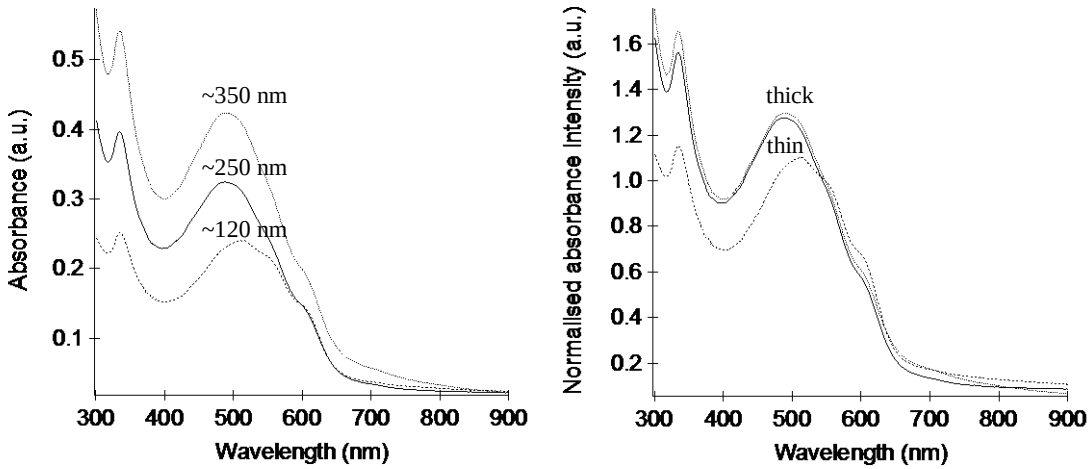

Figure 3.16: UV-vis absorption spectra of ternary blend 40 wt% HDPE, on the left the raw data and on the right the normalized spectra.

After annealing at 125°C, the difference between spectra of ternary films of different thickness was reduced, an annealing at 140°C display the same results (Figure 3.17).

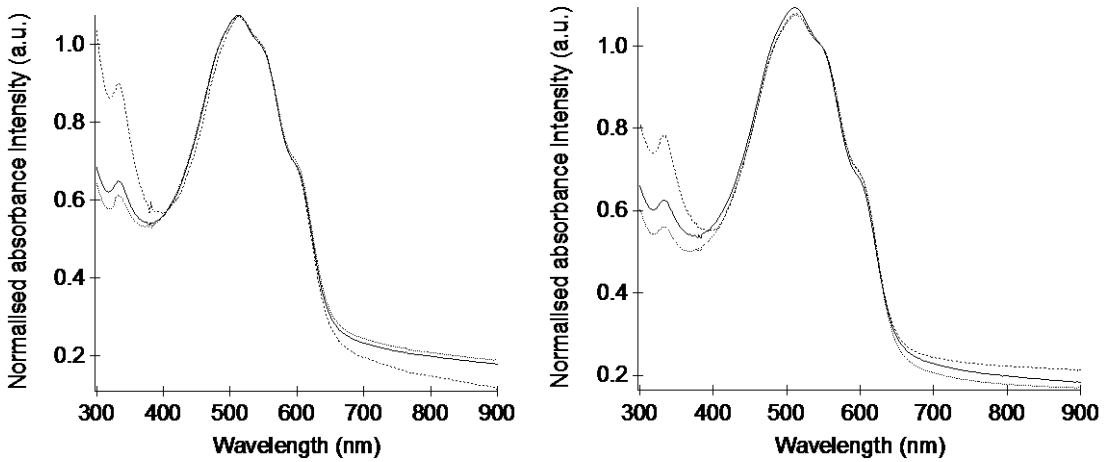

Figure 3.17: UV-vis absorption spectra of ternary blend comprising 40 wt% HDPE, annealed at respectively 125°C (left) and 140°C (right).

This means that even if as-cast films exhibit different aggregation depending on the thickness of the film, an annealing treatment homogenises the difference in structure.

Indeed, the absorption spectra of thin films did not significantly change during annealing. In contrast, for thicker films we observed that the heat treatment led to a noticeable increase at the A_0 absorption while the A_2 transition decreased (Figure 3.18).

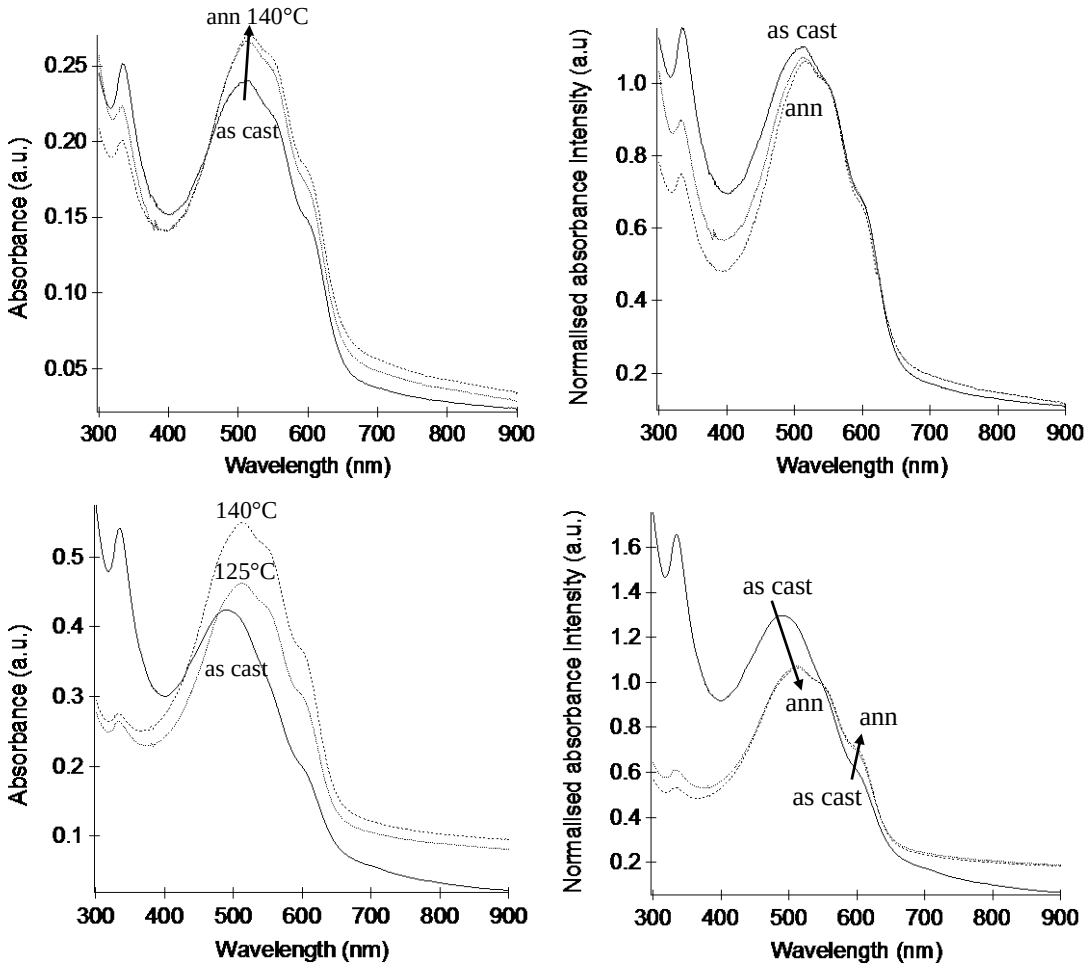

Figure 3.18: UV-vis absorption spectra of ternary blends comprising 40 wt% HDPE. Solid line is for films before annealing. Top: spectra of thin films (~120 nm). Bottom: spectra of thick films (~350 nm). The data are normalised in the right panel.

Further information was obtained from optical microscopy. We observe larger phase separation in thick films (Figure 3.19). In addition we find that after annealing, the quantity of PCBM aggregates is higher for thicker films. This can be attributed to the fact that aggregation is the consequence of phase separation of PCBM from P3HT. At higher PCBM content, this is separated from P3HT and therefore aggregates more. An explanation of the phenomenon of aggregation of PCBM in ternary blends is proposed below. Note that thick films showed are ~350 nm, while thin films are ~80 nm.

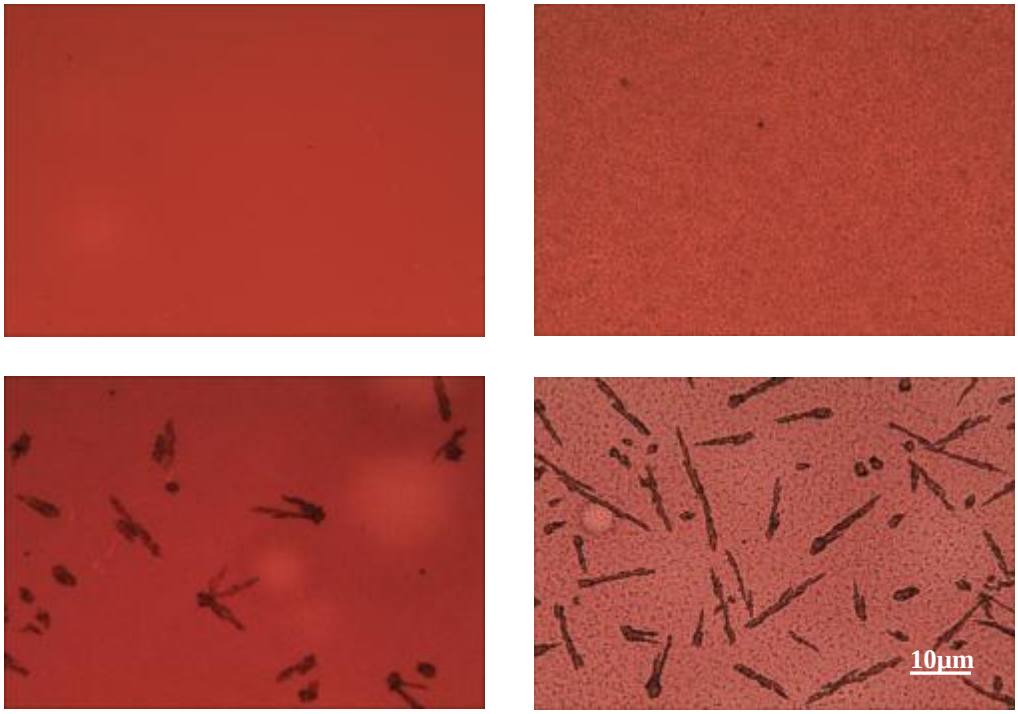

Figure 3.19: Optical micrograph of ternary blend films comprising 40 wt% HDPE. Left: thin film (~80 nm). Right: thick films (~350 nm). Top micrographs show as-cast films, bottom panels are the same structures after annealing.

It is important to mention that blends of different HDPE content produce different microstructures. First of all, as observed for binary blends of P3HT:HDPE, films of a very high or very low content of polyethylene have a homogeneous microstructure where different phases are not readily distinguishable. At a blend composition 1:1 different phases become evident (Figure 3.20).

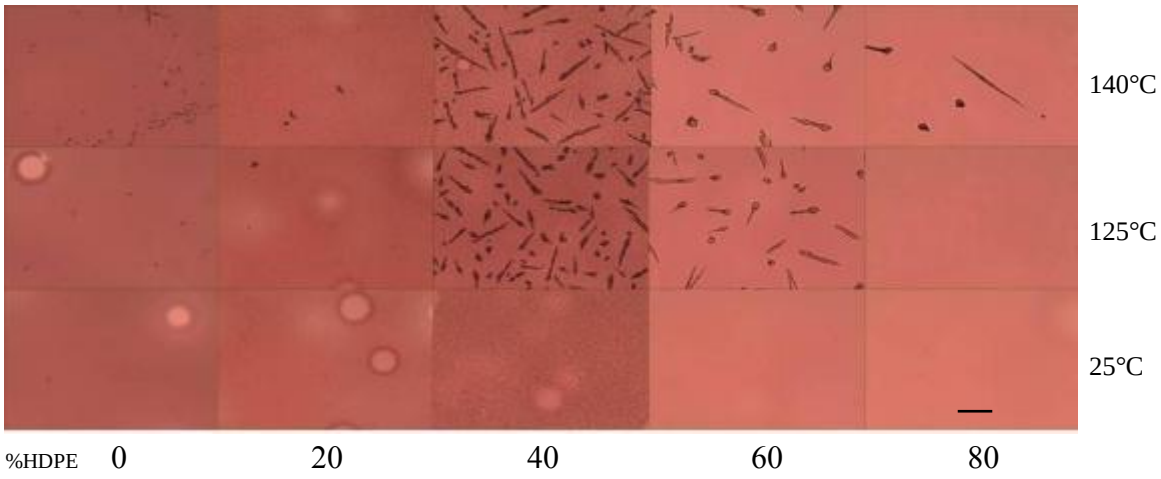

Figure 3.20: Optical micrographs of ternary blends of different compositions after different annealing treatments. Thickness of the films is ~350nm. Scale bar 10µm.

Annealing at temperatures close to the melting of the polyethylene induced crystallization of PCBM into aggregates that are visible in OM. It is important to note that the melting temperature of HDPE (~130°C for the neat polymer) is lowered by the presence of P3HT:PCBM (Figure 3.21).

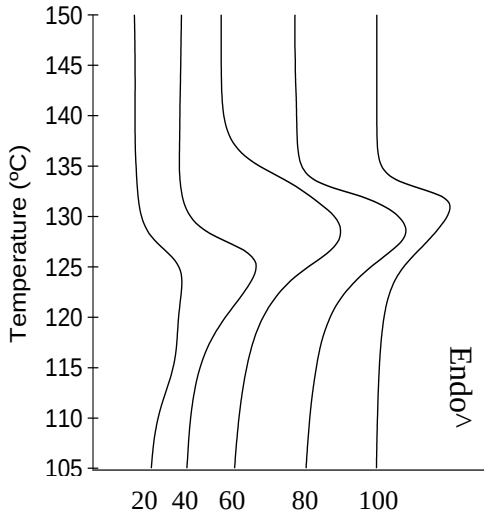

Figure 3.21: DSC thermograms, of P3HT:PCBM:HDPE ternaries showing the melting point depression of HDPE upon addition of the donor:acceptor materials.

Indeed, the melting point recorded for a blend of 60-80 wt% is ~128°C, which is reduced to ~125°C for a ternary comprising 20-40 wt% HDPE. In the blend comprising 20 wt% of polyethylene the melting endotherm is broadened, probably producted by the superposition of two endotherms. This decrease could be related with the presence of an eutectic point. This is supported by the fact that blend comprising 20 wt% HDPE features a broad endotherm related to the melting of the pure component and another one related to the melting of the eutectic composition (Figure 3.21).

The dependence of the content of HDPE is now addressed. Because of the differences explained above, in the next chapters the results related to thin (~80 nm) and thick (~500 nm) films are treated separately.

3.3.1 Ternary blend thin films

Thin films of ternary blends feature different opto-electronical properties compared to the P3HT:PCBM binary. The influence of HDPE content on UV-vis absorption is for instance different from those observed for the P3HT:HDPE blend. For as cast ternary films, the A_0 absorbance intensity increased when adding to 40 wt% HDPE. If the content of the insulating polymer is further increased, the tendency is the opposite. Indeed there is a decrease of the absorbance for higher contents of HDPE. For the A_2 transition there is a decrease of the absorbance for the blend comprising 40 wt% HDPE, while in the other blends there is a slightly increase (Figure 3.22). Note though that the shifts observed are relatively small.

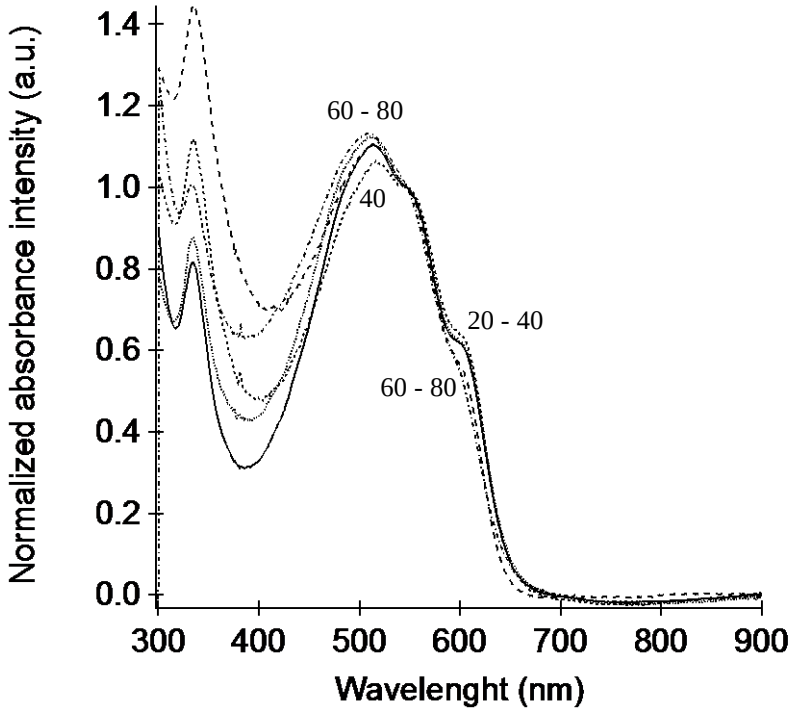

Figure 3.22: UV-vis absorption spectra of ternary blends. Solid line is the binary P3HT:PCBM, dashed lines are ternary films. Numbers indicate the HDPE content.

We now like to focuse on the charge separation efficiency of the ternary blends, i.e. on the PL quenching. First, we discuss our data obtained with blends comprising 20, 40 and 60 wt% of HDPE. Interestingly the ternaries display a less pronounced PL quenching compared to the binary. The HDPE content thereby seems not to have a significant influence, since all the spectra of the ternary films are comparable (Figure 3.23).

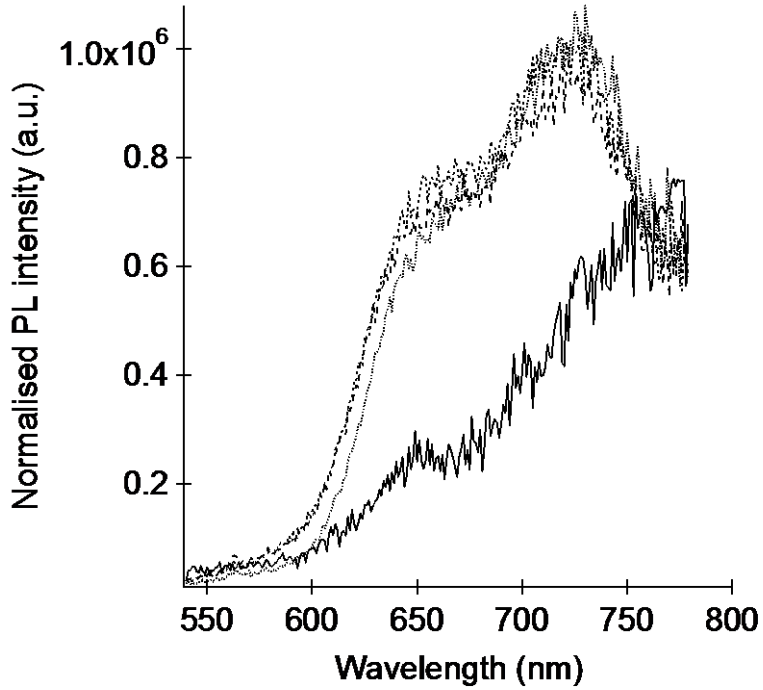

Figure 3.23: Normalised PL spectra, of P3HT:PCBM binary (solid line) and the ternary blends (dashed lines).

This observation indicates that the presence of the HDPE phase reduces the molecular interaction of the P3HT in the donor:acceptor blend.

We now consider the effect of annealing at 125°C for 15 minutes on the opto-electronic properties of such ternaries. UV-vis absorption measurement indicate that the A_0 of the P3HT:PCBM blend is more pronounced, while there is a gradual decrease of the absorption with incerasing content of HDPE. The binary P3HT:PCBM blend film shows also the lowest A_2 peak. The blends with polyethylene display only a slightly more intense absoprtion at these wavelength. The difference becomes notable only for a high content of HDPE, i.e. > 80 wt% (Figure 3.24). This reflects a higher aggregation of P3HT in the binary in respect to the ternary which gradually decreases with HDPE.

An annealing of the films produces aggregation of PCBM that leads to a reduction of the emission quenching. This seems to be due to the smaller intermixing between P3HT and PCBM with a consequent decreased probability to be able to dissociate the exciton and to transfer the electrons from the donor to the acceptor. [21] Annealing at 125°C leads to a more intense PL of blends comprising 40 to 60 wt% HDPE. In contrast, such a heat treatment did not affect blends of lower content of insulator. This is consistent with the Figure 3.20, in which aggregation is present for films of 40-60 wt% HDPE content.

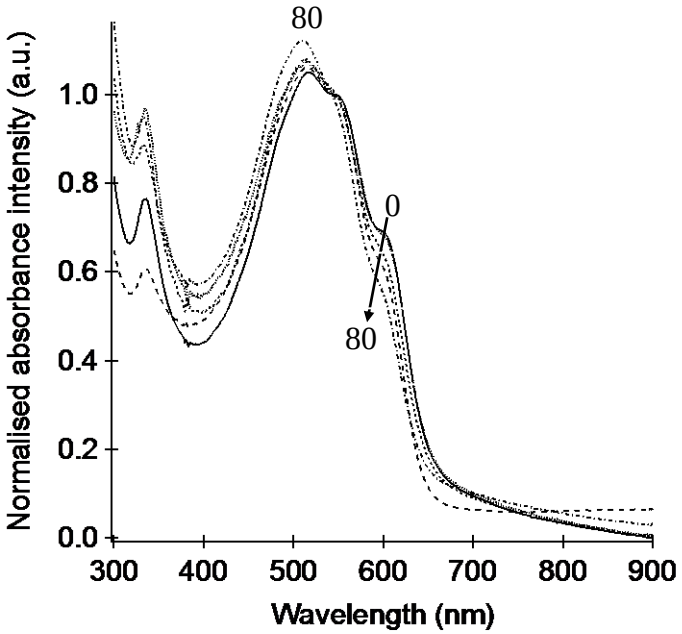

Figure 3.24: UV-vis absorption spectra of ternary blends annealed at 125°C. Solid line is the binary P3HT:PCBM, dashed lines are ternary films. Numbers indicate the HDPE content.

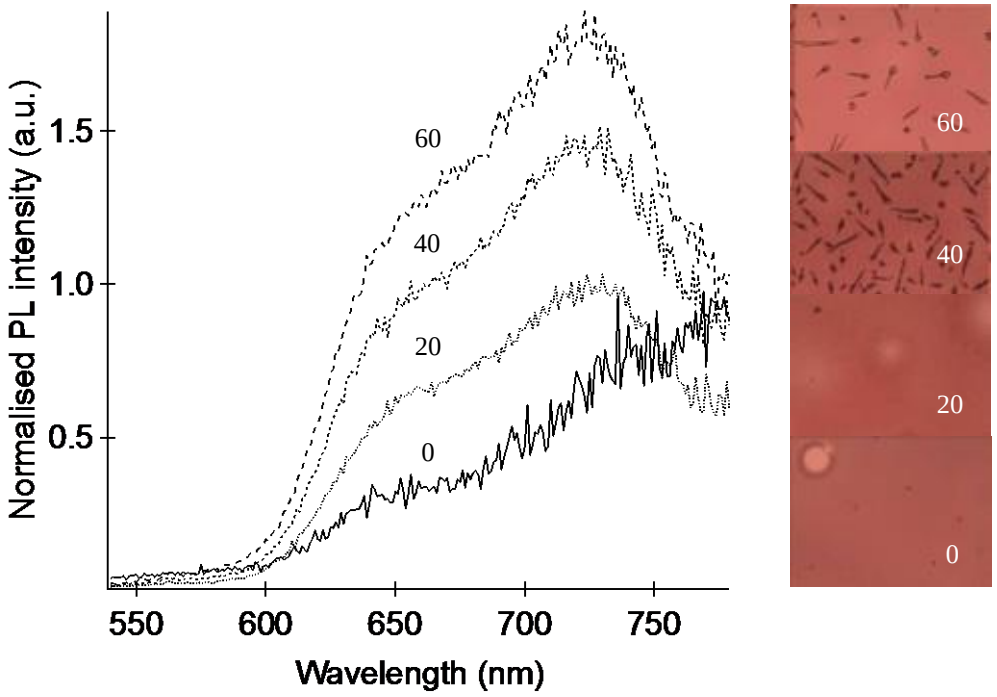

Figure 3.25: Normalised PL spectra of ternary blend films annealed at 125°C. The numbers indicate the wt% of HDPE. On the right optical micrographs of the corresponding films are shown, scale bar 10µm.

When the annealing temperature is raised to 140°C, a hypochromic shift of the A_2 transition is observed for ternary blend films. Films of a content of HDPE of 40-60 wt% indeed absorb less compared to the films prepared with the binary. Only the 80 wt% HDPE display a higher A_2 transition. The A_0 absorption of blends up to 40 wt%

were comparable to the binary and slightly more pronounced, while blends comprising higher contents of HDPE (60-80 wt%) display a lower intensity (Figure 3.26).

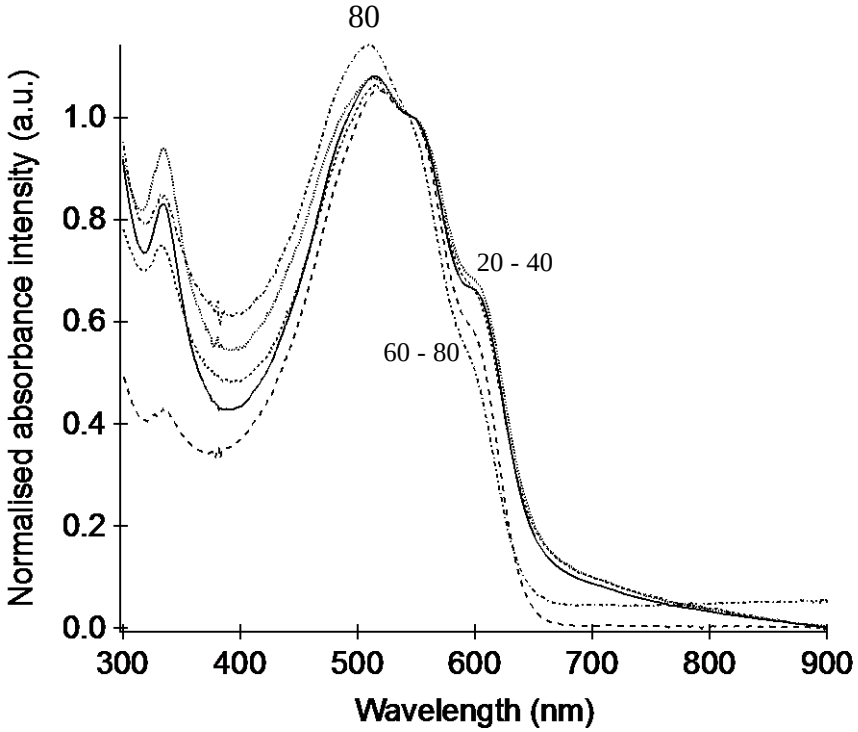

Figure 3.26: UV-vis absorption spectra of ternary blends annealed at 140°C. Solid line is the binary P3HT:PCBM, dashed lines are ternary films. Numbers indicate the HDPE content.

This results demostrate that an annealing 140°C lead to a reorganization of P3HT in blends of an HDPE content of up to 40 wt%. This indicates enhanced aggregation and thus, likely, improved molecular order of P3HT. Addition of more than 80 wt% HDPE, however affects the aggregation of P3HT negatively.

Increasing the annealing temperature to 140°C, produces a further decrease of the PL quenching (increase of the emission). The intensity of the shift is more intense for blends with lower content of HDPE and the ternary comprising 20 wt% content of HDPE appears more shifted compared to blends of 40 to 60 wt%. This is in agreement with an increase of aggregation of PCBM. At this temperature the fullerene derivative can aggregate also for blends comprising smaller content of HDPE (20 wt%). The difference in aggregation between 125°C and 140°C becomes however less pronounced at higher HDPE content, since strong aggregation occurs already at 125°C.

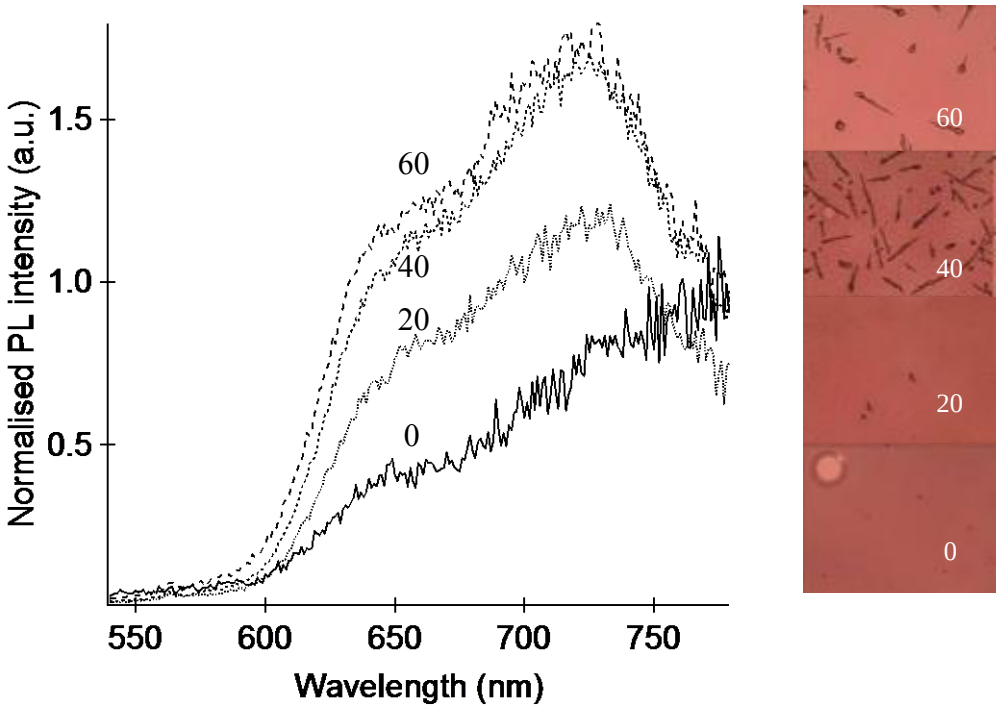

Figure 3.27: Normalised PL spectra of films annealed at 140°C. The numbers indicate the wt% of HDPE. Right: optical micrographs of the corresponding films, scale bar 10µm

The same films used for PL experiments were used for TAS. P3HT shows photoinduced absorption (PA) signal at λ = 640 nm in the crystalline phase, whichis related to photogenerated charge pairs (also called polaron pairs) that rapidly recombine. For PCBM, at the same wavelength, a PA due to singlet-singlet annihilation is present. But interestingly, in the blend, a long lived PA state is present due to the CTS formation. [20] The kinetics of the decay of the signals are of the order of the picoseconds and give information on the recombinations that take place on the excited state formed. The CTS have got a longer lifetime compared to that one of charge pairs and the signal decays completely in 100 ps.

Other transient species, probing P3HT at different wavelengths lead to the conclusion that polarons give a signal at ~1000 nm, the decays in the ns timescale, while the signal resulting from singlet excitons at ~1200 nm decays in the ps timescale. [37] When PCBM is present with compositions close to 50 wt% significantly longer lived charge are observed with a lifetime in the µs timescale.

We were interested to investigate free charges. Hereby we excited this donor material at 520 nm and probed at 980 nm, i.e. where P3HT was reported to display photoinduced signal for polarons. Elucidating the decay dynamics over a timescale from µs to ms, we obtained a low intensity noisy signal. However we can distinguish the different PA

(Figure 3.28). Binary systems (black line) featured the highest photoinduced absorption. A trend related to the addition of HDPE is observed, the decrease of the signal and therefore to the decrease of charges generation is proportional to the HDPE content (Figure 3.28). This is consistent with the above observation (Figure 3.27), where for the ternary blend films less quenching and thus less charge separation was detected.

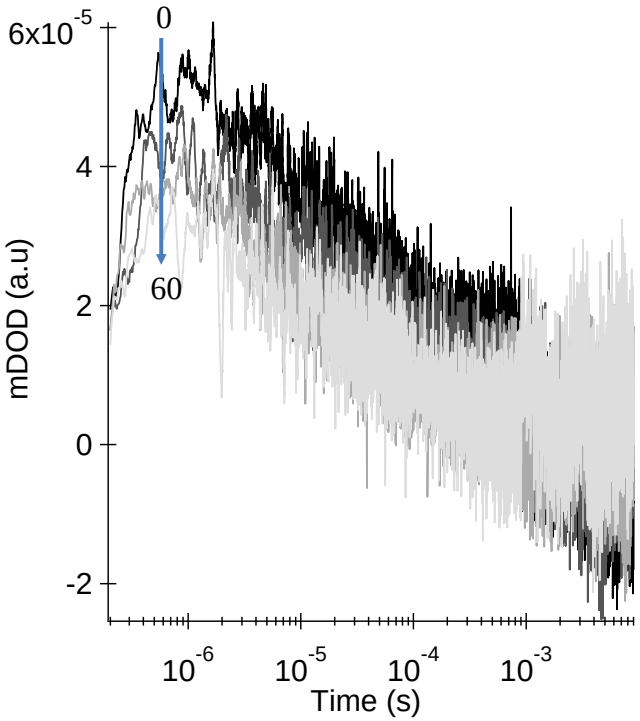

Figure 3.28: Transient absorbance spectra, (excitation wavelength 520 nm). Black: binary system, grey: ternary blends.

The decay of the signal appears similar for all the films, except for the blend comprising 60 wt% HDPE which features a slower decay, especially at longer timescales, (after 10^{-4} seconds). The decay is related with the geminative recombination of charges and takes place in a time scale from μs to ms.

3.3.2 Ternary blend thick films

Different results are obtained for thick ternary blends. In absorption, UV-vis P3HT:PCBM blends display the highest A_2 absorption and the lowest A_0 transition. The difference with the ternary blends films is significant. An addition of HDPE leads to a decrease of the A_2 transition and to an increase of the A_0, which is most pronounced for blends comprising 60 wt% of HDPE.

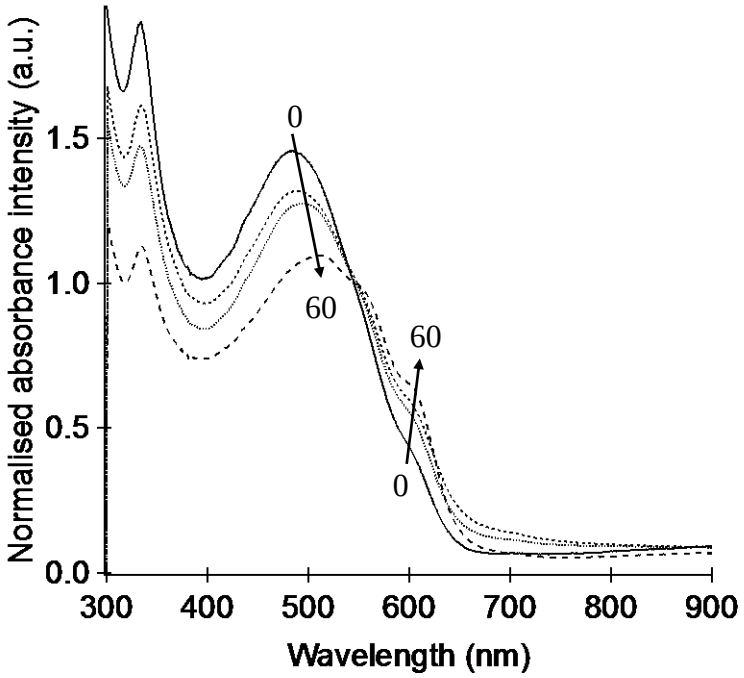

Figure 3.29: UV-vis absorption spectra of thick ternary blend films, solid line is the binary P3HT:PCBM, dashed lines are ternary films. The HDPE content is given in the graph.

These results highlight how thick films of ternary blends show a stronger tendency to aggregate compared to the binary. After annealing at 125°C, the differences between the A_2 and A_0 absorptions is reduced and all the spectra show a more pronunced vibronic structure. The blend comprising 40 wt% polyethylene features very similar spectra as recorded for ternaries of 60 wt%. The peaks A_2 and A_0 change with content of HDPE, while after annealing at 140°C no remarkable modifications are found (Figure 3.30). This behaviour is in agreement with the results shown above. Thicker films of both binary and ternary blends are subjected to a molecular reorganization during annealing that leads to P3HT aggregation. The binary has a less pronounced effect than the ternary, which may be due to the melting of HDPE facilitating this process.

As described for the binary P3HT:HDPE, the phase segregation can lead to a better order of the system. It is possible that when PCBM is present, this process is not effective enough and a system far from the equilibrium is reached. In the ternary the P3HT within the polyethylene molten matrix can diffuse, ann as a consequence aggregates.

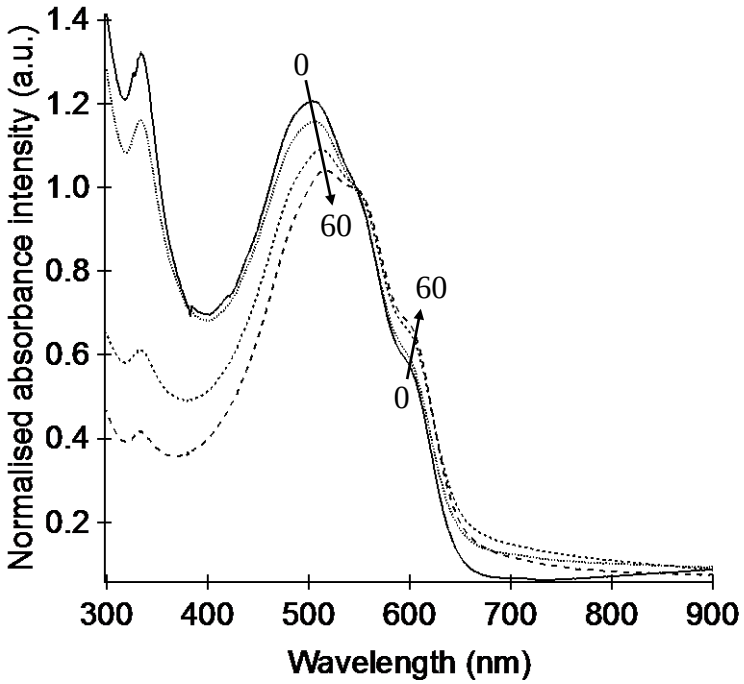

Figure 3.30 UV-vis absorption spectra of thick ternary blend films annealed at 125°C. Solid line is the binary P3HT:PCBM, dashed lines are ternary films. The HDPE content is given in the graph.

We focus now the attention on the PL of annealed films at 140°C, in contrast to our observations made on thin films, the PL quenching of binary and ternary blend films is similar and 20-40 wt% HDPE show stronger quenching than the binary (Figure 3.31). It is interesting to note that the luminescence of P3HT:PCBM remains unchanged in respect to the case of thin films, while the PL quenching of ternary blend is considerably lower. This is probably due to the fact that thick films of ternaries have in this case a stronger interaction between donor and acceptor, while this was reduced in thinner films probably due to the more limited bulk interaction between P3HT and PCBM.

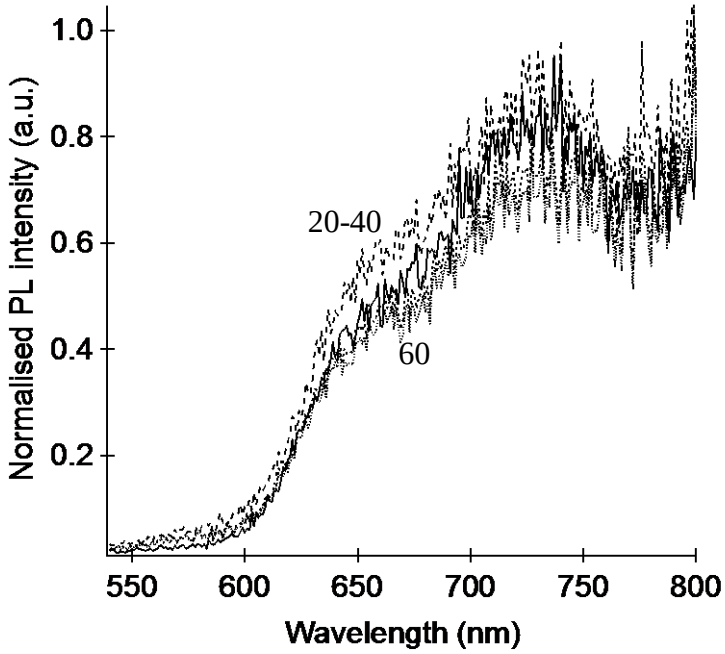

Figure 3.31: Normalised PL spectra of thick films annealed at 140°C. Solid line is the binary P3HT:PCBM, dashed lines are ternary films. The numbers indicate the wt% of HDPE.

While charge separation is efficient in ternary blend films, the charge generation remains smaller than that in binary blend films. This is evident from the TAS data for thick ternary blend films presents in Figure 3.32. The highest signal is obtained for the P3HT:PCBM films, where more active material is present than in the ternaries.

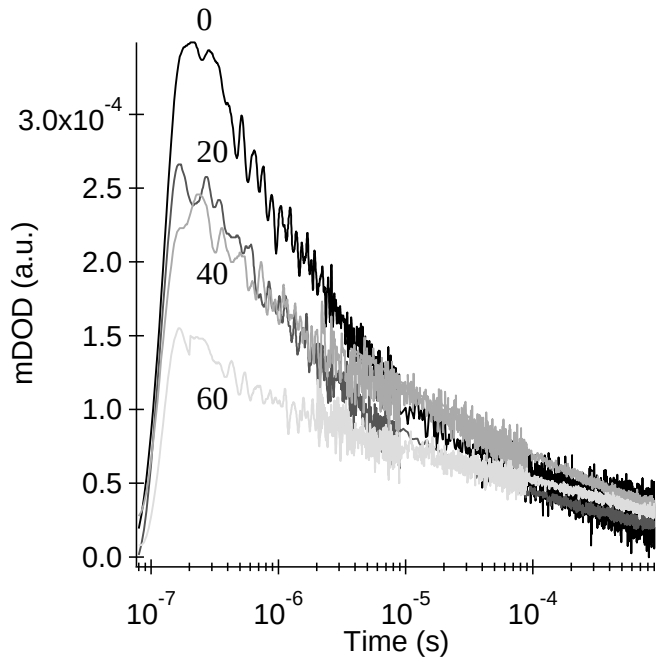

Figure 3.32: Transient absorbance decay signal for thick films (excitation wavelength = 520nm). Black: binary system, grey: ternary blend.

However it is important to note that the charge generation of ternary blend films is now higher than that of thin films of the binary, resulting therefore adequate for photovoltaic applications. Another interesting feature is the decay of the signal. In Figure 3.33 the normalization of the signals at the maximum is reported, an addition of HDPE causes a decreasing of the decay. Films with 40-60 wt% HDPE show a slower decay and thus recombination process especially after 10^{-5} seconds, possibly related to the less charge density consequent to the presence of the insulating polymer.

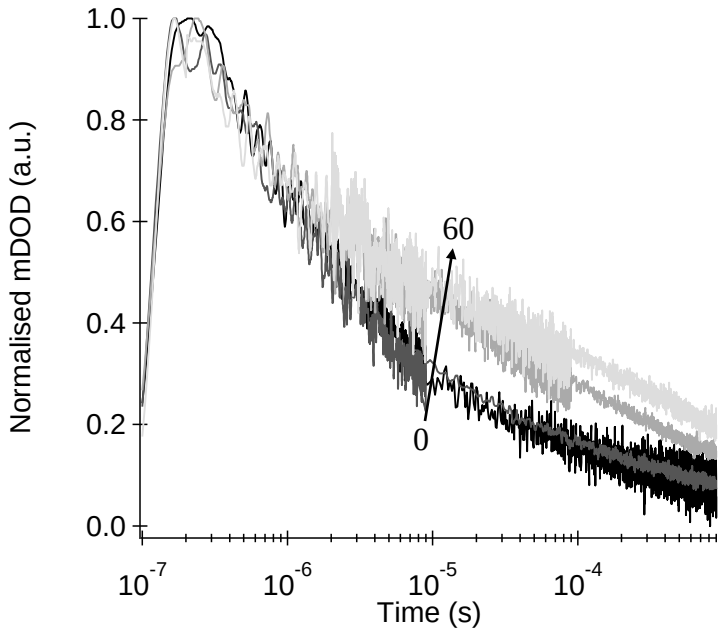

Figure 3.33 Transient absorbance spectra, (excitation wavelength 520 nm), signal normalised at the maximum. Black: binary system, grey: ternary blends.

3.3.3 Performances of photovoltaic devices

In this work the attention was focused on the materials characterization, while devices preparation was not the predominant interest. However a limited number of photovoltaic devices were produced and the voltage-current characteristic under simulated solar illumination (Air Mass 1.5, 100 $mWcm^{-2}$) was measured.

Devices were prepared in air in a lab without control of environmental pollutants (not in a cleanroom), only the electrodes deposition was performed in a glove-box. OPV solar cells were fabricated on glass substrates with the following structure: indium tin oxide (ITO)/poly(3,4-ethylenedioxythiophene)(PEDOT:PSS)/P3HT:PCBM:HDPE/Al.

The ITO substrate was first cleaned by sonification with acetone and isopropanol, dried and then placed in a UV ozone chamber for 20 min. The substrate was then coated with approximately 20 nm thick layer of PEDOT:PSS by spin-coating at 2500 rpm for 60 seconds, afterwards the substrate was heated at 125 °C for twenty minutes. Film

deposition of the active layer is then performed via wire-bar coater and then annealed at 140°C for 15 minutes. Al is finally deposited via evaporation with a mask design showed in Figure 2.8.

Results relative to a ternary blend with 40 wt% HDPE are here presented and compared with devices produced with a binary blend (Figure 3.34). The thickness of the active layer is ~250 nm for the ternary and ~100 nm for the binary.

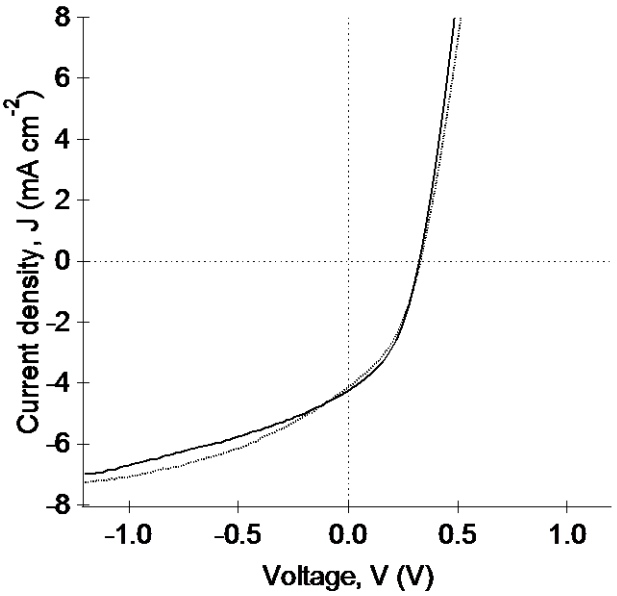

Figure 3.34: Current density–voltage characteristics under simulated solar illumination (Air Mass 1.5, 100mWcm^{-2}) of photovoltaic devices made from P3HT:PCBM blends (solid line) and P3HT:PCBM:HDPE 40 wt% HDPE (dashed line). Films annealed at 140°C for 15 minutes.

Values of open-circuit voltage (Voc), short-circuit current (Jsc), fill factor (FF) and power conversion efficiency (PCE) are showed in Table 3.1.

	Voc (V)	**Jsc (mA/cm2)**	**FF**	**PCE (%)**
Ternary 40 wt% HDPE	0.33005	-4.128667	0.391813	0.533911
P3HT:PCBM	0.32484	-4.257556	0.411979	0.569778

Table 3.1: Voc, Jsc, FF and PCE of photovoltaic devices of Figure 3.34.

The characteristic J-V curve is almost the same for the two blends and therefore also the efficiency. This is an example of how doubling the thickness of the active layer, the efficiency of the ternary blend can be comparable to that of the binary. The values of V_{oc} are quite low and affect the PCE of the cells, this is related to the preparation of the device in a normal lab and not in a cleanroom and to the non-optimization of the cell.

3.4 DPP-TTT films

Before blending DPPTTT with polyethylene a previous study on the neat polymer was conducted. Solutions in chlorobenzene, that provide a good dissolution of the material, are casted at 30°C, 60°C, 90°C, 120°C. These films were subjected to DSC and XRD analysis, the former was performed in order to obtain information on the transitions occurring. A scan from 25°C to 350°C was executed but no phase transitions were observed (the thermograph appear flat). Since the polymer is semicrystalline, the melting temperature and the crystallization temperature are probably at higher temperatures.

XRD analysis provides additional information. We observe the h00 diffraction attributed to the lamellar stacking, with the 100 around 2θ = 4.45 and the 0k0 diffraction attributed to the π-stacking, with the 010 at 2θ = 25 (Figure 3.35). The wavelength used is λ = 1.54 Å, inserting these values in the Bragg's law (eq. 17), a distance d = 19.83 Å for the lamellar stacking and d = 3.5 Å for the π-stacking are obtained.

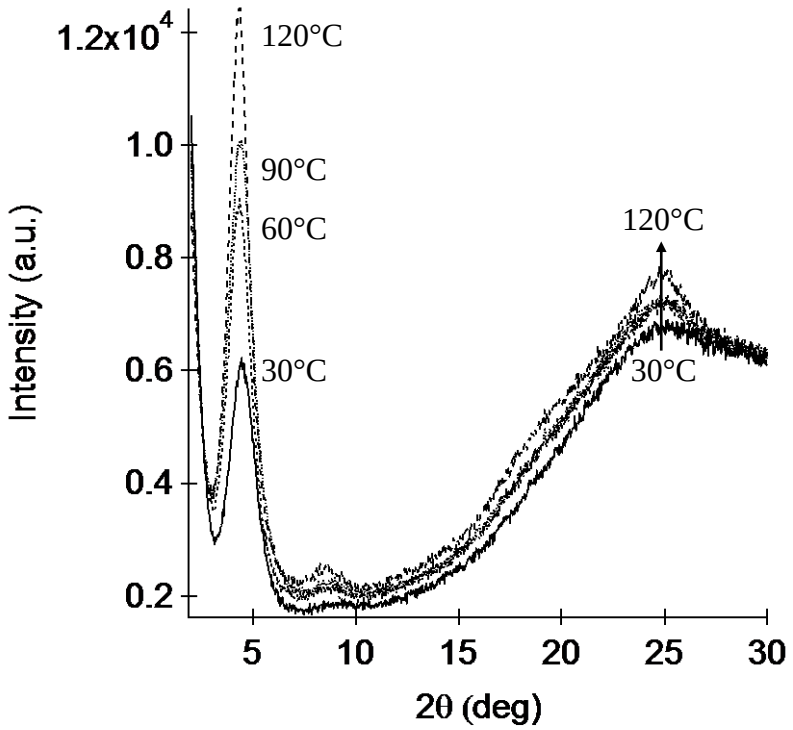

Figure 3.35: XRD spectra of drop-casted films of DPPTTT, different deposition temperature are indicated.

An increase in intensity of the peaks is noticed with the increase of the deposition temperature, as an evidence of the increase of the quality of the lamellar packing.

Films were also deposited via wire-bar coating, with the same casting temperature used for the XRD and DSC analysis. UV-vis absorption was then performed on this films, three absorptions are visible: at 800, 740 and 440 nm (Figure 3.36).

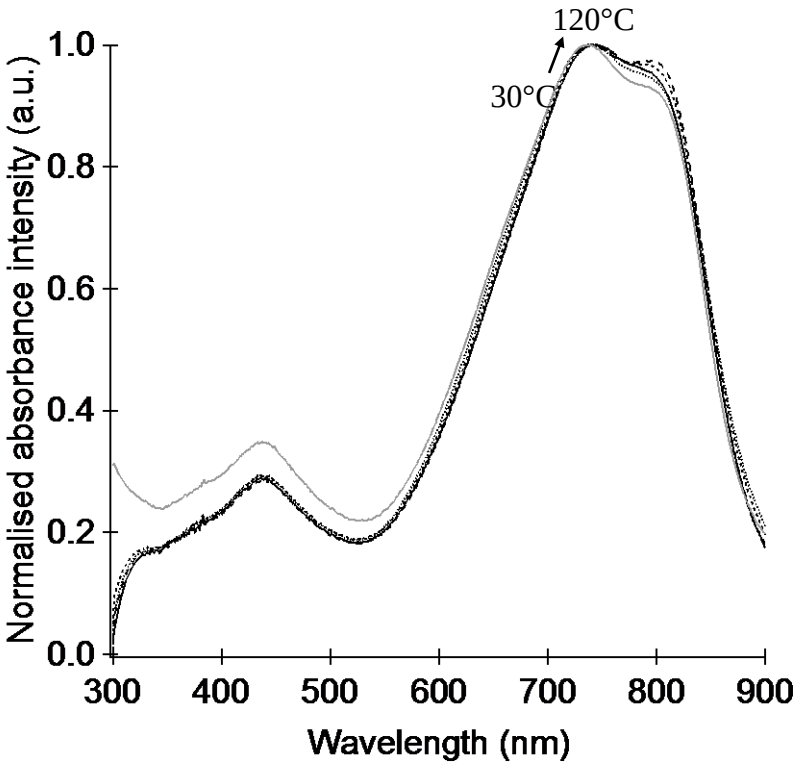

Figure 3.36: UV-vis absorption of DPPTTT films, different temperatures of deposition are indicated. DPPTTT:HDPE 1:1 in grey.

Reflecting the lower energy gap (~1.38 eV), the absorption maxima is red-shifted compared to the P3HT. As stated by Bronstein et al., [10] the presence of the shoulder at 440 nm can be addressed to the presence of low molecular weight oligomers, to a vibronic shoulder arising from aggregates in solution or to a spectral feature of the polymer chain.

A slight dependence on the deposition temperature was observed, indeed the less energetic absorbance appears slightly shifted at higher intensity as the deposition temperature increases. This may reflect a better aggregation of these films. Changes in thicknesses do not appear to alter to absorption behaviour.

A blend DPPTTT:HDPE 1:1 was studied to check the applicability of the insulating polymer to DPPTTT. Films with different deposition temperature were coated and their UV-vis spectra measured, a limited difference in respect to the same films with neat

DPPTTT is appreciable, the first absorption is indeed slightly less intense (grey line in Figure 3.36). Deposition temperatures from 110°C to 140°C did not seem to have influences on the spectra, as well as different thicknesses.

Optical microscopy was also used to study the microstructure, which appears quite homogeneous, although it is possible to observe the presence of two phases (Figure 3.37).

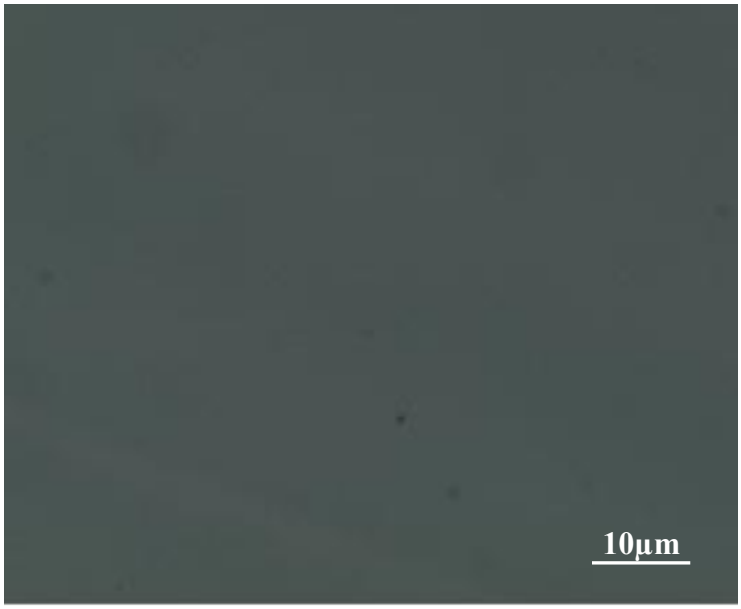

Figure 3.37: Image of DPPTTT:HDPE microstructure via optical microscope.

The blend of DPPTTT with PCBM was then examined. $PC_{71}BM$ was employed because previous studies with films casted via spin-coating gave good results with this fullerene derivative. A composition DPPTTT:PCBM 1:1 was chosen.

DSC and XRD analysis were performed. A it was observed for the neat DPPTTT, also in this case no useful information was obtained via DSC. XRD samples were prepared by drop-casting at 30°C and 120°C. The position of the 100 lamellar stacking and 010 π-stacking peaks are unaltered, but a new peak around $2\theta = 18°$ appears for the blend casted at 120°C. Also the blend casted at 30°C shows a limited higher intensity at that angle, but a peak is not clearly detectable. In both the blend films there is also an enlargement of the 200 diffraction (Figure 3.38).

The interesting datum is the presence of the new peak, attributed to PCBM, it is apparently possible to achieve phase separation of the acceptor material by changing the deposition temperature.

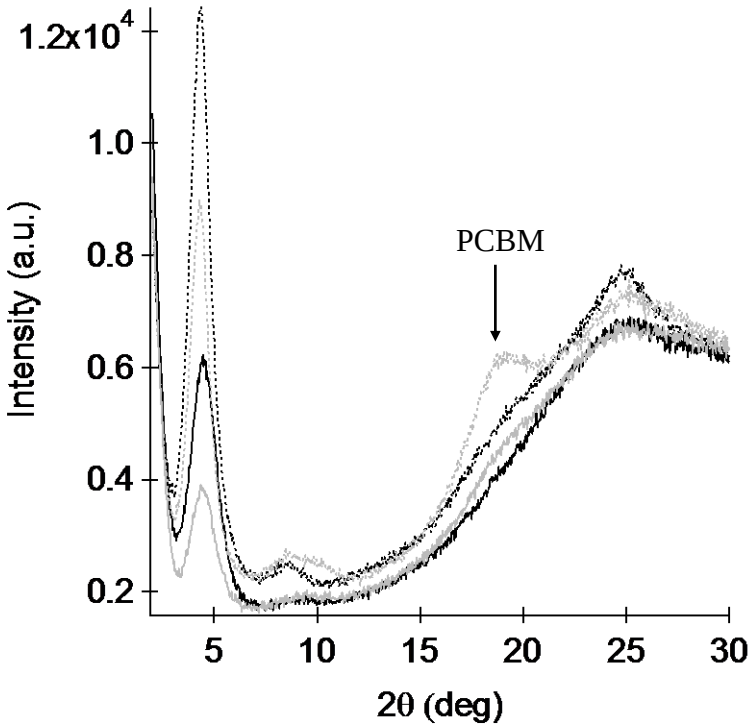

Figure 3.38: XRD spectra of drop-casted films of DPPTTT:PCBM 1:1 (grey) and DPPTTT (black). Deposition temperature of 30°C in solid lines, 120°C in dashed lines.

This last observation is important because an analysis of the microstructure of the blend DPPTTT:PCBM via optical microscope shows how aggregation of PCBM is not visible in the film even after annealing at high temperature, only at 180°C a little aggregation is visible at the microscope. This doesn't mean that phase separation doesn't occur, but for sure it is in a small scale. Even if this behaviour is positive from an exciton quenching point of view, an aggregation of crystals of PCBM is needed for obtaining an efficient spatial separation of the charges. [21] For this reason a deposition treatment at 120°C can be beneficial.

The absence of aggregation noticed via microscope analysis is confirmed by XRD data of annealed films. The film deposited at 30°C was annealed at 120°C, while the film deposited at 120°C was annealed at 180°C, in both cases the annealing duration was 15 minutes. The signal relative to the PCBM is not affected by the thermal treatment as a further evidence of our hypothesis, while the lamellar stacking signal is increased as a consequence of the improved lamellar packing.

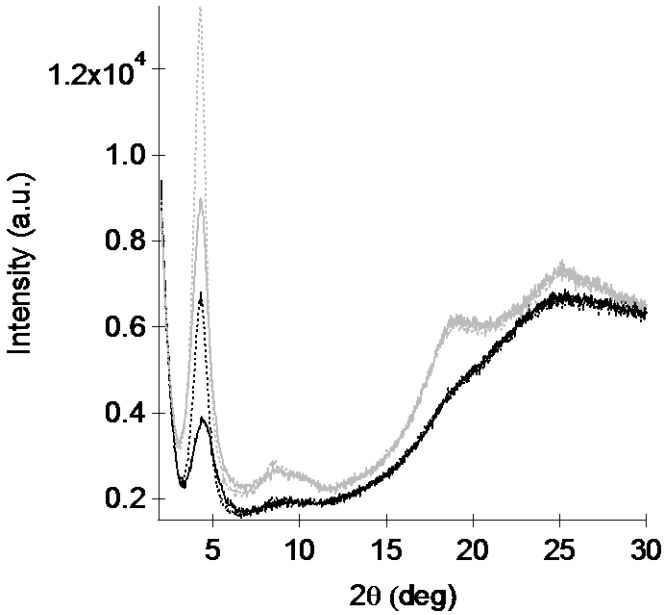

Figure 3.39: XRD spectra of drop-casted films of DPPTTT:PCBM deposited at 120°C (grey) and 30°C (black). Annealing at 120°C and 180°C respectively, are represented with dashed lines.

UV-vis on the binary system DPPTTT:PCBM was also performed. First of all the deposition temperature does not have the same decisive influence noticed for the XRD, there is only a slightly increasing of the absorption at higher wavelength (A_0), likewise it was observed for the neat polymer. The parameter that definitely influences the absorbance is the thickness and the effect is the same of that one observed for the binary blend P3HT:PCBM. Indeed an increase of the thickness leads to a decreasing of the A_0 absorbance, as an indication of a lower aggregation.

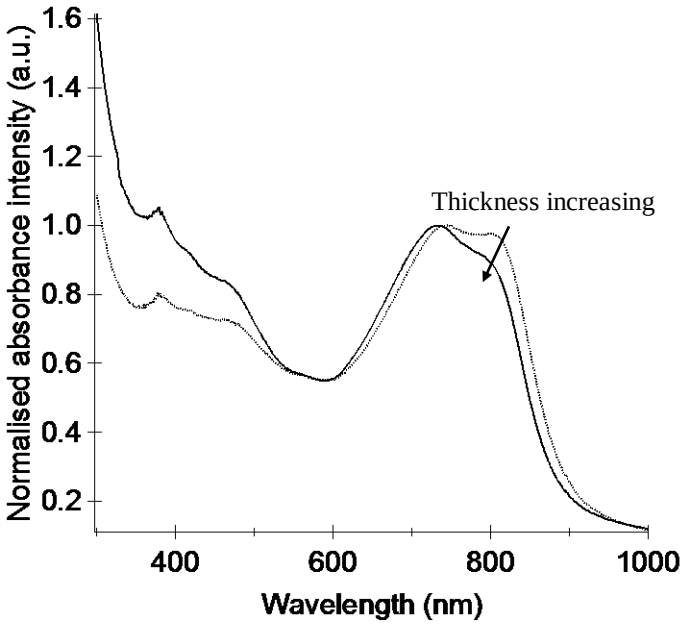

Figure 3.40: UV-vis absorption of DPPTTT:PCBM films, different thicknesses are indicated.

Furthermore, attention was focused on ternary blend films of (DPPTTT:PCBM):HDPE. The insulating polymer content was 50wt% and the ratio between DPPTTT:PCBM was 1:1. UV-vis absorption of these films doesn't demonstrate any effect provided by HDPE. Similarly to what was observed for the binary DPPTTT:HDPE, also for the ternary blend in the microstructure it is difficult to observe different phases (Figure 3.41).

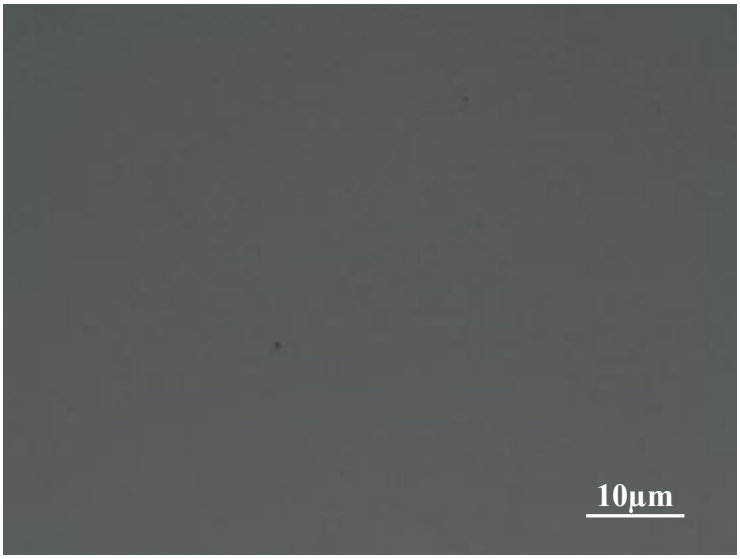

Figure 3.41: Optical micrographs of DPPTTT:PCBM:HDPE.

An annealing treatment was then performed on the ternary blend films. An analysis at microscope demonstrates surprisingly an absence of aggregation even at temperature above the melting point of HDPE.

For studying this phenomenon, films with a composition $PC_{71}BM$:HDPE 1:1 from a CB solution were prepared and the annealing effect on the microstructure was analysed via optical microscope. Aggregation doesn't occur either for these films, as an evidence that the absence of aggregation in ternary blend films is the consequence of a non-aggregation of $PC_{71}BM$ in HDPE when the solution is prepared in CB. In order to understand if this behaviour was related just to the solvent, solutions of the same blend in TCB were prepared. In this case a small amount of aggregation is present, but still much less than what was observed for the blend HDPE:$PC_{60}BM$ (Figure 3.42).

The increased aggregation observed for TCB could be attributed to the higher boiling point of the solvent and therefore its slower evaporation or to a co-crystallization of the solvent with the polymer that lead to different PCBM structure, like explained by Rispens and al. [38]

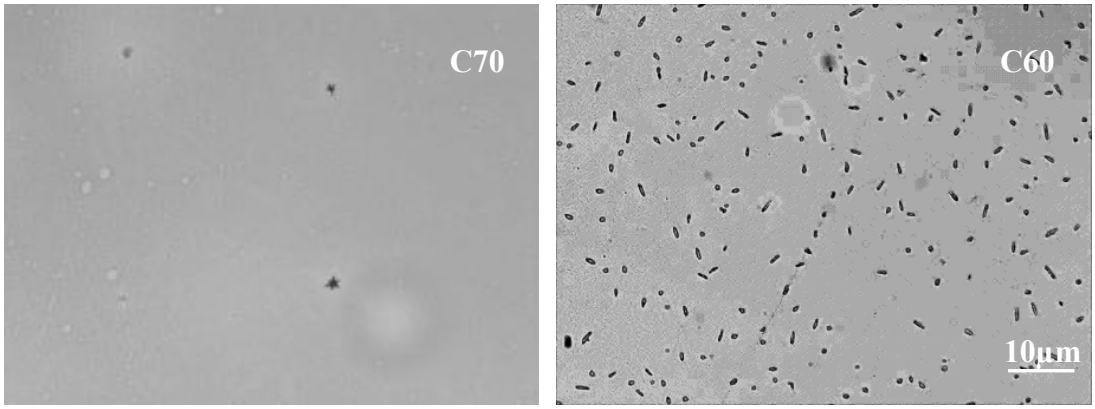

Figure 3.42: Optical micrographs of PCBM. [C70] on the left, [C60] on the right. Annealing temperature 130°C.

The difference between $PC_{71}BM$ and $PC_{61}BM$ is probably related to the different in dimensions and so to the difference in solubility and diffusion rate of the two materials. Films with composition $PC_{71}BM$:HDPE 1:1 were also treated at temperature higher but the microstructure remains the same.

TCB was then used to prepare solutions of the ternary blend. Films were annealed at different temperatures and consistently with the observation just exposed, aggregation was oberved, even if in a much lower scale than the ternary blend P3HT:$PC_{61}BM$:HDPE.

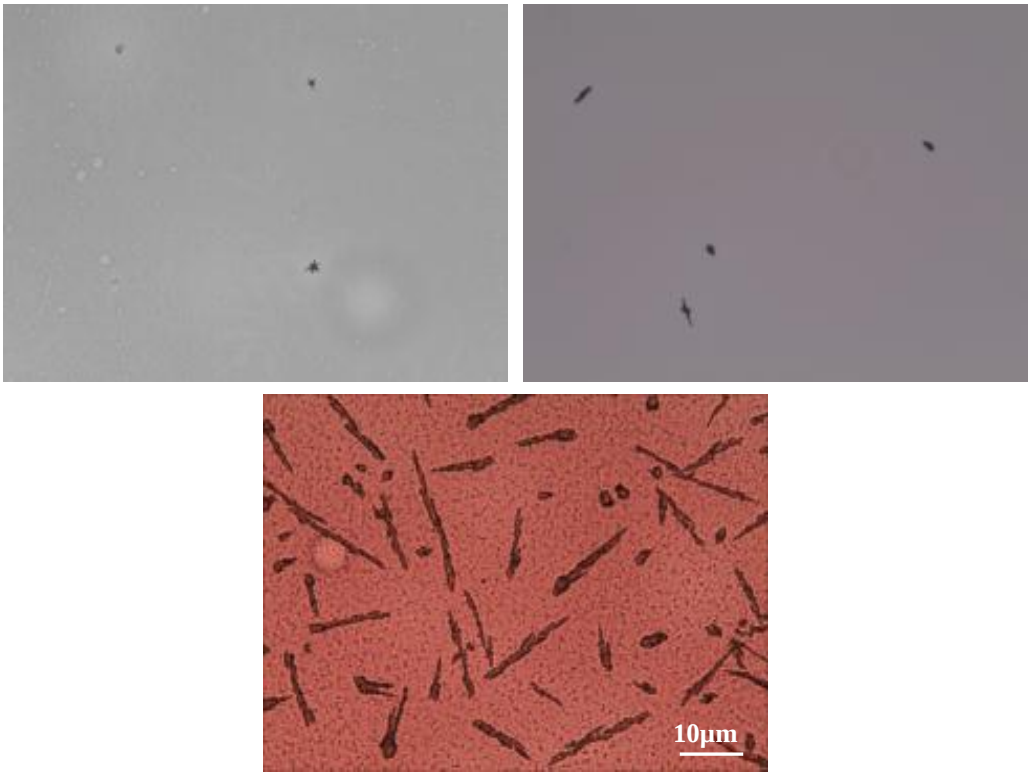

Figure 3.43: Optical micrographs of $PC_{71}BM$:HDPE (top left) DPPTTT:$PC_{71}BM$:HDPE (top right) and P3HT:PCBM61:HDPE (bottom). Annealing temperature 140°C.

UV-vis analysis on ternary blend films of DPPTTT:PCBM:HDPE were also performed. The spectrum doesn't appear different from the binary DPPTTT:PCBM, confirming the observation proposed before for DPPTTT:HDPE that HDPE doesn't affect the absorption of these films. An increase of the thickness has got also in this case the effect of inducing less aggregation to DPPTTT.

4. Conclusions and outlooks

The influence of HDPE on optical, structural and electronic properties of different blend films was studied and a further evidence for the potential applicability of a ternary blend P3HT:PCBM:HDPE for photovoltaic applications has been provided.

A binary blend P3HT:HDPE demonstrate how the insulating material is able to provide an increase of order and aggregation to P3HT. This observation is in agreement with the results of Goffri et al. [1] who showed that field-effect mobility of binary blends was comparable or higher than that of neat P3HT. This is attributed to the presence of the insulating polymer, the crystallinity of which provides the driving force for the segregation of P3HT.

The UV-vis measurements of P3HT:PCBM films deposited via wire-bar coating show that thicker films are less aggregated and highly disordered. Although a better reorganization is achieved with an annealing treatment, the lower aggregation persists. An addition of HDPE leads to the same amount of aggregation for films with different thickness, inducing a better uniformity of results. This is an important advantage, since this behaviour could be determinant for obtaining regularity of properties and for a large scale production of devices.

Ternary blend thin films (~80-100 nm) display poor performances in terms of exciton quenching and free charge formation in respect to P3HT:PCBM films. This was explained as the consequence of the reduced quantity of active material present. Because one of the objectives was to obtain thick and robust films, the impracticality of ternary blend thin films is not a problem. The increase of the thickness results in an improvement of the performance, exciton quenching is nearly the same of that of the binary and charge generation is satisfactory. Moreover the recombination rate of the charges is lower for films with HDPE, demonstrating improved properties in respect to the binary.

Thus, thick films of P3HT:PCBM:HDPE display properties agreeable with the requisites of blends for photovoltaic applications. Further evidence is given by the efficiencies of the devices reported, which are in the same order of magnitude of those of the P3HT:PCBM solar cells. These results are in agreement with those proposed by Ferenczi et al., [2] although it is important to point out that films used in that work are

deposited via spin-coating. An optimization of the cells, including for instance the usage of new solvents, and a wider number of devices is needed to obtain further information on the performances of the devices produced via wire-bar coating.

The studies on the aggregation of PCBM in HDPE demonstrate how the use of a third material can be used to modulate the dimensions of aggregates. An annealing at temperature close to the melting point of HDPE can lead to the segregation of PCBM possibly without affecting the intermixing between P3HT and PCBM. This could explain why in thick films the exciton quenching is high and the geminative recombination of charges is reduced.

The use of $PC_{71}BM$ can produce different microstructures, a further study of blends with this material is needed to clarify the reason of the different behaviour compared with the C_{60} counterpart. This could helpful for a further study of a DPPTTT:PCBM:HDPE system. In fact the absence of aggregation of PCBM in the binary blend DPPTTT:PCBM could be solved exploiting the segregation behaviour of PCBM in HDPE, without the need of adding a higher concentration of PCBM. As explained previously, this can be solved also choosing a deposition temperature around 120°C.

[1] S. Goffri et al., “Multicomponent semiconducting polymer systems with low crystallization-induced percolation threshold.,” *Nature materials*, vol. 5, no. 12, pp. 950-6, Dec. 2006.

[2] T. a M. Ferenczi, C. Müller, D. D. C. Bradley, P. Smith, J. Nelson, and N. Stingelin, “Organic semiconductor:insulator polymer ternary blends for photovoltaics.,” *Advanced materials (Deerfield Beach, Fla.)*, vol. 23, no. 35, pp. 4093-7, Sep. 2011.

[3] H. Akamatu, H. Inokuchi, and Y. Matsunaga, “Electrical Conuctivity of the Perylene-Bromine Complex.” Nature, vol.173, p. 168, 1954.

[4] T. N. Prize, “The Nobel Prize in Chemistry , 2000 : Conductive polymers,” pp. 1-16, 2000.

[5] T. Kobayashi, *Relaxation in Polymers*. 1993, pp. 269-308.

[6] J. Clark, J.-F. Chang, F. C. Spano, R. H. Friend, and C. Silva, “Determining exciton bandwidth and film microstructure in polythiophene films using linear absorption spectroscopy,” *Applied Physics Letters*, vol. 94, no. 16, p. 163306, 2009.

[7] J. Clark, C. Silva, R. Friend, and F. Spano, “Role of Intermolecular Coupling in the Photophysics of Disordered Organic Semiconductors: Aggregate Emission in Regioregular Polythiophene,” *Physical Review Letters*, vol. 98, no. 20, pp. 1-4, May 2007.

[8] C. Winder and N. S. Sariciftci, “Low bandgap polymers for photon harvesting in bulk heterojunction solar cells,” *Journal of Materials Chemistry*, vol. 14, no. 7, p. 1077, 2004.

[9] I. Kaur et al., “Substituent effects in pentacenes: gaining control over HOMO-LUMO gaps and photooxidative resistances.,” *Journal of the American Chemical Society*, vol. 130, no. 48, pp. 16274-86, Dec. 2008.

[10] H. Bronstein et al., “Thieno[3,2-b]thiophene-diketopyrrolopyrrole-containing polymers for high-performance organic field-effect transistors and organic photovoltaic devices.,” *Journal of the American Chemical Society*, vol. 133, no. 10, pp. 3272-5, Mar. 2011.

[11] Michael Kasha, *Energy Transfer Mechanisms and the Molecular Exciton Model for Molecular Aggregates*. Radiation Research Society, pp. 55-70.

[12] F. Würthner, T. E. Kaiser, and C. R. Saha-Möller, “J-aggregates: from serendipitous discovery to supramolecular engineering of functional dye materials.,” *Angewandte Chemie (International ed. in English)*, vol. 50, no. 15, pp. 3376-410, Apr. 2011.

[13] F. C. Spano and I. Introduction, “The Spectral Signatures of Frenkel Polarons in,” *Accounts of Chemical Research*, vol. 43, no. 3, pp. 429-439, 2010.

[14] F. C. Spano, “Modeling disorder in polymer aggregates: the optical spectroscopy of regioregular poly(3-hexylthiophene) thin films.,” *The Journal of chemical physics*, vol. 122, no. 23, p. 234701, Jun. 2005.

[15] E. S. Manas and F. C. Spano, “Absorption and spontaneous emission in aggregates of conjugated polymers,” *The Journal of Chemical Physics*, vol. 109, no. 18, p. 8087, 1998.

[16] S. Westenhoff et al., “Supramolecular Electronic Coupling in Chiral Oligothiophene Nanostructures,” *Advanced Materials*, vol. 18, no. 10, pp. 1281-1285, May 2006.

[17] F. Spano, “Absorption in regio-regular poly(3-hexyl)thiophene thin films: Fermi resonances, interband coupling and disorder,” *Chemical Physics*, vol. 325, no. 1, pp. 22-35, Jun. 2006.

[18] B. Kippelen and J.-L. Brédas, “Organic photovoltaics,” *Energy & Environmental Science*, vol. 2, no. 3, p. 251, 2009.

[19] C. Deibel, T. Strobel, and V. Dyakonov, “Role of the charge transfer state in organic donor-acceptor solar cells.,” *Advanced materials (Deerfield Beach, Fla.)*, vol. 22, no. 37, pp. 4097-111, Oct. 2010.

[20] G. Grancini, D. Polli, D. Fazzi, J. Cabanillas-gonzalez, G. Cerullo, and G. Lanzani, “Transient Absorption Imaging of P3HT : PCBM Photovoltaic Blend :,” *Technology*, pp. 1099-1105, 2011.

[21] F. C. Jamieson, E. B. Domingo, T. McCarthy-Ward, M. Heeney, N. Stingelin, and J. R. Durrant, “Fullerene crystallisation as a key driver of charge separation in polymer/fullerene bulk heterojunction solar cells,” *Chemical Science*, vol. 3, no. 2, p. 485, 2012.

[22] N. Stingelin, “On the phase behaviour of organic semiconductors,” *Polymer International*, no. February, p. n/a-n/a, Apr. 2012.

[23] B. A. Collins, J. R. Tumbleston, and H. Ade, “Solar Cells : Toward an Enlightened Understanding of Device,” *Perspective*, 2011.

[24] O. G. Reid et al., “The influence of solid-state microstructure on the origin and yield of long-lived photogenerated charge in neat semiconducting polymers,” *Journal of Polymer Science Part B: Polymer Physics*, vol. 50, no. 1, pp. 27-37, Jan. 2012.

[25] A. a Virkar, S. Mannsfeld, Z. Bao, and N. Stingelin, “Organic semiconductor growth and morphology considerations for organic thin-film transistors.,” *Advanced materials (Deerfield Beach, Fla.)*, vol. 22, no. 34, pp. 3857-75, Sep. 2010.

[26] J. Nelson, “Polymer:fullerene bulk heterojunction solar cells,” *Materials Today*, vol. 14, no. 10, pp. 462-470, Oct. 2011.

[27] L. Mascia, *The Role of Additives in Plastics*. 1985.

[28] D. Credgington, R. Hamilton, P. Atienzar, J. Nelson, and J. R. Durrant, “Non-Geminate Recombination as the Primary Determinant of Open-Circuit Voltage in Polythiophene:Fullerene Blend Solar Cells: an Analysis of the Influence of Device Processing Conditions,” *Advanced Functional Materials*, vol. 21, no. 14, pp. 2744-2753, Jul. 2011.

[29] F. C. Krebs, “Fabrication and processing of polymer solar cells: A review of printing and coating techniques,” *Solar Energy Materials and Solar Cells*, vol. 93, no. 4, pp. 394-412, Apr. 2009.

[30] B. O’Connor et al., “Correlations between mechanical and electrical properties of polythiophenes.,” *ACS nano*, vol. 4, no. 12, pp. 7538-44, Dec. 2010.

[31] Y. Galagan et al., “Technology development for roll-to-roll production of organic photovoltaics,” *Chemical Engineering and Processing: Process Intensification*, vol. 50, no. 5–6, pp. 454-461, May 2011.

[32] T. a M. Ferenczi, C. Müller, D. D. C. Bradley, P. Smith, J. Nelson, and N. Stingelin, “Organic Semiconductor:Insulator Polymer Ternary Blends for Photovoltaics.,” *Advanced materials (Deerfield Beach, Fla.)*, pp. 4093-4097, Aug. 2011.

[33] C. E. Murphy, L. Yang, S. Ray, L. Yu, S. Knox, and N. Stingelin, “Wire-bar coating of semiconducting polythiophene/insulating polyethylene blend thin films for organic transistors,” *Journal of Applied Physics*, vol. 110, no. 9, p. 093523, 2011.

[34] C. Müller, C. P. Radano, P. Smith, and N. Stingelin-Stutzmann, “Crystalline–crystalline poly(3-hexylthiophene)–polyethylene diblock copolymers: Solidification from the melt,” *Polymer*, vol. 49, no. 18, pp. 3973-3978, Aug. 2008.

[35] A. Kumar, M. a. Baklar, K. Scott, T. Kreouzis, and N. Stingelin-Stutzmann, “Efficient, Stable Bulk Charge Transport in Crystalline/Crystalline Semiconductorâ□“Insulator Blends,” *Advanced Materials*, vol. 21, no. 44, pp. 4447-4451, Nov. 2009.

[36] C. Müller et al., “Tough, Semiconducting Polyethylene-poly(3-hexylthiophene) Diblock Copolymers,” *Advanced Functional Materials*, vol. 17, no. 15, pp. 2674-2679, Oct. 2007.

[37] J. Guo, H. Ohkita, H. Benten, and S. Ito, “Near-IR femtosecond transient absorption spectroscopy of ultrafast polaron and triplet exciton formation in polythiophene films with different regioregularities.,” *Journal of the American Chemical Society*, vol. 131, no. 46, pp. 16869-80, Nov. 2009.

[38] M. T. Rispens, A. Meetsma, R. Rittberger, C. J. Brabec, N. S. Sariciftci, and J. C. Hummelen, “Influence of the solvent on the crystal structure of PCBM and the efficiency of MDMO-PPV:PCBM ‘plastic’ solar cells.,” *Chemical communications (Cambridge, England)*, no. 17, pp. 2116-8, Sep. 2003.